UNIVERSITÉ DE RENNES 1

IRMAR

HABILITATION À DIRIGER DES RECHERCHES

Mention : Mathématiques

présentée à

L'UNIVERSITÉ DE RENNES 1

par

Éric DARRIGRAND

Opérateurs intégraux, noyaux singuliers, méthodes rapides : Outils mathématiques pour la résolution numérique de problèmes denses et de grande dimension

Soutenue le **28 novembre 2014**

Devant le jury composé de

M.	**Marc BONNET**	**Directeur de Recherches – ENSTA-ParisTech**	**examinateur**
M.	**Martin COSTABEL**	**Professeur – Université de Rennes 1**	**examinateur**
Mme	**Monique DAUGE**	**Directeur de Recherches – Université de Rennes 1**	**examinatrice**
M.	**Christophe GEUZAINE**	**Professeur – Université de Liège (Belgique)**	**examinateur**
M.	**Stéphane LANTERI**	**Directeur de Recherches – INRIA Sophia-Antipolis**	**rapporteur**
Mme	**Francesca RAPETTI**	**Maître de conférences HDR – Université de Nice**	**rapporteur**
M.	**Francisco Javier SAYAS**	**Professeur – Université du Delaware (USA)**	**rapporteur**
Mme	**Isabelle TERRASSE**	**Ingénieur de Recherches HDR – Airbus**	**examinatrice**

à la Nature,

au Héron Cendré et aux Paons de Jour de la saligue d'Arbus,
pour les rendez-vous réguliers,

aux Gypaètes Barbus de la vallée d'Aspe et Balbuzard de la plaine du Gave de Pau,
pour les rencontres furtives,

à la Chouette Effraie qui illumine nos soirées hivernales,

aux Oies du Canada et Oies des Neiges en Delaware,
à la mélodie réconfortante, si loin de mon Béarn,

au Monarque, voyageur éphémère au long cours,
ou la vision inattendue au détour d'un jardin du Delaware,

aux Grues Cendrées, dans leur vol annuel au dessus des Pyrénées,
à l'appel si émouvant, un souvenir inaltérable,

"L'étude approfondie de la nature est la source la plus féconde des découvertes mathématiques"
Joseph Fourier

Puissent, un jour, les mathématiques, contribuer significativement
à la préservation de notre planète et de ses richesses naturelles et sauvages ...

Remerciements

Je tiens tout d'abord à remercier vivement Marc Bonnet, Martin Costabel, Monique Dauge, Christophe Geuzaine, Stéphane Lanteri, Francesca Rapetti, Francisco Javier Sayas et Isabelle Terrasse pour avoir accepté d'être membres du jury de ma soutenance HDR, et plus particulièrement Stéphane Lanteri, Francesca Rapetti et Francisco Javier Sayas pour avoir accepté de rapporter sur ce document.

Je souhaite faire part d'une infinie gratitude à l'ensemble de mes collègues rennais, les collègues de l'IRMAR (plus amicalement ceux des équipes EDP, Mécanique et Analyse Numérique), de l'UFR Mathématiques, de l'INSA ou de l'ENS Rennes, de l'IREM, de l'INRIA de Rennes, de l'IETR, ... Je m'adresse plus chaleureusement à certains d'entre eux qui ont marqué sensiblement mes années à l'IRMAR : Monique Dauge et Martin Costabel, mes premiers contacts avec l'équipe d'Analyse Numérique de Rennes, de proches collègues et amis, ils ont joué le rôle essentiel et délicat de me soutenir et me guider tout au long de la rédaction de ce document ; Gabriel Caloz et Michel Pierre qui ont assuré un exceptionnel triple recrutement de l'équipe en 2003 ; Rozenn Texier-Picard et Julien Vovelle, mes co-bureau et co-recrutés 2003 ; Daniel Martin, le concepteur de MÉLINA++ qui m'a formé au développement de bibliothèques numériques – je lui dois l'expérience et la confiance avec lesquelles j'ai initié l'aventure FastMMLib et contribue à XLiFE++ ; Yvon Lafranche, il fut mon premier collègue sur le plan de l'enseignement à Rennes, il est mon plus proche collaborateur sur le plan du développement numérique, mon expert C++ – je lui dois l'enthousiasme avec lequel je poursuis l'aventure FastMMLib ; Michel Crouzeix, notamment pour ce cours d'optimisation en 2003 – un fabuleux héritage désormais élément central du Master Calcul Scientifique et Applications ; Grégory Vial, pour son accueil lors de ma première venue en terrain rennais, pour les leçons d'agreg et un cours construit ensemble; Benjamin Boutin, notre dernier recruté ; l'équipe projet IPSO de l'INRIA de Rennes, notamment François Castella, Philippe Chartier et Erwan Faou, pour leur accueil joyeux pendant deux années de délégation pour une mise en orbite réussie de la FMM ; Florian Méhats et Mohammed Lemou arrivés en renfort du Sud-Ouest nous offrir une exploration galactique ; l'équipe pédagogique du Master Calcul Scientifique et Applications, notamment Stéphane Balac, Mariko Dunseath-Terao, Fabrice Mahé, Loïc Le Marrec – un Master époustouflant, dynamique, novateur et de nouvelles perspectives sur le plan recherche ... ; les doctorants rennais avec lesquels j'ai ou ai eu le plaisir d'interagir, El-Hadji, Frédérique, Rania, Hamdi, Julie, Maher, Adrien. J'aimerais aussi exprimer mes remerciements à nos partenaires du SFC, du SAI, du SOIE ou de la Fondation Rennes 1, ainsi qu'à mes étudiants, ceux qui ont suivi et ceux qui suivent les cours d'optimisation, EDP elliptiques, méthodes numériques, éléments finis, FMM, C++, ..., pour leur attention, leur curiosité, leurs difficultés, autant d'échanges qui font de ces heures d'activité professionnelle des moments passionnants.

Nos diverses activités, nos déplacements, nos colloques et soutenances ne seraient pas sans le personnel de gestion, d'entretien des locaux ou de maintenance informatique. De grands mercis à Claude, Carole, Emmanuelle, Xhensila, Marie-Aude, Frédérique, Hélène, Chantal, Marie-Annick, Véronique, Claudine, Jeannick, Leone, André, Patrick, Olivier ... pour leurs

accueils toujours si chaleureux et si dévoués ... sans oublier celles et ceux qui ne sont plus dans nos locaux ... et une pensée emplie d'émotion pour Marie-France. De grands mercis aussi à Lalao et Bachir nos directeurs du moment, et à celles et ceux qui les ont précédés dans ce rôle.

Je tiens également à adresser mes remerciements à mes compagnons d'étude, mes collaborateurs et collègues des quatre coins de monde, des universités de Pau, Bordeaux, Toulouse, Nancy, Amiens, Nantes, Clermont-Ferrand, ..., du CERMICS, de l'ENSTA, du Delaware, de Caltech, universités de Reading, de Göttingen, UCL, WIAS de Berlin, MPI de Leipzig, LAMSIN, universités de Tunis, de Santiago de Chile, de Zhengzhou, ... Notamment : mes amis et mes enseignants de l'école d'Arbus, des collège et lycée de Lescar ; mes enseignants ou collègues de l'Université de Pau avec une pensée particulière pour Ovide Arino ; mes collègues et compagnons de DEA et de thèse – université de Bordeaux, les amis du CESTA, un clin d'oeil particulier à Alain Bachelot, Katherine Mer-Nkonga et Hélène Barucq qui m'ont initié au monde de la Recherche ; mes amis et collègues du Delaware lors de mon accueil post-doctoral par Peter Monk ; un collègue et ami à la fois de Reading, Göttingen et Frankfurt, Roland Potthast ; les membres collègues et amis du projet ANR Microwave à Nancy, Liège, Lille, Amiens, ... sans oublier ses joyeux [anciens] thésards dont Bertrand mon allié GMSH, ...

Merci à Amel pour notre extraordinaire réalisation conjointe pour le plus grand bonheur de nos juments Horiane et Édelweiss, nos chiens et chats sur notre petit domaine de Percou avec ses occupants non déclarés qui illuminent notre quotidien de leurs naissances chaque printemps (pinsons, hirondelles, hérissons, crapauds, chouettes effraies, écailles du séneçon, grimpereaux, mésanges, ...) et rythment nos saisons (châtaigniers, rosés des prés, mûres sauvages, pommes à cidre, ...). Merci à nos familles pour leurs nombreux coups de main dans cette aventure. Merci à tout Percou pour son accueil chaleureux et son assistance à notre arrivée en pays de Brocéliande. Merci à l'AACIV et nombreux amis *amis des chevaux*. Merci aussi aux voisins de l'avenue du Général Patton (plus particulièrement Marie et Christian), au Cercle Celtique de Rennes et la Petite Hublais de Betton pour leur accueil à mon arrivée en Bretagne.

Mille mercis à l'ensemble de ma famille pour sa présence sans faille à mes côtés malgré l'éloignement géographique et mes visites trop espacées. Merci à mes parents, mes sœurs, mes beaux-frères, mes nièces et neveu qui emplissent de joie chacun de mes passages en Béarn.

Pour chacune de leurs œuvres, Alexandre le charpentier, Gabriel le forgeron, Yves le plombier, imaginaient l'ouvrage futur (*de mon côté, je choisis une méthode numérique à mettre en œuvre, ou j'ai à l'esprit un problème physique à résoudre*), pensaient des stratégies de réalisation (*pour ma part, je réfléchis un algorithme, j'identifie des inconnues du problème physique*), dessinaient des plans (*j'écris l'algorithme, ou un modèle mathématique*), décidaient l'outillage et une stratégie de réalisation (*j'organise la programmation, je choisis des outils de résolution appropriés*) pour enfin réaliser l'ouvrage dont le résultat était tout aussi artistique que fonctionnel (*j'écris le programme de mise en œuvre de la méthode numérique, ou j'obtiens une simulation numérique du phénomène physique*). Mon activité ne serait-elle que le reflet des réalisations exceptionnelles du charpentier, du forgeron et du plombier ? À mes parents et mes grands-parents, mille mercis pour le souci permanent de qualité et de bienveillance avec lequel ils m'ont prodigué leurs enseignements.

Contents

Introduction (version française)

La modélisation des phénomènes physiques, biologiques, chimiques, conduit souvent à des équations mathématiques complexes. Les problèmes à N corps, la dynamique moléculaire, la propagation d'onde en domaine extérieur, sont des applications dont la modélisation et la discrétisation conduisent à des systèmes dont la résolution est particulièrement compliquée à cause de leur taille ainsi que des propriétés mathématiques des opérateurs impliqués. La propagation d'onde en domaine extérieur, l'application principale de ce document, est un phénomène physique présent dans de nombreux domaines : détection radar, communication, assistance à la conduite, imagerie, traitement médical des cancers, ... Cependant, la simulation de ce phénomène est toujours un véritable challenge : il nécessite la prise en compte du caractère infini du domaine de résolution vis à vis duquel de nombreuses solutions mathématiques et numériques sont proposées et analysées. En raison des caractéristiques physiques des applications, chaque stratégie présente des avantages et des inconvénients. Il convient de s'intéresser à chacune d'elles, de les confronter voire les combiner. Dans ce document, nous nous intéressons essentiellement aux opérateurs intégraux surfaciques et volumiques impliqués dans deux approches différentes : les représentations intégrales dans le cadre d'approches par équations aux dérivées partielles, ou les équations intégrales. Des caractéristiques de ces opérateurs rendent leur mise en œuvre numérique difficile : ce sont des opérateurs globaux, singuliers et généralement mal conditionnés. Pour faire face à l'aspect global, l'usage de méthodes rapides est indispensable à haute fréquence. La méthode dite "Panel Clustering" [HN89, Sau00], la méthode multipôle rapide [GR88, CRW93, SC95, Dar00a], la méthode "fast high order solver" [BK01b, BK01a], les "H-matrices" et leur "Adaptive Cross Approximation" [Hac99, BGH06, Beb08] sont développées pour rendre moins coûteuse la résolution numérique des systèmes denses de grande taille définis par un noyau de Green. Des préconditionneurs ou des formulations bien conditionnées [BC00, CN02, BET12, AD07, ABL07] sont proposées dans la littérature. Des formules de quadrature et des formules analytiques sont élaborées pour le traitement des singularités [LS12, SS11, DLS14a, DLSon, DLS14b].

Cet ouvrage concerne des concepts mathématiques élaborés pour améliorer l'efficacité et la robustesse des méthodes numériques de résolution des problèmes denses de grande dimension, tels que les équations intégrales pour la propagation d'onde en domaine extérieur. Quatre principaux sujets sont abordés dans cette synthèse, contribuant tous au développement et à la mise en œuvre d'algorithmes de résolution. Chacun correspond à un chapitre du document :

- ⋆ **FMM – une solution numérique pour compenser le caractère dense des opérateurs intégraux :** La méthode multipôle rapide (FMM pour "Fast Multipole Method") a été initialement introduite pour les problèmes à N corps [GR88, GR97] puis rapidement appliquée aux formulations intégrales de l'équation de Laplace. Par la suite, la méthode a été adaptée aux problèmes de propagation d'onde acoustique et électromagnétique [CJL+97, Dar00a, Dar00b, KSC99, Rah96]. La FMM est utilisée dans une opération bien

spécifique de la résolution numérique de sorte qu'elle peut être combinée à d'autres outils numériques tels que les préconditionneurs et s'applique à toute formulation impliquant des opérateurs intégraux, noyaux de Green ou potentiels de Coulomb. Le chapitre 1 montre l'application de la FMM à différentes configurations : couplage à une discrétisation microlocale pour la résolution des équations intégrales de Després [Dar02b, BDMN03] ; couplage avec un préconditionneur analytique basé sur la stratégie dite "On Surface Radiation Condition" (OSRC) [DDL13] ; une version régularisée de la FMM pour les systèmes Hamiltoniens [CDF10] ; application au couplage entre éléments finis et représentation intégrale [Dar08].

Résumé du chapitre 1 :
La FMM a pour action d'approcher les interactions induites par le noyau de Green en équations intégrales et par le potentiel de Coulomb en dynamique particulaire. Dans la section 1.1, j'écris l'approximation FMM sous une forme générique (équation 1.1). Cette méthode est généralement utilisée pour accélérer les produits matrice-vecteur d'une résolution numérique itérative où la matrice impliquée est définie par un noyau de Green ou un potentiel de Coulomb. Dans ce chapitre, la FMM est adaptée à des configurations originales où elle est utilisée pour l'assemblage d'une matrice plutôt que pour un produit matrice-vecteur (section 1.2), ou alors combinée à un préconditionneur (section 1.3), développée sous une forme régularisée pour l'intégration de systèmes Hamiltoniens (section 1.4), ou encore appliquée à une représentation intégrale (section 1.5).

Dans le cadre d'un couplage avec la discrétisation microlocale [ANZ94, ANZ95, Zho95], la FMM ne consiste pas à accélérer des produits matrice-vecteur mais bien à calculer une matrice. En fait, la discrétisation microlocale prend en considération des paramètres physiques pour relâcher l'interpolation de l'inconnue du problème. Ainsi la taille du système discret est fortement réduite mais le coût d'évaluation de cette dernière reste prohibitif car il s'appuie sur la discrétisation habituelle nettement plus fine. De ce fait, les calculs généralement approchés par la FMM interviennent dans l'évaluation de la matrice. Ce couplage original a été appliqué avec succès aux équations intégrales de Després [Des97, SD99, Stu01], dans le cadre de ma thèse à Bordeaux I, avec Alain Bachelot et Katherine Mer-Nkonga [Dar02b, BDMN03]. Les figures 1.7-1.8 donnent des résultats satisfaisants avec un coût relativement optimal et des discrétisations où la longueur moyenne des éléments du maillage est de l'ordre de 2λ au lieu du classique $\lambda/10$ (λ désignant la longueur d'onde).

L'association de la FMM au préconditionneur OSRC a permis d'analyser numériquement cet outil en 3D pour la résolution de l'équation de Helmholtz [DDL13]. Le préconditionneur OSRC modifie l'équation par l'introduction de facteurs impliquant exclusivement des opérateurs différentiels classiques. De ce fait, l'utilisation de la FMM pour les opérateurs intégraux n'est pas altérée et s'applique de manière transparente à l'équation préconditionnée. Avec Marion Darbas et Yvon Lafranche, dans le cadre du projet ANR Microwave, ce couplage a permis une investigation précise du spectre numérique de l'équation préconditionnée (section 1.3.1) et une résolution numérique efficace permettant de percevoir l'impact remarquable du préconditionnement sur la vitesse de convergence des solveurs itératifs : réduction du nombre d'itérations à la dizaine au lieu de plusieurs centaines sans préconditionnement. Des exemples divers, pour des objets tels que le cône-sphère, un domaine à cavité sphérique, un sous-marin, jusqu'à plusieurs centaines de milliers de degrés de liberté, sont présentés dans la section 1.3.2.

La résolution des systèmes Hamiltoniens requiert d'excellentes propriétés de préservation de la régularité du potentiel du système. Hors, l'approximation FMM est par définition irrégulière. Avec Philippe Chartier et Erwan Faou, lors d'un accueil en délégation INRIA dont j'ai bénéficié au sein de l'équipe IPSO, nous avons développé une forme régularisée de la FMM [CDF10].

Son implémentation a permis de confirmer l'impact bénéfique sur la résolution des systèmes Hamiltoniens : dans la section 1.4, une application numérique à un problème modèle, le système solaire, montre que la FMM régularisée permet d'assurer la conservation de l'Hamiltonien.

La résolution par équation intégrale est rendue difficile par les caractéristiques des opérateurs intégraux. Lorsque l'on résout un problème en domaine extérieur par éléments finis avec condition artificielle, la considération d'une représentation intégrale introduit ces opérateurs dans le système éléments finis. L'utilisation de la FMM assure que le coût induit par l'ajout de ces opérateurs dans la formulation éléments finis n'augmente pas la complexité numérique. Cela a été scrupuleusement vérifié dans le cadre de l'utilisation d'une représentation intégrale pour la formulation variationnelle ultra-faible [Ces96, CD03]. La formulation variationnelle ultra-faible est une variante des éléments finis décrite précisément dans le chapitre 3. L'analyse de la complexité est donnée dans la table 1.4 de la section 1.5 et les tests numériques de cette section confirment ce résultat.

⋆ **Analyse mathématique et numérique des opérateurs intégraux volumiques :** Même si les opérateurs intégraux volumiques sont très utilisés par les physiciens [KM00, Lu03, Bot06, SSVVA06, BS06, Rah00, SF11], la littérature mathématique sur ces outils est relativement pauvre. Un cadre mathématique a été proposé dans [Kir07, KL09], quelques propriétés mathématiques et spectrales figurent dans [FP84]. Nous avons récemment contribué à compléter les résultats d'existence et d'unicité, le choix des espaces fonctionnels, les propriétés spectrales, dans le but d'analyser mathématiquement et d'implémenter des méthodes de résolution. Le chapitre 2 est dédié aux propriétés mathématiques et numériques des opérateurs intégraux volumiques établies avec la participation d'El-Hadji Koné et Hamdi Sakly dans le cadre de leurs thèses [CDK10, Kon10, CDS12, Sak14, CDSonb, CDSona].

Résumé du chapitre 2 :
Les opérateurs intégraux volumiques étaient dans la littérature assez mal connus sur le plan mathématique. Dans la section 2.2, les propriétés mathématiques des opérateurs intégraux sont explorées : choix des espaces fonctionnels, existence et unicité de la solution des équations intégrales de volume, équivalence avec des formulations mieux connues. Notamment, les opérateurs électrique et magnétique ont des propriétés assez différentes qui peuvent facilement conduire à des erreurs de formulation si trop peu d'attention est prêtée au choix des espaces fonctionnels.

La section 2.3 concerne l'analyse du spectre essentiel des opérateurs volumiques électrique et magnétique. Le résultat est établi pour des équations en domaine extérieur autour d'un objet ou bien régulier ou bien Lipschitzien. Dans le cas régulier, on trouve notamment, selon certaines conditions sur les paramètres physiques, que les deux opérateurs ont même spectre essentiel, $\{0, 1/2, 1\}$, mais avec des sous-espaces propres différents.

L'implémentation de l'opérateur électrique dans la librairie MÉLINA++ avec la participation d'El-Hadji Koné, a permis de vérifier numériquement quelques propriétés établies. Les figures 2.2-2.3 offrent des exemples de résolution des équations intégrales volumiques, et la figure 2.4 présente le spectre numérique de l'opérateur électrique.

⋆ **Analyse de la représentation intégrale comme condition au bord exacte :** Afin de résoudre le problème de propagation d'onde en domaine extérieur selon une approche d'équations aux dérivées partielles, il est nécessaire de se ramener à un domaine borné délimité par une frontière artificielle (figure 3.1). Une représentation intégrale permet

de définir une condition artificielle exacte par l'implication d'opérateurs intégraux. De ce fait, ce choix proposé dans [JL77, HL96] a succité quelque intérêt dans la littérature [LJ01, BBFGJ05] malgré les nombreuses difficultés de mise en œuvre qu'il induit. Dans le chapitre 3, nous analysons cette utilisation des représentations intégrales dans le contexte d'une approximation éléments finis [DGR14, Rai14, DGRon] ou d'une formulation variationnelle ultra-faible [DM07, DM12].

Résumé du chapitre 3 :
Le choix d'une représentation intégrale [HL96] comme condition artificielle exacte induit des difficultés numériques majeures : perte des propriétés classiques du système discret (ajout d'une contribution non symétrique et dense à un système initialement creux et symétrique), introduction des opérateurs intégraux dans la formulation. L'impact numérique de l'utilisation de la représentation intégrale pour la résolution des équations de Maxwell a été analysé dans le cadre d'une formulation éléments finis et dans le cadre d'une formulation variationnelle ultra-faible (UWVF pour "ultra-weak variational formulation").

La UWVF [Ces96, CD03] est une alternative aux éléments finis qui combine des idées des méthodes de décomposition de domaine et d'éléments finis enrichis. La méthode a inspiré Peter Monk et co-auteurs [HMK02, HKM04, HMM07]. Avec Peter Monk, nous avons analysé l'impact de l'application d'une représentation intégrale à la UWVF [DM07, Dar08, DM12]. La section 3.2 présente l'algorithme de résolution établi et donne des résultats numériques permettant d'évaluer le gain engendré par l'usage de la représentation intégrale (figures 3.2 à 3.5).

L'application de la représentation intégrale dans le cadre d'une approche éléments finis est considérée dans la section 3.3 où le modèle standard [LJ01] est justifié comme une méthode de Schwarz avec recouvrement, ce qui inspire un préconditionneur pour l'utilisation de solveurs itératifs de type Krylov [DGR14, Rai14, DGRon]. Avec Nabil Gmati et Rania Rais, nous avons justifié un algorithme de résolution de type Krylov comme alternative à l'algorithme de type point fixe proposé par [LJ01]. L'implémentation de cette approche par le développement de nouveaux intégrands dans MÉLINA++ a permis d'illustrer numériquement la vitesse de convergence superlinéaire du GMRES, un solveur de Krylov (figure 3.10).

⋆ **Traitement des singularités :** Les opérateurs intégraux sont faiblement singuliers, singuliers ou même fortement singuliers pour certains d'entre eux. L'évaluation de la forme discrète de ces opérateurs requiert une attention toute particulière et correspond toujours à une difficulté majeure de mise en œuvre numérique de la résolution des équations intégrales. Des solutions numériques existent [SS11] mais conduisent à un coût de calcul élevé. Des expressions analytiques sont proposées [LS12] mais sont non génériques et difficiles à établir. Le dernier chapitre est dédié au traitement des singularités.

Résumé du chapitre 4 :
Le traitement des singularités est requis dans chacune des applications précédemment présentées des formulations intégrales. La stratégie utilisée dans le cadre de ces applications est basée sur des changements de variables singuliers impliquant la transformation de Duffy [Duf82]. Le cas des opérateurs surfaciques est décrit explicitement dans la section 4.2 et est traité selon une méthode développée par Jean Gay, ingénieur retraité du CEA-CESTA, méthode essentiellement décrite dans des thèses de l'université de Bordeaux I ([Lec97, Lan95, Dar02a]). Le cas des opérateurs intégraux volumiques est traité selon une méthode que j'ai élaborée sur le modèle de celle pour le cas surfacique. La mise en œuvre numérique a été réalisée avec la participation

d'El-Hadji Koné pendant sa thèse à l'université de Rennes 1 et les détails de la méthode sont visibles dans [Kon10].

La méthode retenue dans nos travaux s'apparente à celle présentée dans [SS11], avec des différences sur les cas les plus singuliers. D'autre part, des solutions analytiques sont développées autour de Marc Lenoir [LS12]. Dans le cadre de sa thèse avec Marc Lenoir, Nicolas Salles m'a rendu visite à l'IRMAR à plusieurs reprises afin d'implémenter leurs expressions analytiques dans la librairie éléments finis MÉLINA++ [Sal13]. De récents travaux par Francisco Javier Sayas et co-auteurs [DLS14b, DLS14a, DLSon] offrent, dans le cas bi-dimensionnel, des méthodes numériques très peu coûteuses. L'ensemble de ces solutions méritent d'être comparées ou combinées.

Ces travaux ont systématiquement été menés avec un important travail de programmation numérique dans le cadre du développement de bibliothèques de calcul numérique open-source : FastMMLib [DLnt] (une bibliothèque numérique générique de méthodes rapides), MÉLINA++ [MDL14] (bibliothèque numérique éléments finis), XLiFE++ [KLss] (bibliothèque numérique d'éléments finis étendue), le projet d'une bibliothèque numérique du traitement des singularités.

Par de nombreuses applications de la méthode multipôle rapide (voir les chapitres 1 et 3) avec différents noyaux (potentiel de Coulomb, solution fondamentale de Helmholtz, et leurs dérivées), dans différentes configurations (dynamique moléculaire, équations intégrales, représentations intégrales), combinées ou non à d'autres outils numériques (préconditionneurs, discrétisation microlocale), j'ai acquis une expertise qui me permet aujourd'hui de diriger le développement d'une bibliothèque numérique de méthodes rapides : FastMMLib [DLnt]. L'originalité et l'intérêt de la bibliothèque résident dans l'aspect générique selon lequel sont définies les méthodes rapides implémentées. La bibliothèque permettra de traiter de nombreuses applications selon un canevas générique et sera utilisable par tout code de résolution d'équation intégrale ou de résolution de problèmes denses de même catégorie.

La bibliothèque libre MÉLINA++ [MDL14], principalement développée par Daniel Martin à l'IRMAR, Université de Rennes 1, est une bibliothèque éléments finis initialement dédiée à la résolution des équations aux dérivées partielles elliptiques. Avec Daniel Martin, nous avons intégré les opérateurs intégraux de surface dans la bibliothèque de sorte que MÉLINA++ puisse résoudre les équations intégrales. Rapidement, nous avons validé ce travail par la résolution des équations intégrales de Després [DM09] (voir la section 1.2 pour des détails sur ces équations) et l'avons utilisé pour l'étude du préconditionneur OSRC (voir la section 1.3). Par la suite, nous avons implémenté les opérateurs intégraux de volume (chapitre 2) dans MÉLINA++ avec la participation d'El-Hadji Koné dans le cadre de sa thèse. L'ingrédient essentiel de la mise en œuvre de ces opérateurs est le traitement des singularités (voir chapitre 4). Pour cela, dans le cas volumique, nous avons adapté la stratégie implémentée dans le cas surfacique (detaillée dans le chapitre 4) que j'avais expérimentée lors de ma première mise en œuvre des équations intégrales de Després (résultats numériques relatifs dans la section 1.2). La plus récente contribution à MÉLINA++ concerne l'intégration des opérateurs relatifs aux représentations intégrales comme conditions au bord exactes pour la résolution d'équations aux dérivées partielles en domaine extérieur. Avec le soutien de Daniel Martin et Yvon Lafranche, Rania Rais, dans le cadre de sa thèse, et moi-même avons ajouté de nombreux intégrands dans la bibliothèque de sorte à pouvoir résoudre les équations de Maxwell dans des configurations complexes (voir la section 3.3). La difficulté majeure consistait à valider les nombreux outils numériques combinés pour la résolution de ces équations.

Suite au départ à la retraite de Daniel Martin, la bibliothèque MÉLINA++ est maintenue par Yvon Lafranche et moi-même mais nous n'y apportons plus de nouveaux développements. Un nouveau projet, la bibliothèque libre XLiFE++ [KLss], a récemment été initié par Éric Lunéville de l'ENSTA-ParisTech. La bibliothèque dérive de MÉLINA++ et a pour objectif principal de permettre un élargissement des champs d'application. XLiFE++ est développée dans le cadre d'un projet ANR avec des partenaires industriels. Yvon Lafranche et moi-même contribuons à son développement.

Les résolutions d'équations intégrales proposées dans ce document (sections 1.2, 1.3, chapitre 2) nécessitent le traitement des singularités. Comme indiqué précédemment, la méthode numérique implémentée dans MÉLINA++ (section 4.2) a rendu possible la résolution d'équations intégrales avec cette bibliothèque mais d'autres techniques, numériques ou analytiques, existent et méritent d'être considérées (see Section 4.3). J'ai de ce fait le projet d'une bibliothèque libre de méthodes de traitement de singularités, à l'image de la bibliothèque FastMMLib.

Introduction (English version)

Integral operators, singular kernels, fast methods: Mathematical tools for the numerical resolution of large dense problems

Physical, biological, chemical modelizations usually lead to very challenging mathematical equations. N-body problems, molecular dynamics, wave propagation in exterior domain are applications which are modelized by systems the resolution of which is extremely challenging either due to the size or the sensitive mathematical properties of the involved operators. The wave propagation in exterior domain, the leading application of this document, is a physical phenomenon which is present in many applications: radar detection, communication, driving assistance, imaging, medical treatments of cancers, ... However the simulation of this phenomenon has always been a difficult issue: one has to deal with the unbounded character of the domain and many different mathematical and numerical strategies have been developed and studied. Due to the physical parameters of the applications, any strategy has its own limitations and requires improvements in different directions. Combinations are often considered. In this document, we essentially evoke surface and volume integral operators which are ingredients of two different approaches: integral representation in the framework of a differential approach or integral equations. Such operators have particularities which make difficult the numerical resolution: they are global operators, singular and generally lead to bad conditioned systems. To overcome the global character of integral operators, the use of fast methods is essential at high-frequency regime. Panel Clustering [HN89, Sau00], Fast Multipole Methods [GR88, CRW93, SC95, Dar00a], fast high order solver [BK01b, BK01a], H-matrices and Adaptive Cross Approximation [Hac99, BGH06, Beb08] were developed to speed up the resolution of large-size dense systems related to Green kernels. Different preconditioners or well conditioned formulations [BC00, CN02, BET12, AD07, ABL07] have been studied in literature. Specific quadrature formulae or analytical calculation address solutions for the treatment of the singularities [LS12, SS11, DLS14a, DLSon, DLS14b].

The work presented in this document concerns mathematical concepts elaborated in order to improve the efficiency and robustness of the numerical strategies considered for the resolution of large-size problems such as integral equations for wave propagation in exterior domains. Four main subjects are tackled in this collection. All of them contributed to the development and the implementation of new algorithms for the resolution of large dense problems. Each one of them corresponds to a chapter of the document:

- ⋆ **FMM – a numerical solution to deal with the dense character of discrete integral equations**: Initially designed for the fast evaluation of Coulomb potentials in the study of N-body problems, the Fast Multipole Method (FMM) [GR88, GR97] has quickly been applied to the integral operators involved in integral formulations of Laplace equation.

Then the method has been adapted to wave propagation problems [CJL+97, Dar00a, Dar00b, KSC99, Rah96]. The FMM is used in a specific operation of the numerical resolution. This enables one to combine the method with different tools such as preconditioners and to apply the method in any formulation involving integral operators, Green kernels or Coulomb potentials. The next chapter exhibits the application of the Fast Multipole Method in four different configurations: combination to a microlocal discretization within the context of Després's integral equations [Dar02b, BDMN03]; combination to an analytical preconditioner based on On Surface Radiation Condition (OSRC) [DDL13]; a regularized version of FMM for Hamiltonian systems [CDF10]; application to integral representation for the Ultra-Weak Variational Formulation [Dar08].

⋆ **Mathematical and numerical analysis of the volume integral operators**: Even if the volume integral operators are often used by physicists [KM00, Lu03, Bot06, SSVVA06, BS06, Rah00, SF11], the mathematical literature on these operators is rather poor. A mathematical framework was proposed in [Kir07, KL09], some mathematical and spectral properties were investigated in [FP84]. Our contribution has complemented existence and uniqueness results, mapping properties and spectral properties with the aim to mathematically analyze and implement different numerical resolution algorithms. Chapter 2 is devoted to mathematical properties of volume integral operators derived within the PhD theses of El-Hadji Koné and Hamdi Sakly [CDK10, Kon10, CDS12, Sak14, CDSonb, CDSona]. We firstly present results on existence and uniqueness for the electric and magnetic volume integral equations. Then, spectral properties of both operators are given in the case of wave propagation around either smooth or Lipschitz domains.

⋆ **Analysis of the integral representation as an exact artificial boundary condition**: To deal with the exterior wave propagation problem, one can choose the use of a volume differential formulation written on a bounded domain delimited by the domain and an artificial boundary which simulates the behavior at infinity. An integral representation offers an exact artificial boundary condition. Such application of integral operators was proposed in [JL77, HL96] and have aroused some interest [LJ01, BBFGJ05]. In Chapter 3, we examine the consideration of such application of integral representations in the framework of differential formulations of wave propagation problems. First of all, the impact of this approach is evaluated with the Ultra-Weak Variational Formulation [DM07, DM12]. A second study consists in a mathematical justification of the coupling of integral representation and finite elements. Within the PhD thesis of Rania Rais, this work shows the relevance of such a combination and suggests a preconditioner for the use of Krylov solvers [DGR14, Rai14, DGRon].

⋆ **Treatment of the singularities of the integral operators**: Integral equations and integral representations involve weakly singular, singular or strongly singular operators. The evaluation of the discrete form of these operators require some attention and is still a difficult issue to deal with: numerical approaches lead to costly calculus [SS11] and analytical expressions are non generic and difficult to establish [LS12]. Last chapter is dedicated to the treatment of the singularities: 3D numerical solutions based on Duffy transformation are well known [SS11], analytical solutions are under development [LS12], new numerical tools are derived in 2D by Sayas et al [DLS14b, DLS14a, DLSon]. A library of integration of singular operators would help for comparisons and development of efficient algorithms.

All this work has always been done with a large amount of programming activity, contributing to the development of open-source libraries: FastMMLib [DLnt] (a generic fast methods library), MÉLINA++ [MDL14] (finite element library), XLiFE++ [KLss] (extended finite element library), the project of a library on the treatment of the singularities of integral operators.

Through the different applications of the Fast Multipole Method (see Chapters 1, 2 and 3) with different kernels (Coulomb potential, Helmholtz fundamental solution, and derivatives) in different configurations (molecular dynamics, integral equations, integral representation), by itself or combined to other numerical tools (preconditioners, microlocal discretization), I acquired a strong expertise on the method such that I can manage the development of a library of fast methods: FastMMLib [DLnt]. The essential and original quality of the library is the generic form chosen to define the implemented algorithms. The library will be able to deal with different applications using a generic framework and will be usable by any code which aims to solve integral equations or comparable large dense problems.

The open-source library MÉLINA++ [MDL14], initiated essentially by Daniel Martin at IRMAR, Université de Rennes 1, is a finite element library initially oriented to the resolution of elliptic partial derivative equations (PDE). With Daniel Martin, we integrated the surface integral operators in the library such that MÉLINA++ could solve integral equations. We quickly validated the integration by solving Després's integral equations (see Section 1.2 for details on these equations) with MÉLINA++ [DM09] and used it to test the OSRC preconditioning technique (see Section 1.3). We implemented the volume integral operators (Chapter 2) in MÉLINA++ with the contribution of El-Hadji Koné in the context of his PhD thesis. An essential ingredient of these operators is the treatment of the singularities (see Chapter 4): for the volume case, we adapted the strategy implemented for the surface case (detailed in Chapter 4) that I experimented in my very first programming of Després's integral equations (numerical results in Section 1.2). The latest contribution to MÉLINA++ was the integration of the operators related to integral representations as artificial boundaries for the resolution of PDE in exterior domains. In the context of the PhD thesis of Rania Rais, with Daniel Martin and Yvon Lafranche, Rania Rais and myself implemented numerous new integrands in the library in order to solve Maxwell equations in complicated configurations (see Section 3.3). The inherent difficulty was the validation of numerous numerical tools specific to Maxwell equations and put all together.

Due to the departure of Daniel Martin after he retired, the library MÉLINA++ is maintained by Yvon Lafranche and myself but not developed anymore toward applications not yet reachable by the library. A new project, the open-source library XLiFE++ [KLss] was recently initiated at ENSTA-ParisTech, by Éric Lunéville. The library is derived from MÉLINA++ and aims to be more generic and to enlarge the range of applications. XLiFE++ is developed in the framework of an ANR-project with industrial partners. Yvon Lafranche and myself are involved in the development of this new library.

All the resolutions of integral equations considered in the document (Sections 1.2, 1.3, Chapter 2) require the treatment of the singularities. As already mentioned just above, the numerical technique which was integrated in the library MÉLINA++ (Section 4.2) was a successful tool which made possible the resolution of integral equations with MÉLINA++ but other techniques either numerical or analytical have to be considered (see Section 4.3). I have in mind the project of a generic library dedicated to the treatment of the singularities.

Chapter 1

Fast methods for integral equations and dense linear systems

1.1 Introduction

Similar dense systems arise from the discretization of integral equations or molecular dynamics. In the first case, the dense matrix components are essentially characterized by the Green kernel. In molecular dynamics, the matrix components are defined by a Coulomb interaction. The Fast Multipole Method (FMM) speeds up the calculation of matrix-vector products. The FMM strategy is essentially based on a choice of an expansion of the interaction function which defines the matrix. This is done through a distribution of the interacting particles (either finite element degrees of freedom or molecular particles) into boxes such that the interactions between the particles are replaced by interactions between boxes. The method was initially introduced by Rokhlin et al (e.g. [CRW93]) for N-body problems and was adapted to integral equations of wave propagation in the 90's (e.g. [CJL+97], [Dar00a], [Dar00b], [KSC99], [Rah96]).

More precisely, the FMM splits partially the interactions between both the column and row entries of the matrices. This is done thanks to a separation of variables x and y in the interaction function, either a Green kernel or Coulomb potential $G(x, y)$: the particles are contained in boxes (called FMM boxes – see Figure 1.1), and the interaction between two particles is replaced by a succession of translations through the centers of the boxes that contain these particles. In a single-level FMM (SLFMM), only boxes of a same size, of a same level of an oc-tree, are considered. In a multilevel FMM (MLFMM), boxes from different levels are involved. The FMM strategy is illustrated in Figure 1.2. The main ingredient of a FMM approximation is the choice of the expansion of the interaction function:

$$G(x,y) \approx \sum_{p=1}^{S} c_p \, g_{x,B}^{(p)} \sum_{\tilde{p}=1}^{\widetilde{S}} \mathcal{T}_{B,\widetilde{B}}^{(p,\tilde{p})} \, f_{y,\widetilde{B}}^{(p,\tilde{p})}, \tag{1.1}$$

where

- S and $\widetilde{S}$ are usually truncation or discretization parameters;
- c_p depends only on p;
- $f_{y,\widetilde{B}}^{(p,\tilde{p})}$ does not depend on x; this quantity is named *far moment*;

⋆ $\mathcal{T}_{B,\widetilde{B}}^{(p,\tilde{p})}$ does not depend on x or y but on the boxes B and $\widetilde{B}$ which contain respectively x and y; this quantity is named *translation operator*;

⋆ $g_{x,B}^{(p)}$ does not depend on y; this quantity is named *local moment*.

The success of the method occurs when the parameters S and $\widetilde{S}$ are negligeable compared to the number of particles in the discrete problem.

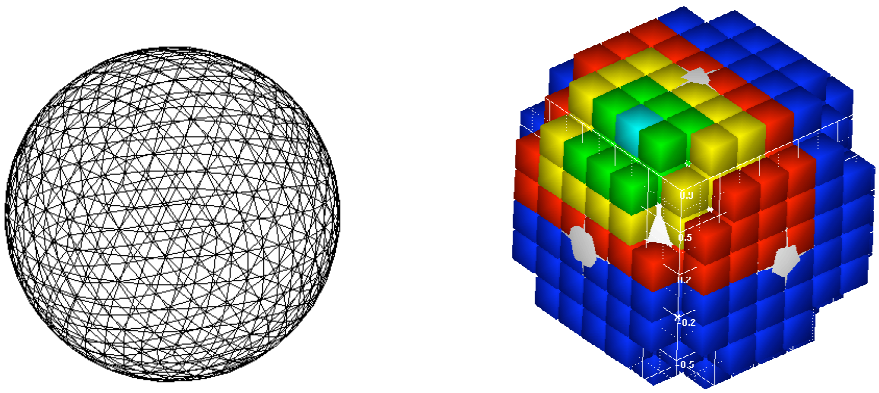

Figure 1.1. FMM boxes: a mesh or set of particles (left) and corresponding FMM boxes (right)

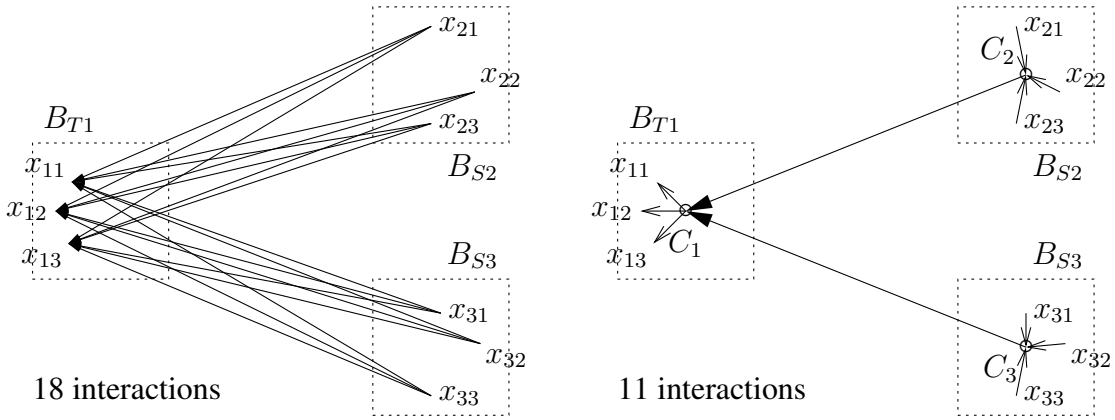

Figure 1.2. (*generated with Fig4TeX* [Laf11]) FMM strategy: without FMM (left), with FMM (right)

In this chapter, we consider the application of the FMM to different configurations

⋆ In the context of my PhD work at the university of Bordeaux I and CEA-CESTA, with Katherine Mer-Nkonga and Alain Bachelot, we combined a Microlocal Discretization and FMM for the resolution of Després integral equation for Helmholtz and Maxwell exterior problems. This application was quite original in the sense that the FMM was used to compute a matrix (see Section 1.2).

- ⋆ With Marion Darbas and Yvon Lafranche, in the framework of the ANR project Microwave, we combined the FMM and an analytical preconditioner. The results obtained for Helmholtz equation were significantly impressive and are very promising (see Section 1.3).
- ⋆ In the context of a 2-years period at INRIA-Rennes, with Philippe Chartier and Erwan Faou, we investigated a regularized version of the FMM for the integration of Hamiltonian systems where the regularity of the potential is of great importance (see Section 1.4).
- ⋆ With Peter Monk, in the context of my postdoc position at the university of Delaware, we implemented an integral representation and the FMM for the ultra-weak variational formulation. This formulation is an alternative to the finite elements which combines, in its original form, ideas of domain decomposition and plane-wave enriched finite elements. The application of the FMM reveals the interest of such a use of integral representation (see Section 1.5).

1.1.1 FMM expansion for the Helmholtz fundamental solution

In order to reduce the computational cost related to the integral operators, the FMM splits partially the interactions between both the column and row entries of the matrices obtained after discretization. In this document, the FMM that we consider is based on the Gegenbauer series and Funk-Hecke formula ([CJL+97], [Dar00a]). For instance, let us consider the matrix $[L]$

$$[L]_{i\,j} = \int_\Gamma \int_\Gamma G(x,y)\varphi_j(y)\varphi_i(x)d\gamma(y)d\gamma(x), \qquad \forall i,j$$

where G is the Helmholtz fundamental solution, $G(x,y) = \frac{e^{ik\|x-y\|}}{4\pi\|x-y\|}$, k the wavenumber, and $(\varphi_i)_i$ a set of finite element basis fonctions. An efficient calculation of the matrix-vector product $[L]\mathbf{X}$ can be expressed thanks to such an expansion for i far from j:

$$[L]_{i\,j} \approx \sum_{p=1}^{S} c_p \sum_{B/B\cap \mathrm{supp}\varphi_i \neq \emptyset} g_{i,B}^{(p)} \sum_{\widetilde{B}/\widetilde{B}\cap \mathrm{supp}\varphi_j \neq \emptyset} \mathcal{T}_{B,\widetilde{B}}^{(p)}\, f_{j,\widetilde{B}}^{(p)},$$

with

$$c_p = \frac{ik}{(4\pi)^2} w_p\,,$$

$$g_{i,B}^{(p)} = \int_{B\cap \mathrm{supp}\varphi_i} e^{ik<s_p, x-C_B>}\varphi_i(x)d\gamma(x)\,,$$

$$f_{j,\widetilde{B}}^{(p)} = \int_{\widetilde{B}\cap \mathrm{supp}\varphi_j} e^{-ik<s_p, y-C_{\widetilde{B}}>}\varphi_j(y)d\gamma(y)\,,$$

and $\mathcal{T}_{B,\widetilde{B}}^{(p)}$ is the translation operator from the FMM box $\widetilde{B}$ to the FMM box B given by the expression

$$\mathcal{T}_{B,\widetilde{B}}^{(p)} = \sum_{\ell=0}^{L} (-i)^\ell (2\ell+1) h_\ell^{(1)}(k|C_B - C_{\widetilde{B}}|) P_\ell(\cos(s_p, C_B - C_{\widetilde{B}})), \tag{1.2}$$

where w_p, s_p are the quadrature weights and points for the integration on the unit sphere involved in the Funk-Hecke formula. The summation "$\sum_{p=1}^{S}$" comes from the discretization of the Funk-Hecke formula while the summation "$\sum_{\ell=0}^{L}$" is a truncation of the Gegenbauer series. Moreover, C_B denotes the center of the FMM box B, $h_\ell^{(1)}$ is the spherical Hankel function of the first kind of degree ℓ, and P_ℓ is the Legendre polynomial of degree ℓ. The parameters L and S are estimated thanks to the empirical formula ([KSC99]) $L = kd + C(kd)^3$, and the choice of the discretization of the unit sphere such that $S = (L+1)(2L+1)$, where d is the diameter of the FMM boxes.

1.1.2 FMM expansion for the Coulomb potential

The FMM approximation is based on the expansions given by the following results:

Result 1 (Multipole expansion): Assume that J source points $\{x_{j_1}, ..., x_{j_J}\}$ are contained in a box B_{src} of center C_{src} and of radius r. Let us denote by $(\rho_{j_p}, \theta_{j_p}, \phi_{j_p})$ the spherical coordinates of $(x_{j_p} - C_{src})$. Then for any x_i such that $\|x_i - C_{src}\|_2 > r$, denoting the spherical coordinates of $(x_i - C_{src})$ by $(\rho_{is}, \theta_{is}, \phi_{is})$, we have the expansion

$$\sum_{p=1}^{J} \frac{1}{\left\|x_i - x_{j_p}\right\|} q_{j_p} = \sum_{n=0}^{\infty} \sum_{m=-n}^{n} \frac{M_n^m}{\rho_{is}^{n+1}} Y_n^m(\theta_{is}, \phi_{is}) \,, \tag{1.3}$$

with

$$M_n^m = \sum_{p=1}^{J} q_{j_p} \rho_{j_p}^n Y_n^{-m}(\theta_{j_p}, \phi_{j_p}) \,,$$

and Y_n^m a spherical harmonic. The corresponding error estimate is

$$\left| \sum_{p=1}^{J} \frac{1}{\left\|x_i - x_{j_p}\right\|} q_{j_p} - \sum_{n=0}^{L} \sum_{m=-n}^{n} \frac{M_n^m}{\rho_{is}^{n+1}} Y_n^m(\theta_{is}, \phi_{is}) \right| \leq \frac{\sum_{p=1}^{J} \left|q_{j_p}\right|}{\rho_{is} - r} \left(\frac{r}{\rho_{is}}\right)^{L+1} . \tag{1.4}$$

Result 2 (Conversion of a multipole expansion to a local expansion): Consider the J source points defined for Result 1. Let us consider that the target point x_i is contained in a box B_{trg} of center C_{trg} and radius r. Denoting by $(\rho_{st}, \theta_{st}, \phi_{st})$ the spherical coordinates of $(C_{src} - C_{trg})$ and by $(\rho_i, \theta_i, \phi_i)$ the spherical coordinates of $(x_i - C_{trg})$, under the condition that $\rho_{st} = \|C_{trg} - C_{src}\| > 2r$, the expansion given by (1.3) can be written

$$\sum_{p=1}^{J} \frac{1}{\left\|x_i - x_{j_p}\right\|} q_{j_p} = \sum_{l=0}^{\infty} \sum_{k=-l}^{l} L_l^k \rho_i^l Y_l^k(\theta_i, \phi_i) \,, \tag{1.5}$$

with the translation operation

$$L_l^k = \sum_{n=0}^{\infty} \sum_{m=-n}^{n} \frac{M_n^m i^{|k-m|-|k|-|m|} A_n^m A_l^k Y_{l+n}^{m-k}(\theta_{st}, \phi_{st})}{(-1)^n A_{l+n}^{m-k} \rho_{st}^{l+n+1}} \,, \tag{1.6}$$

and

$$A_n^m = \frac{(-1)^n}{\sqrt{(n-m)!(n+m)!}} \,.$$

We denote by $\mathcal{T}_{B_{trg}\,B_{src}}$ the translation operator which maps $(M_n^m)_{m,n}$ onto $(L_l^k)_{l,k}$ and write

$$(L_l^k)_{l,k} = \mathcal{T}_{B_{trg}\,B_{src}}((M_n^m)_{m,n})\,. \tag{1.7}$$

The corresponding error estimate is

$$\left|\sum_{p=1}^{J} \frac{1}{\left\|x_i - x_{j_p}\right\|} q_{j_p} - \sum_{l=0}^{L}\sum_{k=-l}^{l} L_l^k \rho_i^l Y_l^k(\theta_i,\phi_i)\right| \leq \frac{\sum_{p=1}^{J}\left|q_{j_p}\right|}{cr-r}\left(\frac{1}{c}\right)^{L+1}, \tag{1.8}$$

with c satisfying $\rho_{st} > (c+1)r$.

The spherical harmonics are given from the associate Legendre functions P_n^m:

$$Y_n^m(\theta,\phi) = \sqrt{\frac{(n-|m|)!}{(n+|m|)!}} P_n^{|m|}(\cos\theta) e^{im\phi}. \tag{1.9}$$

The associate Legendre functions can be evaluated recursively thanks to the relations

$$\left\{\begin{array}{l} \left.\begin{array}{l} P_k^k(\cos\theta) = \frac{(2k)!}{2^k k!}(-\sin\theta)^k \\ P_{k+1}^k(\cos\theta) = (2k+1)\ \cos\theta\ P_k^k(\cos\theta) \end{array}\right\} \quad \forall k \geq 0, \\ \\ (l-k)P_l^k(\cos\theta) = (2l-1)\cos\theta P_{l-1}^k(\cos\theta) - (l+k-1)P_{l-2}^k(\cos\theta) \\ \qquad\qquad \forall l,k\ /\ 0 \leq k \leq l-2 \end{array}\right. \tag{1.10}$$

The derivation of the previous results is given in [GR88] and [GR97]. The definition of the special functions involved in those expansions and further details about their properties can be found in [AS72].

1.2 Combination of Fast Multipole Method and Microlocal Discretization for Després's integral equations

B. Després has written a well-conditioned surface integral formulation of Helmholtz and Maxwell equations posed on the exterior domain. The formulation is initially based on a Lagrange multiplier approach ([Des97], [SD99], [Stu01]) but can be established by rather simple algebraic combinations of more usual integral formulations [BC00]. We hereby focus on a combination of Fast Multipole Method and Microlocal Discretization for the resolution of Després's integral equations. For the sake of simplicity, we present the case of Helmholtz equation [Dar02b] but the work has been extended to the case of Maxwell equations [BDMN03].

In this study, we consider the Microlocal Discretization introduced by T. Abboud, J.-C. Nédélec, B. Zhou [ANZ94], [ANZ95], [Zho95]. The method consists in approximating the phase of the unknown using the geometrical optics method. Consequently, the oscillation of the new unknown is reduced. We can then consider a numerical approximation with a number of degrees of freedom N_d clearly less according to the wavenumber κ. Indeed, in the classical case we have $N_d \sim \kappa^2$, while $N_d \sim \kappa^{2/3}$ after approximation of the phase. Nevertheless, the discretization of the geometry implies to consider $\mathcal{O}(N)$ elements, with $N \sim \kappa^2$, on the surface of the obstacle. Then, the calculation of the matrices of the system needs $\mathcal{O}(N^2)$ operations

with $N \sim \kappa^2$, as in the classical discretizations. Thus, the authors of the method suggested the use of the theory of the stationary phase in order to accelerate the calculation of the matrices ([ANZ95]-[Hör83]). However, this theory does not enable one to have a good estimate of the CPU time needed for a good accuracy, and the extension to the 3-D case implies difficulties not yet solved. In [Dar02b], we have considered the Fast Multipole Method to calculate the reduced-size matrices of the system induced by the Microlocal Discretization in the context of Després's integral formulation.

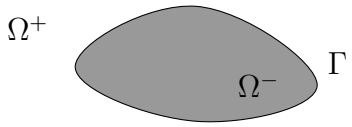

Figure 1.3. (*generated with Fig4TeX* [Laf11]) the exterior unbounded domain Ω^+

In this section, we are concerned with the resolution of the Helmholtz equation with Robin boundary condition (a general impedance boundary condition is considered in [Dar02b]).

$$\left\{ \begin{array}{ll} \Delta u + \kappa^2 u = 0 \ , & \text{in } \Omega^+ \ , \\ \dfrac{\partial u}{\partial n}|_\Gamma + i\kappa u|_\Gamma = g \ , & \text{on } \Gamma \ , \\ \lim\limits_{r\to+\infty} r\left(\dfrac{\partial u}{\partial r} - i\kappa u\right) = 0 \ , & \end{array} \right. \tag{1.11}$$

where Ω^- is a regular bounded domain of $\mathbb{R}^3$, of boundary Γ, and $\Omega^+ = \mathbb{R}^3 \backslash \overline{\Omega^-}$ (Fig. 1.3). g is given as a function of the incident wave. The unit normal n is directed to the exterior domain.

Let us introduce the surface unknowns $q = \kappa u|_\Gamma$, $p = \dfrac{\partial u}{\partial n}|_\Gamma$, and the single and double layer potentials and derivatives S, K, K' and D defined for all x on Γ by

$$\begin{array}{ll} Sp(x) = \displaystyle\int_\Gamma G(x,y)\, p(y)\, d\gamma(y) \ , & Dq(x) = \displaystyle\int_\Gamma \frac{\partial^2 G}{\partial n_x \partial n_y}(x,y)\, q(y)\, d\gamma(y) \ , \\ Kq(x) = \displaystyle\int_\Gamma \frac{\partial G}{\partial n_y}(x,y)\, q(y)\, d\gamma(y) \ , & K'p(x) = \displaystyle\int_\Gamma \frac{\partial G}{\partial n_x}(x,y)\, p(y)\, d\gamma(y) \ . \end{array} \tag{1.12}$$

with $G(x,y) = \dfrac{e^{i\kappa|x-y|}}{4\pi|x-y|}$. The Després's integral formulation uses a plit of the Green kernel G into a regular part $G_i(x,y) = \dfrac{\sin(\kappa|x-y|)}{4\pi|x-y|}$ and a singular part $G_r(x,y) = \dfrac{\cos(\kappa|x-y|)}{4\pi|x-y|}$. Following this decomposition, the operators read

$$S = S_r + iS_i \ , \quad K = K_r + iK_i \ , \quad K' = K'_r + iK'_i \ , \quad D = D_r + iD_i$$

where S_r, K_r, K'_r, D_r, S_i, K_i, K'_i and D_i are real operators.

Finally, we introduce the notations

$$\mathbf{K} = \begin{bmatrix} \frac{1}{\kappa} D_r & -K_r' - \frac{I}{2} \\ -K_r + \frac{I}{2} & \kappa S_r \end{bmatrix} \quad \text{and} \quad \mathbf{M} = \begin{bmatrix} \frac{1}{\kappa} D_i & -K_i' \\ -K_i & \kappa S_i \end{bmatrix} ,$$

and the far field operator defined for all p, q in $L^2(\Gamma)$ and $\hat{s}$ in S^2 by

$$\left(A_\infty \begin{bmatrix} q \\ p \end{bmatrix} \right)(\hat{s}) = \frac{\kappa}{4\pi} \int_\Gamma e^{-i\kappa y \cdot \hat{s}} (p(y) + i(\hat{s} \cdot n_y) q(y)) d\gamma(y) \ . \tag{1.13}$$

Its adjoint is given for all φ in $L^2(S^2)$ by

$$\left(A_\infty^* \varphi\right)(y) = \begin{bmatrix} \frac{-\kappa}{4\pi} \int_{S^2} i(\hat{s} \cdot n_y) e^{i\kappa y \cdot \hat{s}} \varphi(\hat{s}) d\hat{s} \\ \\ \frac{\kappa}{4\pi} \int_{S^2} e^{i\kappa y \cdot \hat{s}} \varphi(\hat{s}) d\hat{s} \end{bmatrix} , \tag{1.14}$$

where $\int_{S^2} . d\hat{s}$ denotes the integral around the unit sphere S^2, such that

$$\mathbf{M} = A_\infty^* A_\infty \ , \tag{1.15}$$

i.e. $\forall p, q \in L^2(\Gamma)$

$$\int_{S^2} A_\infty \begin{bmatrix} q \\ p \end{bmatrix} \cdot \overline{A_\infty \begin{bmatrix} \tilde{q} \\ \tilde{p} \end{bmatrix}} d\hat{s} \ = \ \int_\Gamma (\mathbf{M} \begin{bmatrix} q \\ p \end{bmatrix}) \cdot \overline{\begin{bmatrix} \tilde{q} \\ \tilde{p} \end{bmatrix}} d\gamma \ . \tag{1.16}$$

The Després's integral equations are then written as follows:

$$\begin{cases} X + A_\infty^* A_\infty X - \mathbf{K}^* Y = \tilde{g} \ , \\ \mathbf{K} X + A_\infty^* A_\infty Y = 0 \ , \end{cases} \tag{1.17}$$

where $X = \begin{bmatrix} q \\ p \end{bmatrix}$ and $Y = iX$ the Lagrange multiplier. The theory of the inf-sup condition enables one to check the existence and the uniqueness of X and the existence of Y. In order to gain the uniqueness of Y, B. Després suggested the following modification (see [BC00]), i.e. adding

$$\begin{array}{rl} -\beta X - i\beta Y = 0 & \text{to the first equation} \\ \text{and} \quad -i\beta X + \beta Y = 0 & \text{to the second one,} \end{array} \tag{1.18}$$

$$\begin{cases} (Id - \beta) X + A_\infty^* A_\infty X - \mathbf{K}^* Y - i\beta Y = \tilde{g} \ , \\ (\mathbf{K} - i\beta) X + (\beta + A_\infty^* A_\infty) Y = 0 \ . \end{cases} \tag{1.19}$$

A usual discretization, $\mathbb{P}_1$ Lagrange finite element, would lead to the following system:

$$\begin{cases} X = (\mathcal{D}_{-\beta} + \mathcal{A})^{-1} (F_h + (\mathcal{K}^* + i\mathcal{B}_\beta) Y), \\ ((\mathcal{K} - i\mathcal{B}_\beta)(\mathcal{D}_{-\beta} + \mathcal{A})^{-1} (\mathcal{K}^* + i\mathcal{B}_\beta) + \mathcal{B}_\beta + \mathcal{A}) Y = -(\mathcal{K} - i\mathcal{B}_\beta)(\mathcal{D}_{-\beta} + \mathcal{A})^{-1} F_h, \end{cases} \tag{1.20}$$

with $\mathcal{D}_{-\beta}$, $\mathcal{B}_\beta$, $\mathcal{A}$, $\mathcal{K}$ the matrices resulting respectively from the discretization of the operators $(1 - \beta)I$, βI, $A_\infty^* A_\infty$ and $\mathbf{K}$. Due to the Hermitian property of the positive definite matrix

$((\mathcal{K} - i\mathcal{B}_\beta)(\mathcal{D}_{-\beta} + \mathcal{A})^{-1}(\mathcal{K}^* + i\mathcal{B}_\beta) + \mathcal{B}_\beta + \mathcal{A})$, one can solve the system by using a double conjugate gradient method.

If N denotes the number of degrees of freedom, the matrices $\mathcal{D}_{-\beta}$, $\mathcal{B}_\beta$, $\mathcal{A}$, $\mathcal{K}$ are of size $2N \times 2N$, and involve $N \times N$ matrices of the form

$$[S_r]_{ij} =< S_r\varphi_j, \varphi_i >_{V_h} = \int_{\Gamma_h}\int_{\Gamma_h} G_r(x,y)\,\varphi_i(x)\,\overline{\varphi_j(y)}\,d\gamma(y)\,d\gamma(x) \quad . \tag{1.21}$$

$V_h = \text{Vect}\{\varphi_i \;\; ; \;\; i = 1, ..., N\}$ with φ_i, $i \in \{1, ..., N\}$ the $\mathbb{P}_1$-basis functions associated to the finite element discretization, and Γ_h is the surface defined by the finite element triangulation.

Let us now explain the combination of the Microlocal Discretization and the Fast Multipole Method for the matrix $[S_r]$ defined by (1.21). The same strategy is applied to the entire system. By looking carefully at the matrix $[S_r]$, one can see that the size is highly depending on the wavenumber: $N \times N = \kappa^4$. Moreover, the matrix is dense. The resolution of systems involving such matrices at high frequency is always a difficult issue. Here, we first use the Microlocal Discretization in order to consider a coarser interpolation of the unknown. The idea is based on the integration of the phase of the incident wave into the basis functions. In such a way, we indeed solve a new problem the solution of which is a new unknown with a reduced phase. The new unknown is strongly less oscillating and a theoretical study has shown that the interpolation of the unknown can be done with a number of degrees of freedom of order $\kappa^{2/3}$ instead of κ^2 [ANZ95]. However, for the evaluation of the integral, due to the oscillating Green kernel and new basis functions, one still has to consider the usual discretization for the evaluation of the integrals. To this aim, we consider a coarse mesh Γ_c for the interpolation of the unknown (the basis functions are defined on the nodes of Γ_c), and a fine mesh Γ_f for the geometrical approximations. Let us denote by N_f and N_c the number of nodes of respectively Γ_f and Γ_c ($N_f \sim \kappa^2$ and $N_c \sim \kappa^{2/3}$). In order to make the algorithm easier, the mesh Γ_f is chosen to be a refinement of the mesh Γ_c. We subsequently denote by π the orthogonal projection from the plane triangles of Γ_c to the ones of Γ_f (see Fig. 1.4).

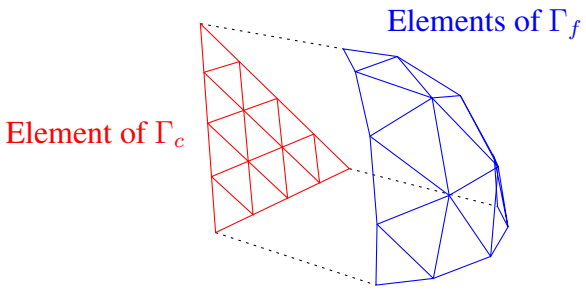

Figure 1.4. (*generated with Fig4TeX* [Laf11]) fine elements of Γ_f obtained from the refinement of a coarse element of Γ_c

We introduce the new basis functions $\widetilde{\varphi}_i = (\varphi_i \circ \pi^{-1})\, e^{i\kappa\phi_0}$ where $i\kappa\phi_0$ is the phase of the incident wave and φ_i, $i \in \{1, ..., N_c\}$ the $\mathbb{P}_1$-basis functions associated to Γ_c.

The matrix $[S_r]$ is now given by

$$\begin{aligned}
[S_r]_{ij} &= \int_{\Gamma_f}\int_{\Gamma_f} G_r(x,y)\,\widetilde{\varphi}_i(x)\,\overline{\widetilde{\varphi}_j(y)}\,d\gamma(y)\,d\gamma(x) \\
&= \sum_{T_k\in\pi(\mathrm{supp}\varphi_i)}\ \sum_{T_l\in\pi(\mathrm{supp}\varphi_j)} \\
&\qquad \int_{T_k}\int_{T_l} G_r(x,y)\,\varphi_i(\pi^{-1}(x))e^{i\kappa\phi_0(x)}\,\overline{\varphi_j(\pi^{-1}(y))e^{i\kappa\phi_0(y)}}\,d\gamma(y)\,d\gamma(x)\quad ,
\end{aligned} \tag{1.22}$$

where $\widetilde{\mathbb{V}}_h = \mathrm{Vect}\{\widetilde{\varphi}_i\ ;\ \ i=1,...,N_c\}$.

This definition shows the term $[S_r]_{ji}$ like a sum of interactions between triangles T_k and T_l satisfying $T_k \in \pi(\mathrm{supp}\varphi_i)$ and $T_l \in \pi(\mathrm{supp}\varphi_j)$. For any degree of freedom i, there is a large amount of triangles T_k satisfying $T_k \in \pi(\mathrm{supp}\varphi_i)$, about $N_f/N_c \sim \kappa^{4/3}$. In the resolution of a system involving such matrices, the difficulty is not the resolution by itself anymore but the calculation of the matrices. In [Dar02b], the Fast Multipole Method is not used to speed up matrix-vector products in the context of a Krylov solver, as usually, but is used to calculate the reduced-size matrices.

Using a kernel expansion of the form (1.1), we get the following approximation of the matrix $[S_r]$

$$\begin{aligned}
[S_r]_{ij} &= \sum_{B/B\cap\pi(\mathrm{supp}\varphi_i)\neq\varnothing}\ \sum_{T_k\in B}\ \sum_{\widetilde{B}/\widetilde{B}\cap\pi(\mathrm{supp}\varphi_j)\neq\varnothing}\ \sum_{T_l\in\widetilde{B}} \\
&\qquad \int_{T_k}\int_{T_l}\sum_{p=1}^{S} c_p\, g_{x,B}^{(p)} \sum_{\tilde{p}=1}^{\widetilde{S}} \mathcal{T}_{B,\widetilde{B}}^{(p,\tilde{p})}\, f_{y,\widetilde{B}}^{(p,\tilde{p})}\,\widetilde{\varphi}_i(x)\,\overline{\widetilde{\varphi}_j(y)}\,d\gamma(y)\,d\gamma(x) \\
&= \sum_{p=1}^{S} c_p \sum_{B/B\cap\pi(\mathrm{supp}\varphi_i)\neq\varnothing}\ \sum_{T_k\in B}\left(\int_{T_k} g_{x,B}^{(p)}\varphi_i(\pi^{-1}(x))e^{i\kappa\phi_0(x)}\,d\gamma(x)\right) \\
&\qquad \sum_{\tilde{p}=1}^{\widetilde{S}}\ \sum_{\widetilde{B}/\widetilde{B}\cap\pi(\mathrm{supp}\varphi_j)\neq\varnothing} \mathcal{T}_{B,\widetilde{B}}^{(p,\tilde{p})}\ \sum_{T_l\in\widetilde{B}}\left(\int_{T_l} f_{y,\widetilde{B}}^{(p,\tilde{p})}\,\overline{\varphi_j(\pi^{-1}(y))e^{i\kappa\phi_0(y)}}\,d\gamma(y)\right)\ .
\end{aligned} \tag{1.23}$$

Using a SLFMM, the new algorithm has the complexity (memory and CPU for "calculation of the matrices + resolution with a direct solver"):

- ⋆ memory: $\mathcal{O}(N_f + N_c^3) \sim \mathcal{O}(N_f)$,
- ⋆ CPU : $\mathcal{O}(N_f^{3/2} + N_c^3) \sim \mathcal{O}(N_f^{3/2})$.

Using a MLFMM, the complexity is:

- ⋆ memory: $\mathcal{O}(N_f + N_c^3) \sim \mathcal{O}(N_f)$,
- ⋆ CPU : $\mathcal{O}(N_f N_c \log N_f + N_c^3) \sim \mathcal{O}(N_f^{4/3}\log N_f)$.

In this configuration, the usual complexity $N_f \log N_f$ of the MLFMM is not reached because the size of the usable boxes is at most the size of the coarse triangles of Γ_c.

Impressive numerical results were obtained for different boundary conditions (Dirichlet, Neumann or Robin condition on Γ) for the unit sphere (see [Dar02b]). In Fig. 1.8 and Fig. 1.7

we plot the RCS obtained with a number of degrees of freedom particularly small: the average length of the elements of the mesh is 1.6λ for the Neumann and Robin cases and 2λ for the Dirichlet case, instead of the classical $\lambda/10$, with λ the wavelength. Fig. 1.5 gives the gain on the CPU and memory requirements on a processor EV67 of a Compaq cluster ES40.

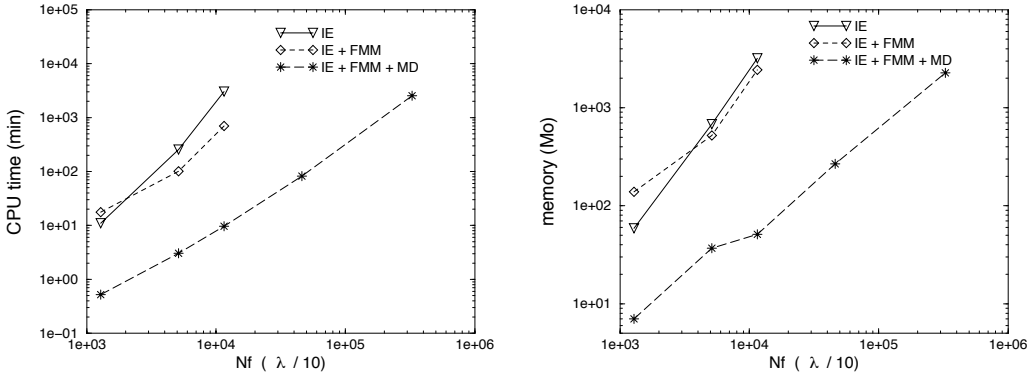

Figure 1.5. CPU time (left) and memory requirements (right)

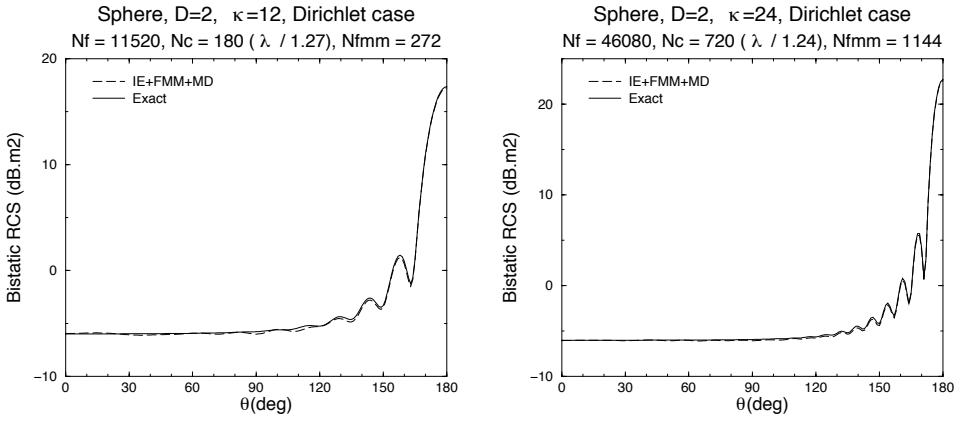

$\kappa = 12$ $\kappa = 24$

Figure 1.6. Dirichlet case, $\kappa = 12$ or 24

An industrial test-case is considered in the paper [Dar02b]. In [BDMN03], we also analyzed the application of the combination to Maxwell equations. The strategy is similar and comparable results are obtained using the MLFMM.

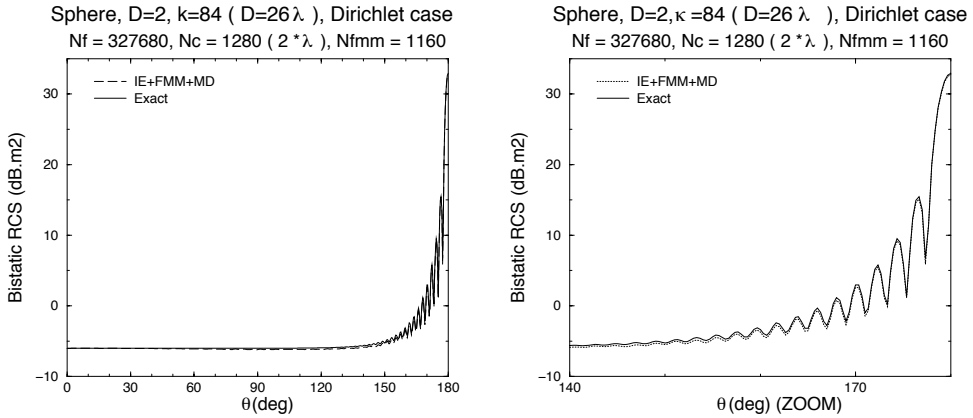

Figure 1.7. Dirichlet case, $D = 26\lambda$, $\kappa = 84$

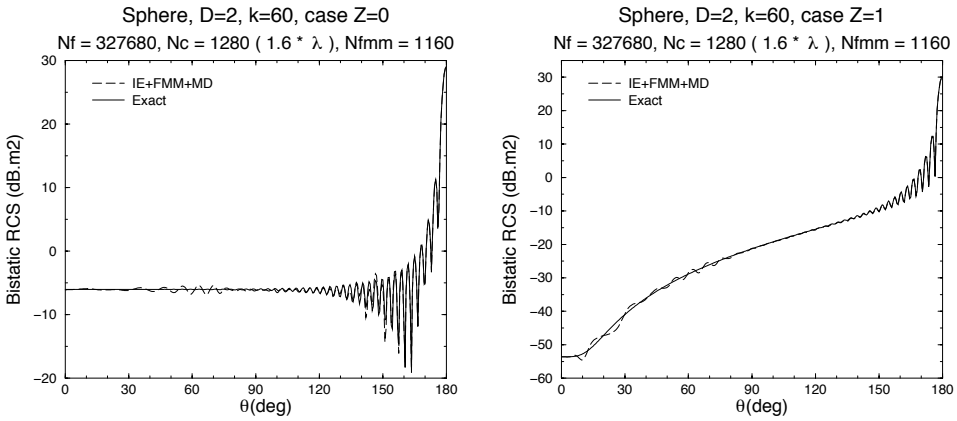

Figure 1.8. Neumann case (left), Robin case (right), $\kappa = 60$

1.3 Analytic preconditioner and Fast Multipole Method

In this section, we focus on the resolution of the Helmholtz equation in exterior domain Ω^+ with Neumann boundary condition on its boundary Γ:

$$\begin{cases} \Delta u + k^2 u = 0, \quad \text{in } \Omega^+, \\ \dfrac{\partial u}{\partial n}|_\Gamma = g = -\dfrac{\partial u^{\text{inc}}}{\partial n}|_\Gamma, \quad \text{on } \Gamma, \\ \lim\limits_{r \to +\infty} r \left(\dfrac{\partial u}{\partial r} - iku \right) = 0, \end{cases} \tag{1.24}$$

where k is the wavenumber and u^{inc} the incident wave. The problem can be solved using a Combined Field Integral Equation (CFIE) involving the integral operators introduced in the previous section. A classical formulation of the CFIE is given in [MH78]. Problem (1.24) can be solved considering the well-known CFIE: find the physical unknown $\varphi = -\gamma_0^+(u - u^{\text{inc}}) \in H^{1/2}(\Gamma)$ solution to

$$\left(\frac{I}{2} - K - \eta D \right) \varphi = -\gamma_0^+ u^{\text{inc}} - \eta \gamma_1^+ u^{\text{inc}}, \quad \text{on } \Gamma, \tag{1.25}$$

with a coupling complex parameter η, K and D the double layer potential and its derivative defined in (1.12), and γ_0^+, γ_1^+ the exterior trace operators of respective orders 0 and 1. Under rather standard conditions on the domain (Lipschitz) and the combination parameter η ($\mathrm{Im}(\eta) \neq 0$), we have existence and uniqueness results [BH05] of the CFIE (1.25) in $H^{1/2}(\Gamma)$ for any wavenumber $k > 0$. However, the equation does not provide an interesting spectral behavior. To expect an eigenvalue clustering and hence a fast convergence of iterative solvers, we adopt the approach of X. Antoine and M. Darbas [AD05, AD07]: composing the operator D with a regularizing operator, the exterior Neumann-to-Dirichlet (NtD) map

$$\begin{array}{rccl} V^{\mathrm{ex}}: & H^{-1/2}(\Gamma) & \to & H^{1/2}(\Gamma) \\ & \gamma_1^+ u & \mapsto & \gamma_0^+ u = V^{\mathrm{ex}} \gamma_1^+ u. \end{array} \tag{1.26}$$

The following integral relations hold: $V^{\mathrm{ex}} D = \frac{I}{2} + K,$ on Γ, and $\frac{I}{2} - K + V^{\mathrm{ex}} D = I,$ on Γ. In this ideal configuration, the solution $\varphi = -\gamma_0^+ u^{\mathrm{inc}} + V^{\mathrm{ex}} \gamma_1^+ u^{\mathrm{inc}} \in H^{1/2}(\Gamma)$ is computed directly. However, as well-known, an expression of the exact NtD is not available for a general surface Γ. Instead, an approximation $\widetilde{V}$ of V^{ex} is introduced to construct the OSRC-preconditioned CFIE: find $\varphi = -\gamma_0^+(u - u^{\mathrm{inc}}) \in H^{1/2}(\Gamma)$ such that

$$\left(\frac{I}{2} - K + \widetilde{V} D\right) \varphi = -\gamma_0^+ u^{\mathrm{inc}} + \widetilde{V} \gamma_1^+ u^{\mathrm{inc}}, \quad \text{on } \Gamma. \tag{1.27}$$

An efficient approximation $\widetilde{V}$ is derived in [ADL06] according to On-Surface Radiation Conditions (OSRC) method [Ant08, ABB99, Jon88, KTU87]

$$\widetilde{V} = \frac{1}{ik} \left(1 + \frac{\Delta_\Gamma}{k_\varepsilon^2}\right)^{-1/2}, \tag{1.28}$$

where Δ_Γ is the Laplace-Beltrami operator over the surface Γ and the parameter $k_\varepsilon = k + i\varepsilon$ is complex-valued. The small damping parameter $\varepsilon \in \mathbb{R}^*$ is introduced to regularize the square-root operator in the transition zone of grazing modes. A suitable choice of ε has been determined in [Dar04]: $\varepsilon = 0.4 k^{1/3} R^{-2/3}$ where R is the radius of the smallest sphere containing Ω. We still have existence and uniqueness of the solution of the OSRC-preconditioned CFIE (1.27) in $H^{1/2}(\Gamma)$ for any wavenumber k and any damping parameter $\varepsilon \neq 0$, under the conditions that Γ is a smooth surface. The OSRC-preconditioned CFIE uses the CFIE integral operators and in addition only some differential operators involved in the OSRC approach. The discretization of the later gives rise to sparse matrices. However, as already mentioned, the discretization of integral operators leads to dense matrices. The operators related to the preconditioner and the integral operators are well separated such that a Krylov resolution of the discretized system involves both the preconditioner and the integral operators in different steps such that

- ⋆ a sparse direct solver is used to apply the OSRC preconditioner,
- ⋆ a Fast Multipole Method can be used to evaluate the dense matrix-vector products related to the integral operators.

In the paper [DDL13] we combine the OSRC preconditioner and a single-level Fast Multipole Method. The application of the OSRC preconditioner requires the evaluation of a square root. Padé approximants localize the square-root operator such that the application of the OSRC preconditioner reduces to the resolution of Helmholtz-type sparse linear systems (we refer to

[DDL13] for more details on this aspect). In order to evaluate efficiently the matrix-vector products related to the discretization of the integral operators, we use the SLFMM introduced in Section 1.1.1. For instance, an efficient calculation of the matrix-vector product with matrix $[L]$ defined by

$$[L]_{ij} = \int_\Gamma \int_\Gamma G(x,y)\varphi_j(y)\varphi_i(x)d\gamma(y)d\gamma(x), \qquad i,j = 1,\cdots,N_V,$$

with G the Helmholtz fundamental solution, can be expressed thanks to such an expansion for i far from j:

$$[L]_{ij} \approx \sum_{p=1}^{P} c_p \sum_{B/B\cap \mathrm{supp}\varphi_i \neq \emptyset} g_{i,B}^{(p)} \sum_{\widetilde{B}/\widetilde{B}\cap \mathrm{supp}\varphi_j \neq \emptyset} \mathcal{T}_{B,\widetilde{B}}^{(p)} f_{j,\widetilde{B}}^{(p)},$$

This leads to an algorithm of complexity which is $N^{3/2}$ for a single-level FMM and $N\log^2 N$ for a multilevel FMM, where N is the number of degrees of Freedom. The chosen expansion, based on the Gegenbauer series and the Funk-Hecke formula leads to a FMM which is known to be unstable at "low-frequency regimes". This occurs for any frequency when the mesh density n_λ is large compared to the usual value $n_\lambda = 10$. This comes from the translation operator $\mathcal{T}_{B,\widetilde{B}}^{(p)}$ which sums Hankel functions (see eq. (1.2)). In the Gegenbauer series, the diverging behavior of the Hankel function is controlled by the converging Bessel function, but the considered FMM expansion separates the Hankel function such that the translation operator (1.2) becomes unstable at low-frequency regimes. In this section, we effectively meet with this issue (cf. Section 1.3.2).

For the numerical results, we have considered several geometries generated using Gmsh [GR09]. First, the unit sphere enables us to validate the code by comparison with the analytical solution. Then, domains with cavity (cube with cubic cavity and sphere with spherical cavity), a cone-sphere and a submarine (Fig. 1.9) offer trapping effects or configurations with singularities. The characteristic length of the cone-sphere and the submarine are respectively $6\times 1\times 1$m and $43\times 7\times 7$m.

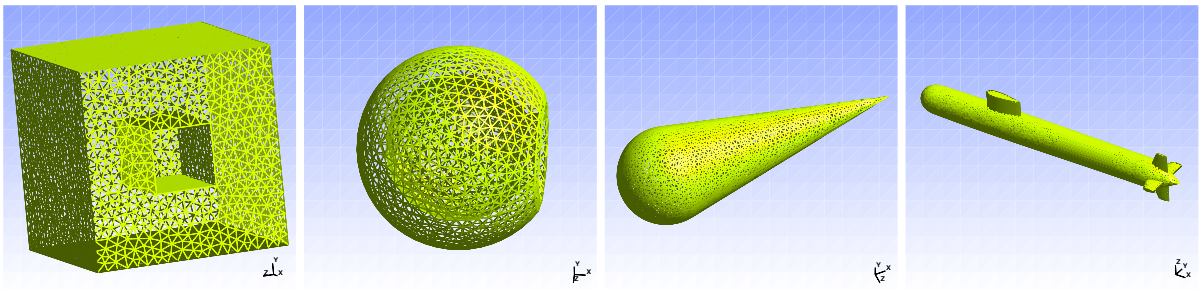

Figure 1.9. cubic cavity, spherical cavity, cone-sphere, submarine

1.3.1 Eigenvalues investigation

The investigation of the eigenvalues behavior of the involved integral operators has been operated using a code implemented with the libraries MÉLINA++ [MDL14] and ARPACK++[1].

[1] http://www.ime.unicamp.br/~chico/arpack++/

MÉLINA++ is the finite element (FE) library developed at IRMAR by the team "Analyse Numérique". It provides the FE discretization of the integral operators and standard differential operators. To compute numerical eigenvalues, ARPACK++ implements the "Implicit Restarted Arnoldi Method" (IRAM), which combines Arnoldi factorizations with an implicitly shifted QR method. A thourough investigation is described in the paper [DDL13]. Some of the most relevant results are given below. For all the geometries, the application of the OSRC preconditioner clearly cluster the eigenvalues around 1. For example, Fig. 1.10-1.11 show the distribution of the eigenvalues without preconditioning (CFIE) and with preconditioning (CFIE+OSRC) for the cone-sphere and the submarine. For the submarine, Fig. 1.13 gives the condition number with respect to the wavenumber k for the mesh density $n_\lambda = 10$, and with respect to n_λ for $k = 1.5$: for the OSRC-preconditioned CFIE, this value lies between 2.5 and 2.9 versus n_λ and between 2.3 and 2.6 versus k. This behavior is very interesting in view of an iterative solution and even remarkable for the considered object.

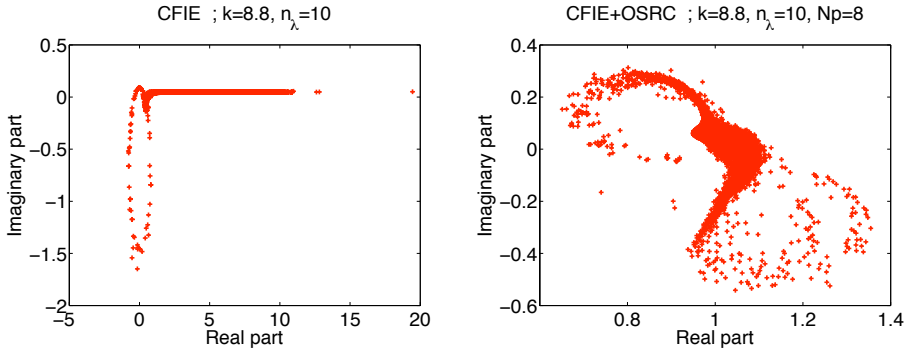

Figure 1.10. Cone-sphere: distribution of the eigenvalues, $k = 8.8$, $n_\lambda = 10$

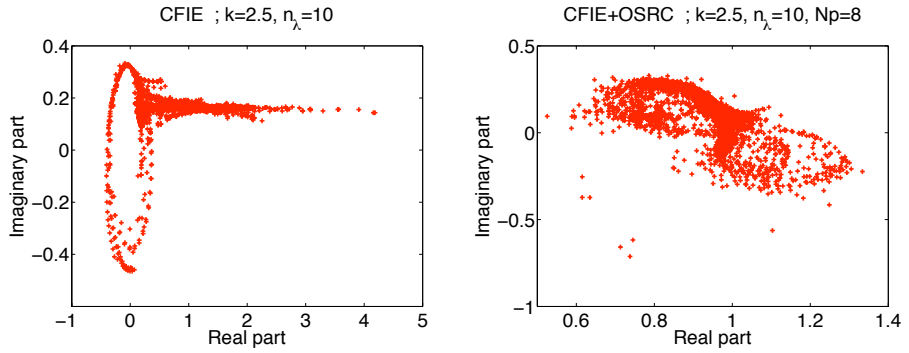

Figure 1.11. Submarine: distribution of the eigenvalues, $k = 2.5$, $n_\lambda = 10$

In the case of the cube with cavity, Fig. 1.14 exhibits a resonance frequency around $k = 5.2$: the OSRC-preconditioned CFIE has an isolated eigenvalue that comes very close to zero. Fig. 1.15 shows the condition number versus k where we considered numerous values of k, with four different meshes. To differentiate the different meshes, the curves are drawn alternatively

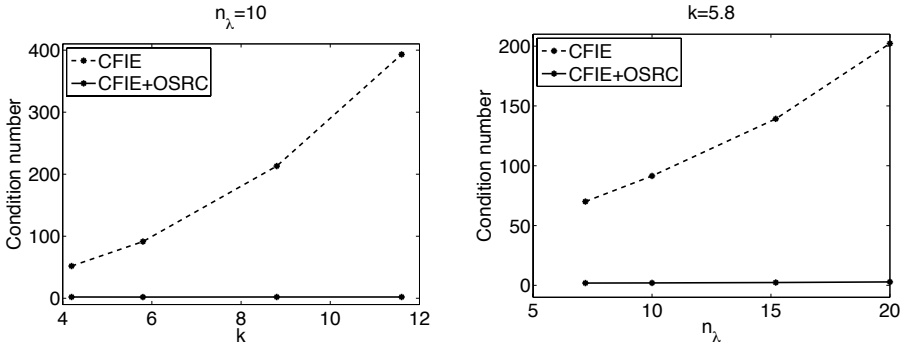

Figure 1.12. Cone-sphere: condition number – left: vs. k, $n_\lambda = 10$; right: vs. n_λ, $k = 5.8$

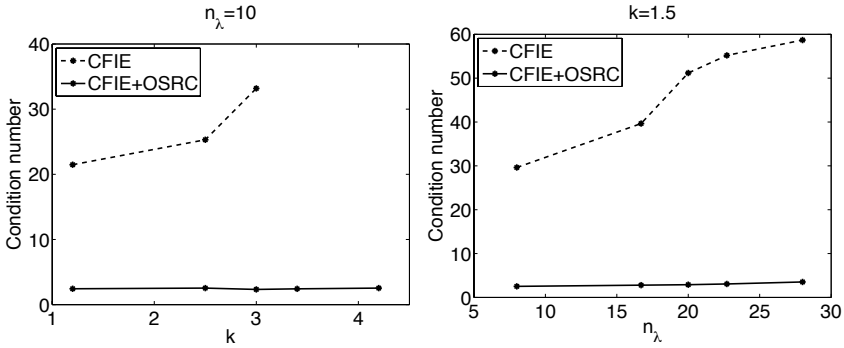

Figure 1.13. Submarine: condition number – left: vs. k, $n_\lambda = 10$; right: vs. n_λ, $k = 1.5$

using dashed and solid lines for the CFIE and using dashed and dotted lines for the OSRC-preconditioned CFIE. Fig. 1.15 clearly indicates that the resonance effect is attenuated by the OSRC-preconditioning. The highlighted resonance frequencies are characterized by the presence of a small number (one or two for the cube with cavity) of eigenvalues close to zero: when two of them are near zero, they are close enough to interpret them as one eigenvalue with multiplicity 2.

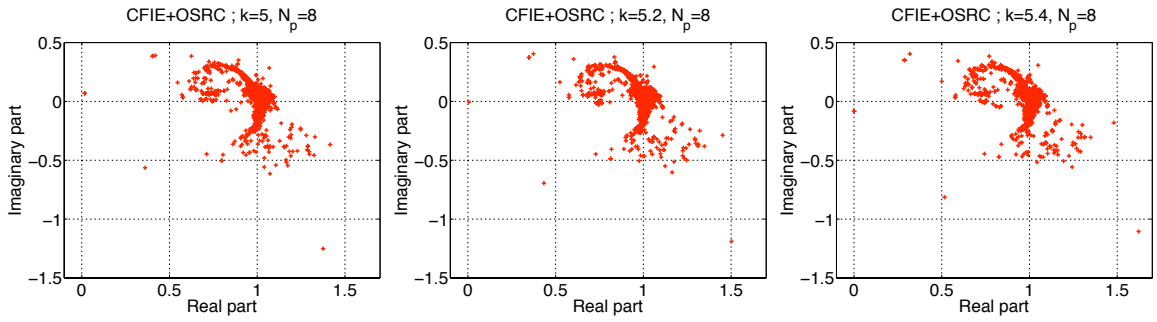

Figure 1.14. Cube with cavity: resonant case, around $k = 5.2$

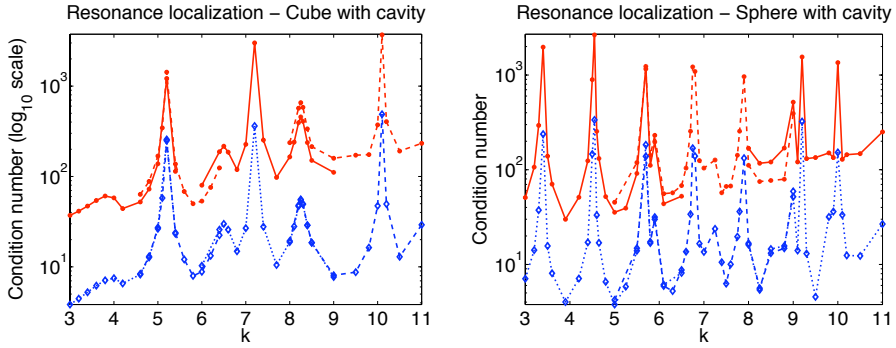

Figure 1.15. Condition number vs. wavenumber (log scale); cube and sphere with cavity

For the unit sphere, an interesting study of the eigenvalues behavior is observed versus the Padé order: Fig. 1.16 gives the numerical eigenvalues and the Padé-analytical ones for different Padé orders where the Padé-analytical eigenvalues are calculated by replacing the square-root operator with the Padé approximants in the analytic expression of the eigenvalues.

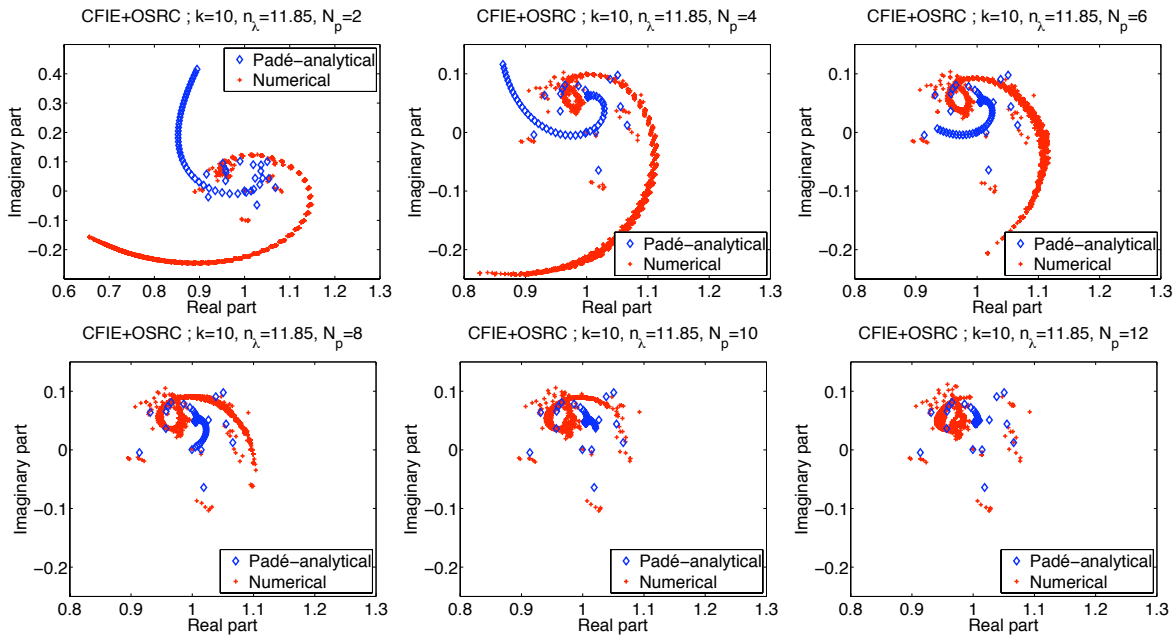

Figure 1.16. Unit sphere: distribution of the eigenvalues vs Padé order N_p, $k = 10$, $n_\lambda = 11.85$

1.3.2 Some of the numerical results

Thanks to the application of a SLFMM we have run tests at significantly high frequencies on an Intel(R) Xeon(R) CPU - E5620- 2.40GHz. The system was solved using GMRES. Fig. 1.17 to 1.23 show the bistatic Radar Cross Section (RCS ; compared to the Mie series solution for the unit sphere) in various configurations: different wavenumbers at the standard mesh density $n_\lambda = 10$, different mesh densities at a fixed wavenumber, using or not using preconditioning, using or not using FMM.

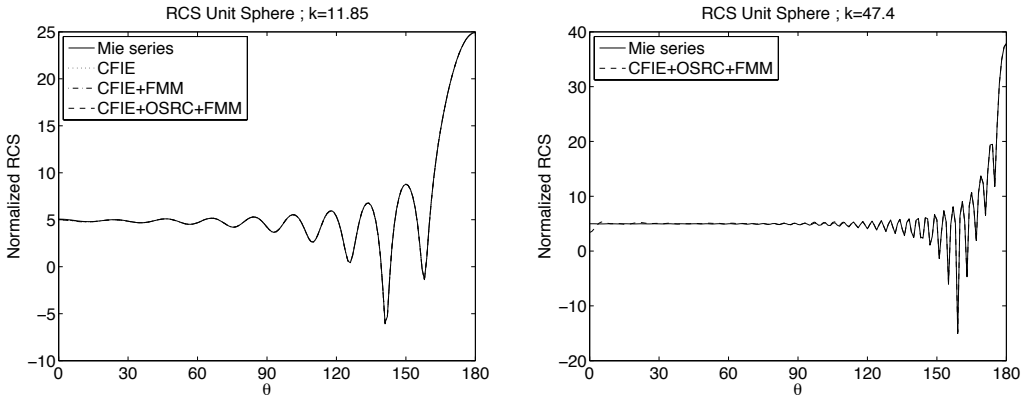

11520 triangles 184320 triangles

Figure 1.17. Normalized RCS for various wavenumbers k ($n_\lambda = 10$)

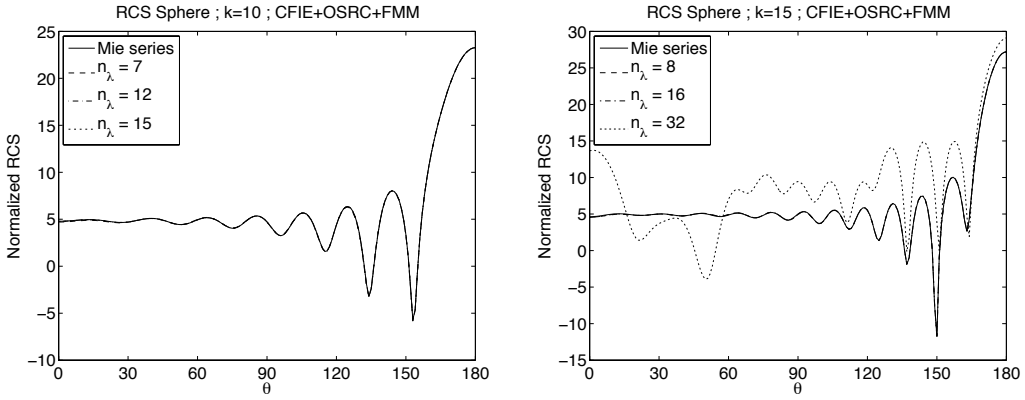

Figure 1.18. Normalized RCS for various discretization densities n_λ

A comment should be made on the use of the FMM: The different tests performed show that the FMM does not affect the OSRC technique as far as the accuracy of the FMM is reasonable. When the mesh density becomes too large, the problem meets with low-frequency regimes. This is clearly visible in Fig. 1.18 for the case $n_\lambda = 32$ where the code has converged to a wrong solution. This is a well-known unstability of the FMM. New expansions of the Green kernel are developed in order to overcome this issue [GHRW98, DH04, LC10].

Concerning the cone-sphere, the essential characteristic is the sharp apex toward the direction $(1, 0, 0)$ from its centroid. We then consider three incident directions: $(-1, 0, 0)$ parallel to the axis of the cone, where the incident wave hits the cone-sphere on the sharp apex, $(1, 0, 0)$ which hits the sphere part of the cone-sphere, and $(0, 0, -1)$ which hits the object perpendicularly to its axis. Table 1.1 indicates how the resolution convergence depends on the incident direction with the code CFIE or CFIE+FMM while it is not the case for the code CFIE+OSRC+FMM. Fig. 1.21 gives the RCS for different incident directions, wavenumbers or mesh densities.

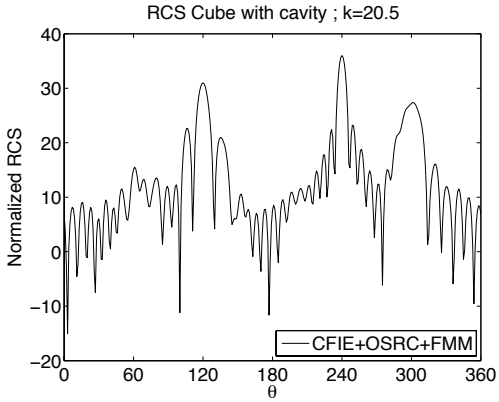

170884 triangles, $k = 20.5$

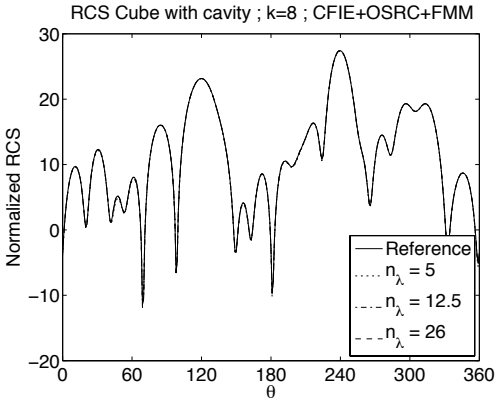

various mesh densities, $k = 8$

Figure 1.19. Normalized RCS

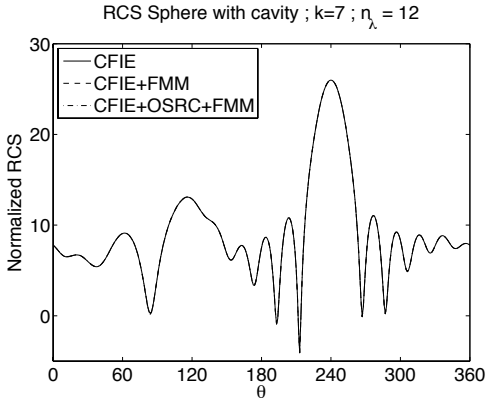

32754 triangles, $k = 7$

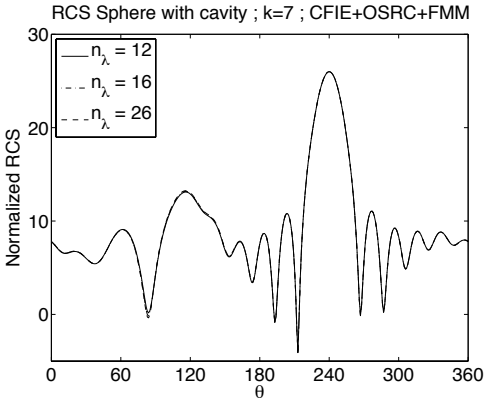

various mesh densities, $k = 7$

Figure 1.20. Normalized RCS

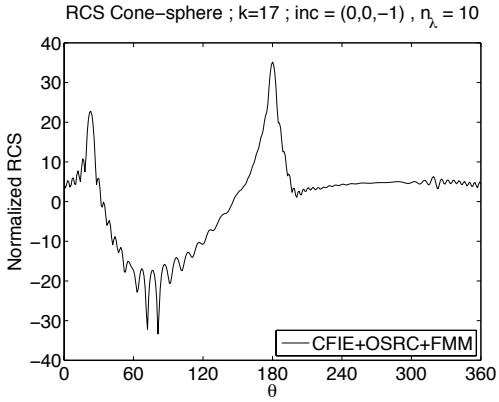

82278 triangles, $k = 17$

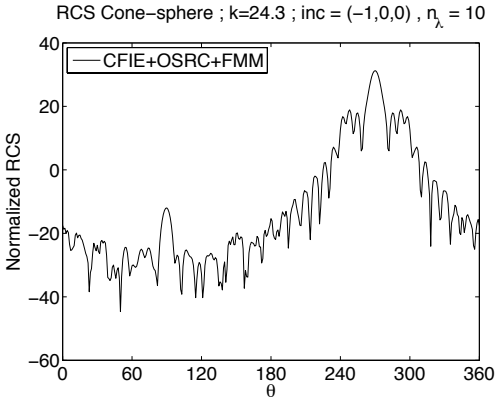

160246 triangles, $k = 24$

Figure 1.21. Normalized RCS for $n_\lambda = 10$

Table 1.1. Number of iterations vs incident direction taking $n_\lambda = 8$, and $k = 8$

Incident direction	CFIE	CFIE+SLFMM	CFIE+SLFMM+OSRC
(-1,0,0)	171	176	7
(1,0,0)	177	182	7
(0,0,-1)	230	235	7

For the submarine, the RCS is illustrated in Fig. 1.22-1.23 when the incident direction is $-(\sqrt{3}/2, 0, 1/2)$. For $k = 2.5$, Fig. 1.23-right exhibits the stability of the RCS versus the mesh density obtained with the code CFIE+OSRC+FMM while Fig. 1.23-left indicates that the code CFIE+FMM does not offer the same property. We can guess that this instability is related to the very low convergence of the GMRES. On Fig. 1.23-left, the results labeled "Ref" were obtained with the code CFIE+FMM for the mesh densities $n_\lambda = 10$ and $n_\lambda = 16.8$ and do not really match (relative (l^2,l^∞) differences: $(0.1846, 0.4127)$). On Fig. 1.23-right, the results are obtained with the code CFIE+OSRC+FMM with mesh densities from 10 to 30 and agree to each other (relative (l^2,l^∞)-differences: $(0.0212, 0.0679)$ to $(0.0280, 0.1051)$). A common curve is visible in both left and right plots of Fig. 1.23: $n_\lambda = 16.8$ in solid-line style. The instability essentially occurs in the illuminated zone which corresponds to the back of the submarine.

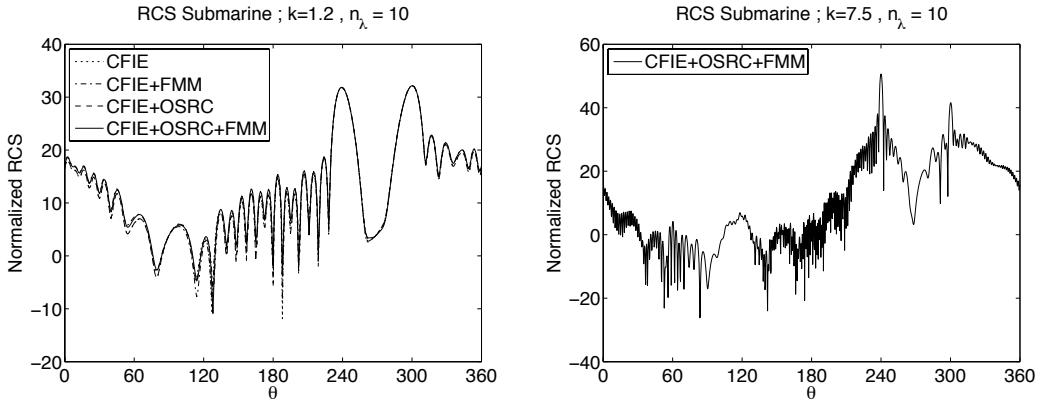

5546 triangles, $k = 1.5$ 215332 triangles, $k = 4.2$

Figure 1.22. Normalized RCS: various wavenumbers, $n_\lambda = 10$

The speed of the GMRES convergence versus the wavenumber or mesh density is illustrated in Fig. 1.24-1.25-1.26 for the different geometries. The use of the OSRC preconditioner clearly reduces the dependence of the GMRES convergence on these parameters.

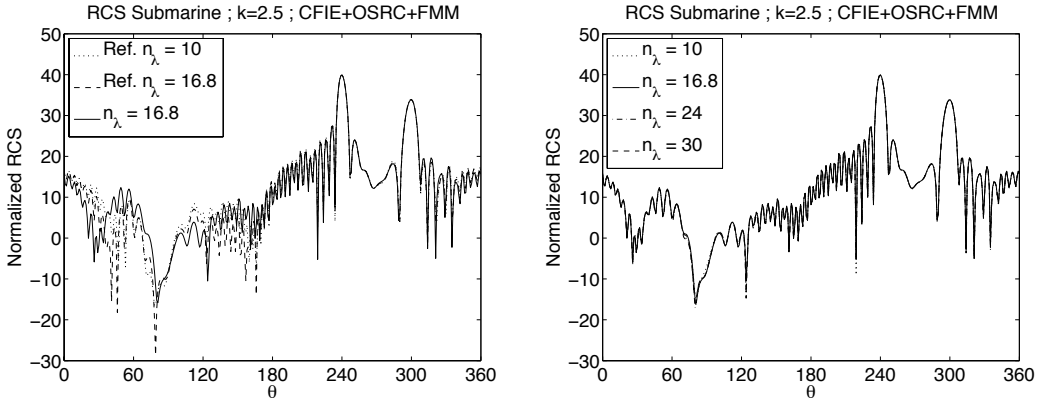

Figure 1.23. Normalized RCS: various mesh densities, $k = 2.5$

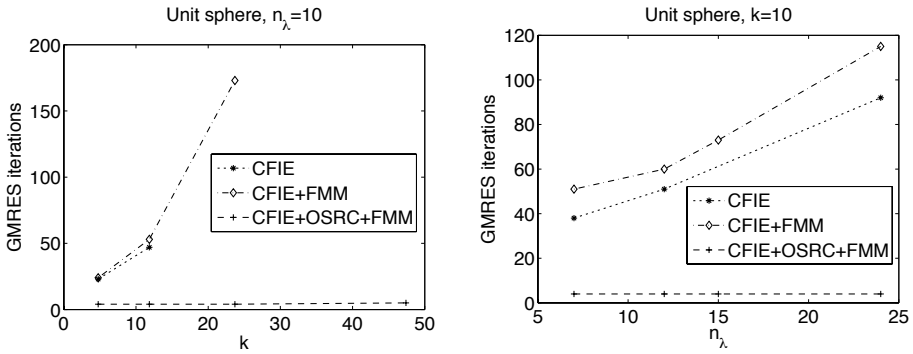

GMRES iterations vs k GMRES iterations vs n_λ

Figure 1.24. Unit sphere: convergence of GMRES

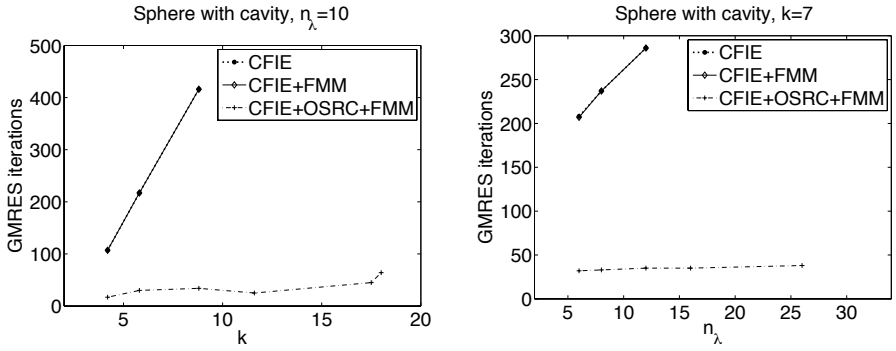

GMRES iterations vs k GMRES iterations vs n_λ

Figure 1.25. Sphere with cavity: convergence of GMRES

GMRES residuals can be observed in Fig. 1.27: in the case of the cube with cavity, at a resonance frequency on right. Close to the resonance frequency, the presence of small eigenvalues, distributed away from the cluster of eigenvalues at $(1, 0)$, slows down convergence of the GMRES. For $k = 5.2$, we can observe a plateau from iteration 7 to 12 in the GMRES residual curve. This plateau is not present in non-resonant cases.

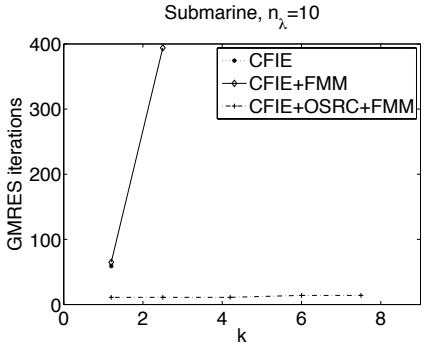

GMRES iterations vs k

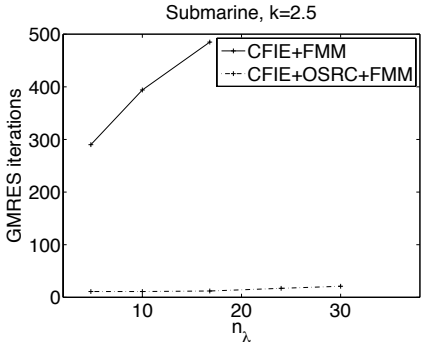

GMRES iterations vs n_λ

Figure 1.26. Submarine: convergence of GMRES

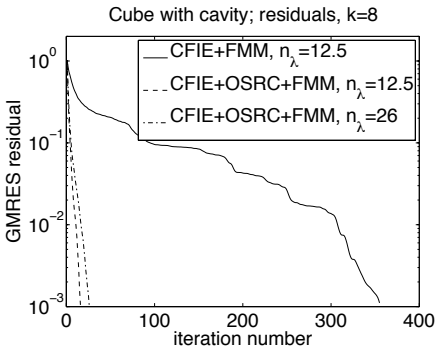

Residual behavior, $k = 8$

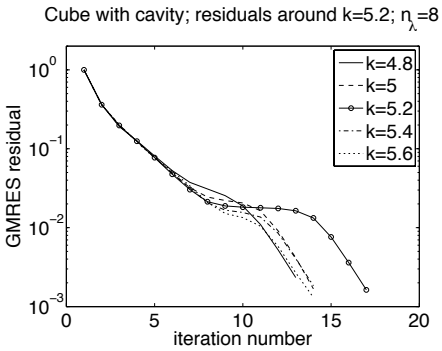

Residual behavior at resonance for CFIE+OSRC+FMM

Figure 1.27. Cube with cavity: convergence of GMRES, residuals

In the case of the unit sphere where we can measure the RCS error in Table 1.2, we have carefully studied the impact of the application of the OSRC preconditioner and of the SLFMM in term of efficiency: in Table 1.3, we show the CPU costs of the different codes (with or without SLFMM; with or without OSRC preconditioning).

Table 1.2. Relative $\|\cdot\|_2$ and $\|\cdot\|_\infty$ errors on the normalized RCS ($n_\lambda = 10$)

	CFIE		CFIE + FMM		CFIE + OSRC + FMM	
k	$\|\cdot\|_2$	$\|\cdot\|_\infty$	$\|\cdot\|_2$	$\|\cdot\|_\infty$	$\|\cdot\|_2$	$\|\cdot\|_\infty$
4.76	6.3e-3	7.9e-3	5.5e-3	6.7e-3	6.8e-3	8.2e-3
11.85	2.5e-3	2.9e-3	3.9e-3	4.9e-3	2.2e-3	2.3e-3
23.7	–	–	1.67e-2	2.07e-2	1.02e-2	9.3e-3
47.4	–	–	–	–	2.46e-2	4.21e-2

As one can see, the application of the OSRC preconditioning technique considerably reduces the global cost of the resolution and does not really affect the cost per iteration. Recall

that the operators involved in the preconditioning technique are differential operators. Then, the cost of applying the regularizing operator $\widetilde{V}$ per iteration is negligible. Thus, the cost per iteration is essentially the one of FMM matrix-vector products. For instance, the global cost is multiplied by 8 when the wavenumber is multiplied by 2 from 23.7 to 47.4. This is precisely the cost of the single-level FMM (SLFMM) since its theoretical complexity is about $(k^2)^{3/2} = k^3$ and $8 = 2^3$.

Table 1.3. Global costs vs k taking $n_\lambda = 10$

k	Total CPU time CFIE	Total CPU time CFIE+SLFMM	Total CPU time CFIE+SLFMM+OSRC
4.76	7 min 42”	13 min 47”	2 min 42”
11.85	9 h 43 min	4 h 33 min	32 min 40”
23.7	$>$ 15 days	214 h 44 min	6 h 20 min
47.4	–	–	48 h 48 min

1.4 A Regularized Fast Multipole Method for Geometric Numerical Integrations of Hamiltonian Systems

1.4.1 Introduction to the Regularized Fast Multipole Method

In applications to molecular dynamics, the evaluation of the potential function involves pairwise interactions (the Coulomb energy) of a large number of particles (typically millions of) and constitutes the bulk of computations. In this context, different strategies have been considered to speed up its evaluation: One of them consists in using the Fast Multipole Method (FMM) as introduced by L. Greengard and V. Rokhlin ([GR88]). This first version was written to deal with point charges, while in papers [WJGHG94], [WJGHG96], [SWHG01], [SSF96] and [KS99], the FMM was extended to and developed for the case of continuous distributions of the charges which corresponds to the charge distributions in molecular dynamics. These improvements led to versions of the FMM referred to as the continuous or gaussian Fast Multipole Method (CFMM or GFMM). However, all these versions share the drawback of producing discontinuities which in turn, when used in combination with a symplectic time discretization of the Hamiltonian dynamics, lead to drift in energy. In molecular dynamics however, it is crucial that the numerical method used to compute the solution preserves the symplecticity, the volume form, the Hamiltonian, or a combination of the three (given that for smooth Hamiltonians, symplecticity implies preservation of volume) and for these properties to show up in long-term integration, quite a lot of smoothness is required. B. Leimkuhler’s work on smooth switches between different symplectic integrators points toward the same direction [KL00, HLL00]. In order to attenuate the effect of discontinuities, one may use a large (sometimes up to twenty) number of multipoles in FMM expansions at the price of a prohibitive increase of the computational cost, despite many efforts to reduce the complexity of the FMM (see Elliot and Board [EB96], Petersen et al [PSPS94], Scuseria et al[KS99, BSSF96a, BSSF96b, SSF96, IS07], and [WHG96, GR97]). In this section, we propose a regularization technique for the FMM with the

aim of recovering the usual benefits of symplectic integration: This new FMM, referred to as the RFMM for regularized FMM in the sequel, is regular at the interface between boxes and thus provides a smooth approximation of the potential.

The FMM aims to offer a fast algorithm for the computation of a matrix-vector product Aq where the matrix A models the energy potential and q refers to the charges involved in the molecular dynamics problem. Let us denote by N the number of charges. For each charge $i \in \{1, ..., N\}$ located at x_i, the FMM approximation of $(Aq)_i = \sum_{j=1}^{N} G(x_i, x_j)q_j$, with G the energy potential function, leads to the expression

$$(Aq)_i \approx (Aq)_i^{\text{close}} + (Aq)_i^{\text{far}}, \tag{1.29}$$

where $(Aq)_i^{\text{close}} = \sum_{x_j \text{ close to } x_i} G(x_i, x_j)q_j$ and $(Aq)_i^{\text{far}}$ is the FMM approximation of the contribution of all the charges which are far from x_i. The latest is given by the development explained in Section 1.1.2 or its derivation when the energy potential is the derivative of a Coulomb potential (see [CDF10] for more details). In this configuration, x_i is said *target* point and is located in a FMM box B_{trg}, and $\{x_j\}_j$ are said the *source* points located in several source boxes B_{src}. x_j and x_i are said far from each other when they are in FMM boxes which are not neighbor, and they are said close to each other otherwise.

In this approximation, the interactions $x_i \leftrightarrow x_j$ are cut into a succession of interactions involving the centers of the boxes containing x_i and x_j. Such an approximation obviously introduces discontinuities in the approximated quantity $G(x_i, x_j)$ for both variables x_i and x_j, whenever x_i or x_j crosses the interface between two boxes. Figure 1.28-a (respectively Figure 1.28-b) shows the critical situation where two target points (respectively two source points) are very close to each other but are not in a same box.

In paper [CDF10], we proposed a regularized FMM (RFMM) where the multi-dimensional regularization is obtained by considering a 1D regularization on each component of the multi-dimensional variable. We perform the 1D regularization with the simple following idea: when a point of a box is close to another box, we view it as a shared point and its contribution to each box is calculated according to its location. This leads to a new distribution of the points. We call boxes associated to this distribution "virtual boxes". In 1D, the boxes are disjoint intervals. Let $[p_i, p_{i+1}]$, $i \in \mathbb{Z}$ define the i-th *geometric* box of the initial FMM distribution. For all i, let p_i^l and p_i^r be two points around p_i. We define the i-th *virtual* box as the interval $[p_i^l, p_{i+1}^r]$. Now for a given point $x \in \mathbb{R}$, we associate virtual boxes and weights depending on the position of x with respect to these virtual boxes. For example in Figure 1.29, the point x_1 belongs to box 2 and its weight is 1; in this case, the relation (1.29) remains unchanged. Point x_2 belongs to boxes 2 and 3, with weights respectively equal to c_2 and c_3 such that:

- $c_2 + c_3 = 1$; obviously, $c_2 > c_3$.
- c_2 and c_3 are given by a regularizing function $\chi : [p_3^l, p_3^r] \to [0, 1]$,

  $c_2 = (1 - \chi(x_2))$, $c_3 = \chi(x_2)$ such that (1.29) becomes

$$\begin{aligned}(Aq)_{x_2} \approx \quad & (1 - \chi(x_2)) \quad [(Aq)^{\text{close}}_{x_2 \in \text{ box } 2} + (Aq)^{\text{far}}_{x_2 \in \text{ box } 2}] \\ + \quad & \chi(x_2) \quad [(Aq)^{\text{close}}_{x_2 \in \text{ box } 3} + (Aq)^{\text{far}}_{x_2 \in \text{ box } 3}]\end{aligned}$$

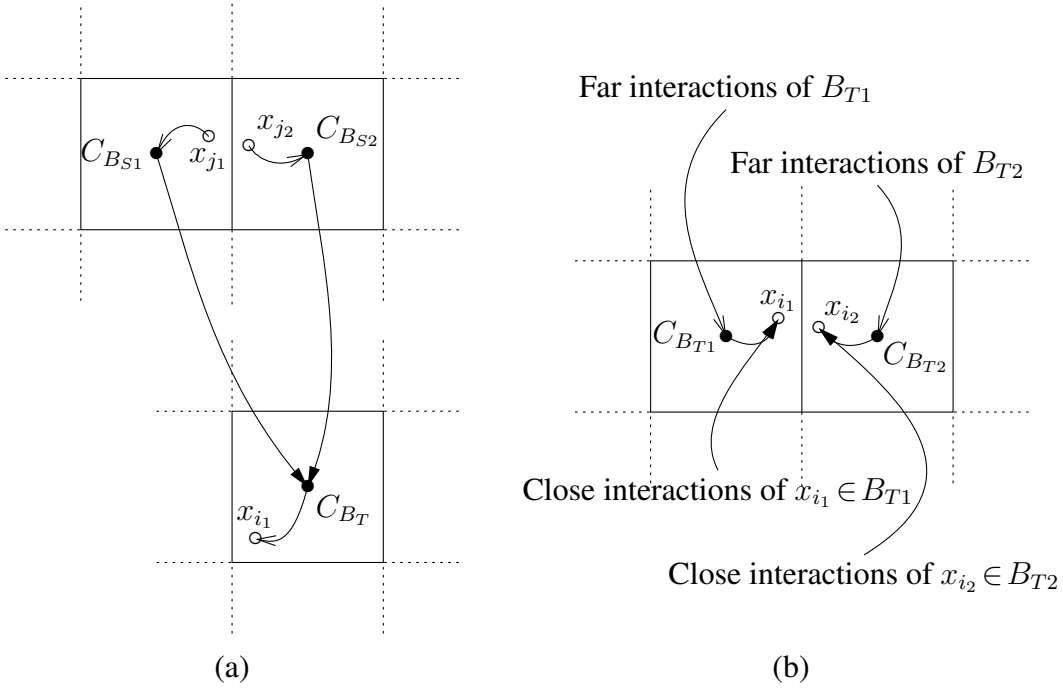

Figure 1.28. (*generated with Fig4TeX* [Laf11]) Exhibition of the discontinuity in the approximation of the interaction between some couples of target and source points. (a) Two source points x_{j_1} and x_{j_2}, close to each other, interact differently with the target point x_i. (b) Two target points, close to each other, receive differently the information from their environment.

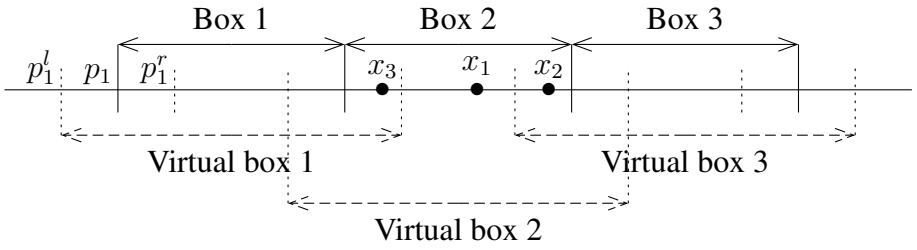

Figure 1.29. (*generated with Fig4TeX* [Laf11]) The virtual boxes for a regularized FMM: when the geometric boxes are next to each other, the virtual boxes overlap like in the partition of unity technique.

The choice of the function χ is discussed in details in [CDF10].

The regularization could be performed for both the first and the second variables of the kernel $G(x_i, x_j)$ but in the application we have in mind, the regularization is required for the target variable only. As an algorithm consequence, an increase of the FMM computational cost is expected due solely to the fact that some target points belong to two boxes: it stems from the last step of the computation of far interactions and from the computation of close interactions. The costs of these steps are indeed multiplied by the ratio between the average number of points in the virtual boxes and the average number of points in the geometric boxes; nevertheless, the complexity of these steps remains the same and the complexity of the whole

algorithm unchanged. Besides computational cost, we should mention that the FMM error estimates (1.4) and (1.8) are still valid for the RFMM.

The regularization technique was derived in the context of the basic single-level FMM introduced by Greengard et al [GR88] but it can be easily adapted to multi-level FMM or to improved versions of the FMM as considered in [EB96, PSPS94, WHG96, GR97].

1.4.2 Velocity Verlet Scheme and Regularized Fast Multipole Method

As a toy test-case, we have chosen to apply the RFMM to the "academic" model of the Outer Solar System as defined in [HLW06], solved by the Verlet's method. Generally speaking and for a separable Hamiltonian system of the form

$$\begin{cases} \dot{q} = M^{-1}p \in \mathbb{R}^{3N} \\ \dot{p} = -\nabla U(q) \in \mathbb{R}^{3N} \end{cases} \tag{1.30}$$

where $M = \text{diag}(m_1 I_{\mathbb{R}^3}, \cdots, m_N I_{\mathbb{R}^3})$ and with Hamiltonian $H(p,q) = T(p) + U(q)$, $T(p) = \frac{1}{2}p^T M^{-1} p$ being the kinetic energy and $U(q)$ the potential function, the Verlet's method reads (see for instance [HLW06])

$$\begin{cases} q_{n+\frac{1}{2}} = q_n + \frac{h}{2} v_n \\ v_{n+1} = v_n - h\nabla U(q_{n+\frac{1}{2}}) \\ q_{n+1} = q_{n+\frac{1}{2}} + \frac{h}{2} v_{n+1} \end{cases} \tag{1.31}$$

where q_n and v_n denote approximations of $q(nh)$ and $v(nh)$ with $v = \dot{q} = M^{-1}p$. It is explicit, symplectic and symmetric, and preserves a modified energy for exponentially long time when the potential U is smooth.

When the scheme is applied in astronomy or molecular dynamics, the bulk of computations lies in the evaluation of ∇U for successive steps (order N^2). It is thus natural to consider its FMM approximation. The Outer Solar System (as defined in [HLW06]) is the Solar system where the Sun is aggregated with the four closest planets (Mercure, Venus, Earth, Mars) and is modeled by Hamiltonian equations with

$$T(p) = \frac{1}{2}\sum_{i=0}^{5} \frac{1}{m_i} p_i^T p_i \text{ and } U(q) = -\gamma \sum_{i=1}^{5}\sum_{j=0}^{i-1} \frac{m_i m_j}{\|q_i - q_j\|}, \tag{1.32}$$

where γ is the gravitational constant. Denoting $G_0(x,y) = \frac{1}{\|x-y\|}$, the k-th component of the $(\mathbb{R}^3)^N$-vector $\nabla U(q)$ is given by the formula

$$\nabla_k U(q) = -\gamma \sum_{j \neq k} m_k m_j \nabla_x G_0(q_k, q_j) = -\gamma \sum_j \mathcal{M}_{k,j} \tag{1.33}$$

with $\mathcal{M}_{k,j} = m_k m_j \nabla_x G_0(q_k, q_j)$ for $k \neq j$ and $\mathcal{M}_{j,j} = 0$. This corresponds to a matrix-vector product commonly computed with the FMM, on which we test the RFMM.

The numerical results are obtain from the initial values taken from [HLW06] and reminded in [CDF10]. In the sequel, distances are expressed in astronomical units = UA (1 UA = 149,597,870 km), times in days, and $\gamma = 2.95912208286 \times 10^{-4}$. The time-step is chosen equal to 10 days. The size of the boxes should take into account the length of the trajectories

and the displacement for one time-step. In this example, one can find that Uranus (resp. Jupiter) requires about 30,700 days (resp. 4,300) to describe one loop around the Sun. With a time-step equal to 10 days, the trajectory around the Sun will be described with about 3,070 locations (resp. 430) on a curve of length about 118 UA (resp. 32) which define a characteristic time-step length equal to 0.04 UA (resp. 0.07). Such reports give enough information to derive the choice of the FMM boxes.

The following experiments are obtained with different values of the parameters:

- $\star$ L: number of multipoles, truncation parameter in (1.4) and (1.8). As is well known, the FMM expansion behaves like a geometric series with respect to L. A typical value for L is around 6, whereas a value around 15 or even 20 gives a very accurate approximation.
- $\star$ $\mathcal{N}_o$: order of neighborhood that defines the close and far interactions in the FMM oc-tree.
- $\star$ $\mathcal{N}_L$: number of levels of the oc-tree. In this experiment, a good tradeoff is $\mathcal{N}_L = 7$.
- $\star$ R_{reg}: ratio of the regularization zone on each side of a geometric box to the length of the geometric box. Example: For the 1D box $[0, 1]$, when $R_{reg} = 0.25$, the virtual corresponding box is $[-0.25, 1.25]$ and the regularization function operates on $[-0.25, 0.25]$ and $[0.75, 1.25]$.

Figure 1.30-a shows the relative error (in log-scale) on the Hamiltonian versus time, for $L = 3, \mathcal{N}_L = 7, \mathcal{N}_o = 1, R_{reg} = 0.25$ and illustrates the impressive improvement brought by the regularization technique.

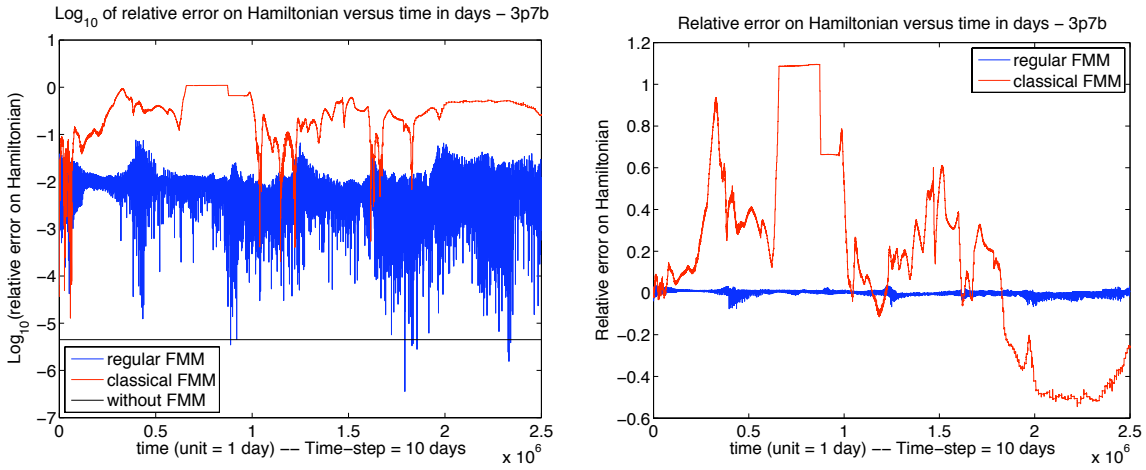

(a) (b)

Figure 1.30. Plot of the relative error on the Hamiltonian of the system, $L = 3$, $\mathcal{N}_L = 7$, $\mathcal{N}_o = 1$, $R_{reg} = 0.25$: (a) $\log_{10}$(relative error); (b) relative error.

Figure 1.31 also shows a significant qualitative improvement, as far as trajectories are concerned. However, as is expected from a low-accuracy approximation of the potential, they are still quantitatively wrong.

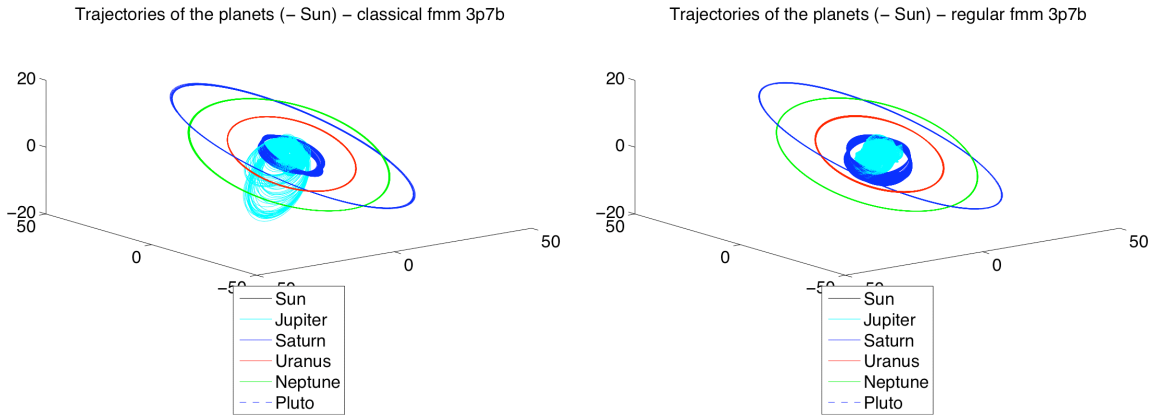

(a) (b)

Figure 1.31. Trajectories of the planets around the Sun, $L = 3$, $\mathcal{N}_L = 7$ and $\mathcal{N}_o = 1$, using: (a) a classical FMM, (b) the regularized FMM with $R_{reg} = 0.25$.

Figures 1.32 and 1.33 show that when L is increased, no gain in the qualitative behavior of the FMM is noticed. In contrast, the regularization technique enables energy preservation. For $L = 10$, the RFMM leads to accuracy comparable with what is obtained with the exact potential.

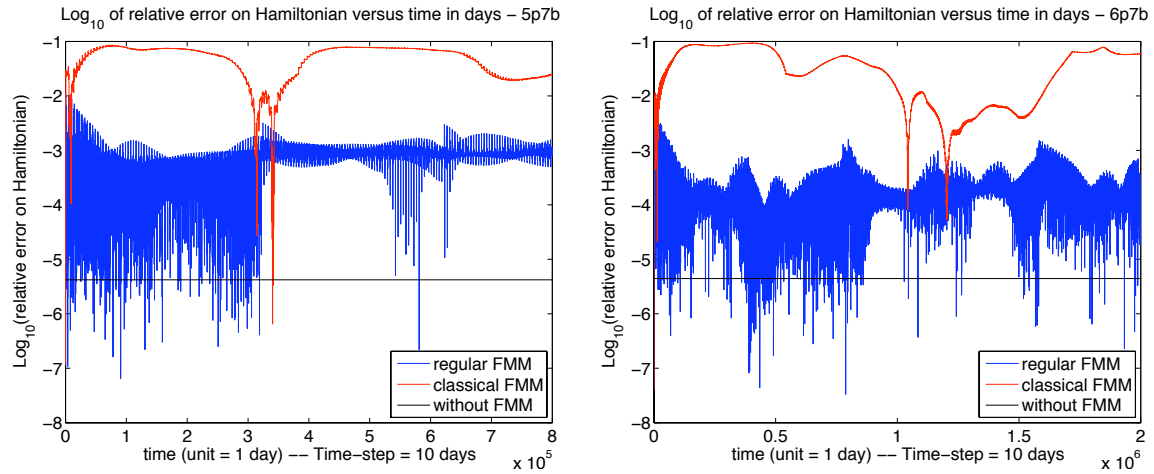

(a) (b)

Figure 1.32. Plot $\log_{10}$ of relative error on the Hamiltonian of the system, with: (a) $L = 5$, $\mathcal{N}_L = 7, \mathcal{N}_o = 1$, $R_{reg} = 0.25$; (b) $L = 6, \mathcal{N}_L = 7, \mathcal{N}_o = 1$, $R_{reg} = 0.25$.

In Figure 1.34, we plot the trajectories of the planets both for the FMM and RFMM approximations, and observe a gain of stability in the regularized case with different regularization ratio and neighborhood definition.

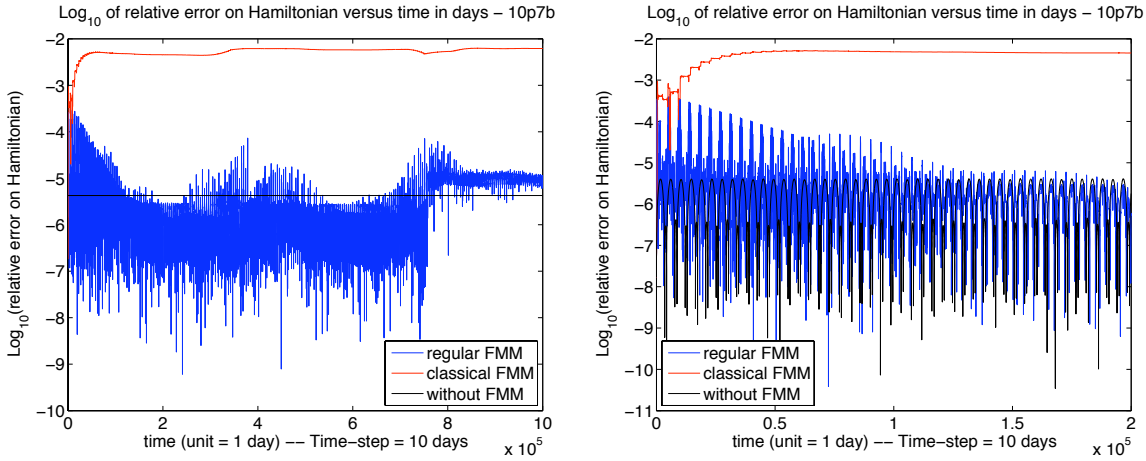

(a) (b)

Figure 1.33. (a) Plot $\log_{10}$ of relative error on the Hamiltonian of the system, $L = 10$, $\mathcal{N}_L = 7$, $\mathcal{N}_o = 1$, $R_{reg} = 0.25$; (b) Zoom.

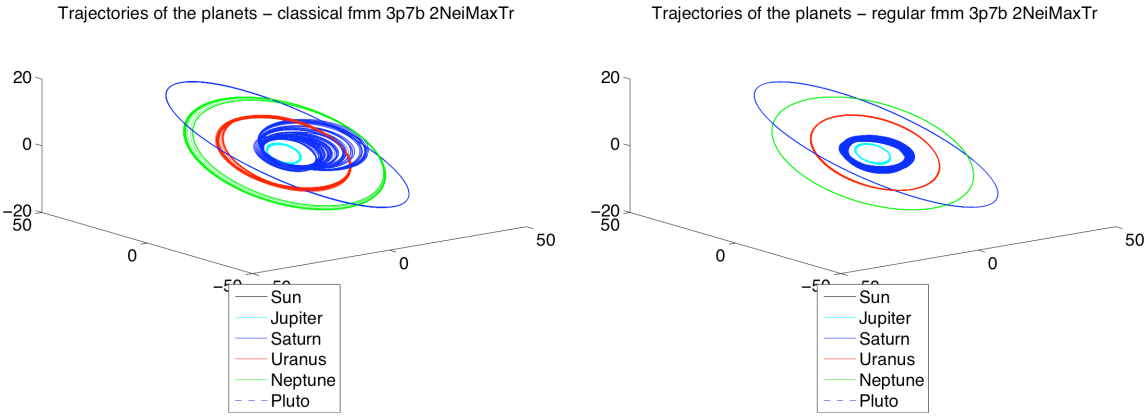

(a) (b)

Figure 1.34. Trajectories of the planets around the Sun, $L = 3$, $\mathcal{N}_L = 7$ and $\mathcal{N}_o = 2$, using: (a) a classical FMM, (b) the regularized FMM with $R_{reg} = 0.45$.

In terms of complexity of the algorithm, the observed overhead between FMM and RFMM is around 20% for $L = 3$, 10% for $L = 5$ or 6 and 1% for $L = 10$. However, in term of computational cost with respect to the accuracy, the RFMM leads to a significant improvement. Indeed, for $L = 10$, the classical FMM only gives an accuracy around $6\,.\,10^{-3}$ on the Hamiltonian. To obtain the same order of accuracy, the RFMM only requires $L = 5$ where the accuracy is somehow behaving between 10^{-3} and $3\,.\,10^{-3}$. On a theoretical point of view, the storage requirements and parts of the calculation cost should be divided by a factor close to $4 = 2^2$ and other parts of the calculation cost by a factor close to $16 = 2^4$ when the RFMM is used with $L = 5$ instead of the classical FMM with $L = 10$. Numerically, we effectively observe that the global CPU is divided by 9.8 for a comparable (even better) accuracy on the Hamiltonian.

1.5 Fast Multipole Method for Ultra-Weak Variational Formulation

To solve the Maxwell exterior problem, the solution evoked in previous sections consisted in the consideration of integral equations on the surface Γ of the scatterer, a bounded domain Ω^-. Another solution is the consideration of finite elements in the exterior domain Ω limited by an artificial boundary Σ which simulates the infinity. To this aim, one has to choose an artificial boundary condition on Σ such that the solution of the truncated exterior domain is close enough to the solution of the initial problem. Absorbing boundary conditions, perfectly matched layers are solutions commonly used. An alternative consists in the consideration of an exact boundary condition on Σ given by an integral representation. In this section, we consider this approach with the use of Fast Multipole Method to speed up the evaluation related to the integral representation, in the framework of the Ultra-Weak Variational Formulation (UWVF). The UWVF introduced by O. Cessenat and B. Després [Ces96, CD03] is an alternative to the finite elements based on the consideration of basis functions which solve the Maxwell equations in each volume element of the mesh discretization. The concept is explained in details in Section 3.2 and can be interpreted as a strategy combining the ideas of domain decomposition methods and of enriched finite elements. The discretization of the problem involves plane wave enriched basis functions: for each tetrahedron of the mesh, the number of basis functions depends on the size of the element. Before a closer consideration of the algorithm complexity, we need to introduce a parameter: K_0 denotes the average number of tetrahedra taken in one dimension so that the number of tetrahedra in the entire volume Ω is $K \sim K_0^3$. As a volume method, the UWVF leads to a sparse system: the number of degrees of freedom is of order $K_0^3\, p$ and the complexity of the algorithm is $\mathcal{O}(K_0^3\, p^2)$ where p denotes the average number of basis functions per tetrahedron which typically satisfies $K_0\, p \sim \kappa$ [HMM07], where κ is the wavenumber.

In this section, we focus on the impact of the use of integral representation and FMM on the algorithm complexity of the resolution of the UWVF. We consider the discretization of the UWVF with integral representation as follows:

$$([A] - [C] - [\widetilde{C}])X = [b]$$

where X is the discretized UWVF unknown, $[A] - [C]$ is the matrix of the discretization of the classical UWVF, and $[\widetilde{C}]$ is related to the integral representation (IR) as boundary condition on Σ. $[A]$ corresponds to the differential operators of the UWVF and $[C]$ is linked to the boundary condition on the surface Γ of the scatterer Ω^-. It is important to note that we never compute $[\widetilde{C}]$ explicitly since we evaluate its action as needed by the FMM.

The integral representation aims to reduce the distance between the artificial boundary Σ and the scatterer Ω^- to a number of elements independent of the wavenumber κ. We then have a number of elements in the mesh of order K_0^2. This reduces the complexity related to the volume calculation. The FMM is used to control the cost of the calculation related to the integral operators which give rise to large dense blocks in the discrete system.

A rigorous expression of the algorithm complexity involves several parameters: the size of the mesh $K \sim K_0^3$ or K_0^2, the average number of basis functions per tetrahedron p, the wavenumber κ, with the correlation $K_0 p \sim \kappa$. Moreover, the integral representation involves oscillating functions such as the Green function, and the exterior normal to the boundaries.

Table 1.4. Complexity estimates for the various versions of the UWVF + IR

Method	Number of elements	Cost of the solution
UWVF	$K_0^3 \sim (\kappa/p)^3$	$K_0^3 p^2 \sim K_0 \kappa^2$
UWVF + IR	$K_0^2 \sim \kappa^2$	$K_0^2 p^2 + K_0^4 p^2 \sim \kappa^2 + \kappa^4$
UWVF + IR + SLFMM	$K_0^2 \sim \kappa^2$	$K_0^2 p^2 + K_0^3\, p \sim \kappa^2 + \kappa^3$
UWVF + IR + MLFMM	$K_0^2 \sim \kappa^2$	$K_0^2 p^2 + K_0^2 \log^2(K_0)\, p \sim \kappa^2 + \kappa^2 \log^2 \kappa$
UWVF + IR + MLFMM with double mesh	$K_0^2 \sim (\kappa/p)^2$	$K_0^2 p^2 + \kappa^2 \log^2(\kappa)\, p \sim \kappa^2 + \kappa^2 \log^2(\kappa) p$
UWVF + IR + SLFMM without close interaction	$K_0^{5/2} \sim \kappa^{5/2}$	$K_0^{5/2} p^2 + K_0^3\, p \sim \kappa^2 + \kappa^3$
UWVF + IR + MLFMM without close interaction	$K_0^2 \sim \kappa^2$	$K_0^2 p^2 + K_0^2 \log^2(K_0)\, p \sim \kappa^2 + \kappa^2 \log^2 \kappa$

Evaluation of these operators requires an accurate discretization of the boundary. These considerations lead to different algorithms with different complexities. In Table 1.4, we give the results developed in [Dar08] which suggest that the UWVF with MLFMM and no close interactions should have attractive work estimates.

Let us illustrate these results with some numerical applications of the MLFMM to the coupling of UWVF and integral representation (UWVF+IR+MLFMM code). More numerical results are given in Section 3.2. We consider here the scattering by a perfectly conducting unit sphere (Γ) with different wavenumbers in order to investigate the κ dependence of the method and determine how well Table 1.4 reflects the practical work needed by the method. To this aim, the exterior boundary Σ is taken to be a concentric sphere rather close to Γ. We use different meshes S040, S025, S017, S010 and S007 defined in Table 1.5, such that the distance between Γ and Σ linearly decreases with the wavelength $\lambda = 2\pi/\kappa$. In the names "Sxxx", "xxx" indicates the distance between Γ and Σ in centimeters. More information on the meshes is given in Table 1.5. They have been generated optimizing the ratio between the average edge-length h and the wavelength λ to $h \approx \lambda/5$ and are quite uniform.

Figures 1.35, 1.36 and 1.37 show the angular dependence of the radar cross section (RCS) from our UWVF+IR+MLFMM code compared to the exact Mie series. Memory, CPU-time (on an Apple Mac Pro with 2×3GHz quad-core Xeon processors using 16 Gb RAM), together with quantitative error results are shown in Table 1.6 (units are seconds and Giga-bytes):

- ⋆ Rel Err 2 = Relative quadratic error on RCS.
- ⋆ Rel Err ∞ = Relative infinity error on RCS.
- ⋆ RMS error = Root mean square error on the scattering amplitude. Like in [CCCS04],

$$\text{RMS error} \;=\; \sqrt{\left(\frac{1}{n}\right)\sum_{i=1}^{n}(\text{RCS}(i) - \text{Exact-RCS}(i))^2}$$

is used as a classical RCS error ([CCCS04]). We have tried to keep the RMS error roughly constant to enable comparison.

We then plot the resulting number of degrees of freedom, CPU and memory requirements against κ in Fig.1.38. We also consider reference lines to enable comparison with results predicted in Table 1.4. These curves support the theoretical results on the complexity.

Table 1.5. The meshes for the unit sphere.

Name	S040	S025	S017	S010	S007
κ	3	4	6	10	15
Radius of Σ in m	1.40	1.25	1.17	1.10	1.07
Distance between Γ and Σ	$\approx \lambda/7.5$	$\approx \lambda/6.3$	$\approx \lambda/6.4$	$\approx \lambda/6.3$	$\approx \lambda/6.6$
Number of tetrahedra	5822	11008	8449	22630	44459
Number of basis functions per tetrahedron	10 to 22	10 to 24	16 to 30	16 to 28	14 to 30
Number of DoF	101814	178146	183108	480226	989238

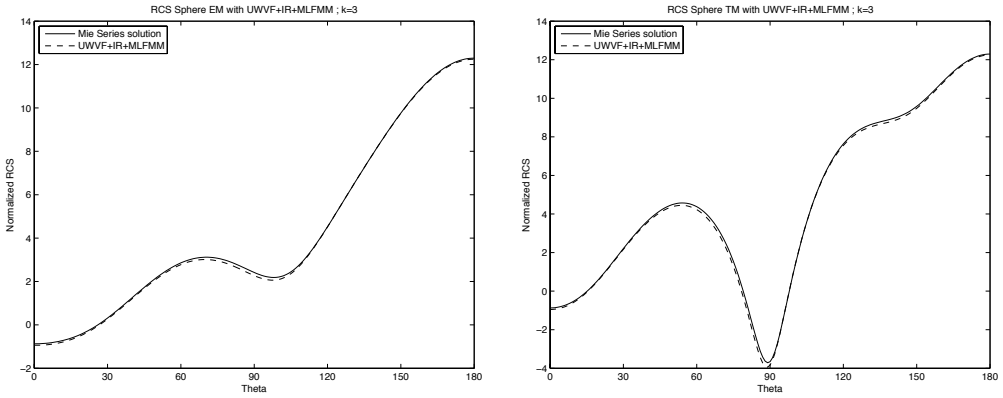

Figure 1.35. The RCS computed using UWVF+IR+MLFMM with the mesh S040, with $\kappa = 3$. Left: TE-polarized RCS. Right: TM-polarized RCS.

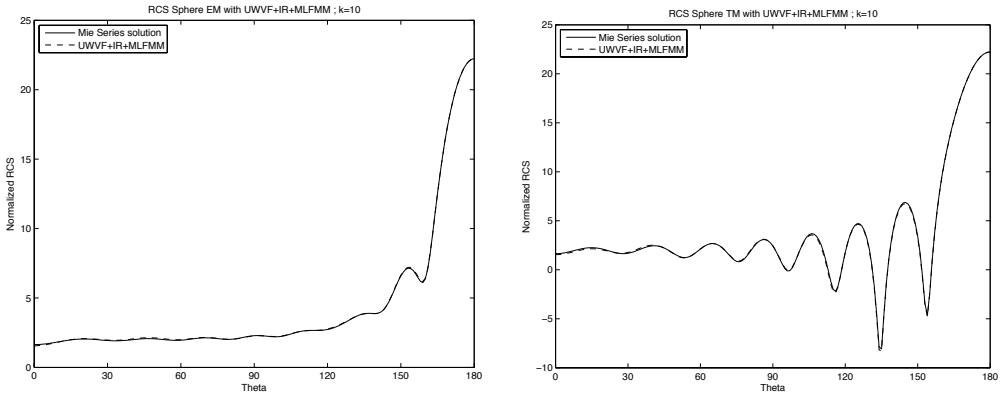

Figure 1.36. The RCS computed using UWVF+IR+MLFMM with the mesh S010, with $\kappa = 10$. Left: TE-polarized RCS. Right: TM-polarized RCS.

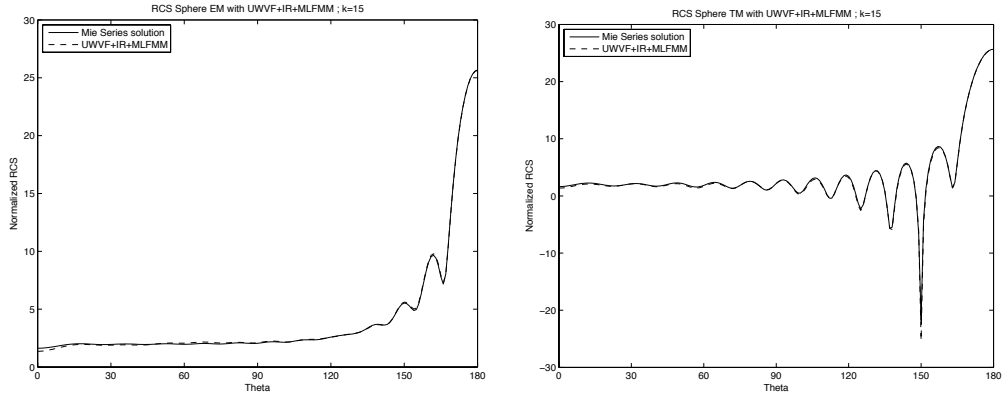

Figure 1.37. The RCS computed using UWVF+IR+MLFMM with the mesh S007, with $\kappa = 15$. Left: TE-polarized RCS. Right: TM-polarized RCS.

Table 1.6. Computational costs comparison for UWVF+IR+MLFMM (S040 ; S025 ; S017 ; S010 ; S007) as κ changes. The RCS error is computed via the Mie series.

Case	κ	CPU	MEM.	Rel Err 2	Rel Err ∞	RMS error
S040	3	558	1.5	$1.2\ \ 10^{-2}$	$1.2\ \ 10^{-2}$	$7.3\ \ 10^{-2}$
S025	4	798	1.6	$1.7\ \ 10^{-2}$	$1.1\ \ 10^{-2}$	$1.1\ \ 10^{-1}$
S017	6	1054	2.99	$6.4\ \ 10^{-3}$	$4.5\ \ 10^{-3}$	$4.1\ \ 10^{-2}$
S010	10	2770	8.38	$5.5\ \ 10^{-3}$	$4.1\ \ 10^{-3}$	$3.6\ \ 10^{-2}$
S007	15	9944	17	$1.3\ \ 10^{-2}$	$1.1\ \ 10^{-2}$	$8.5\ \ 10^{-2}$

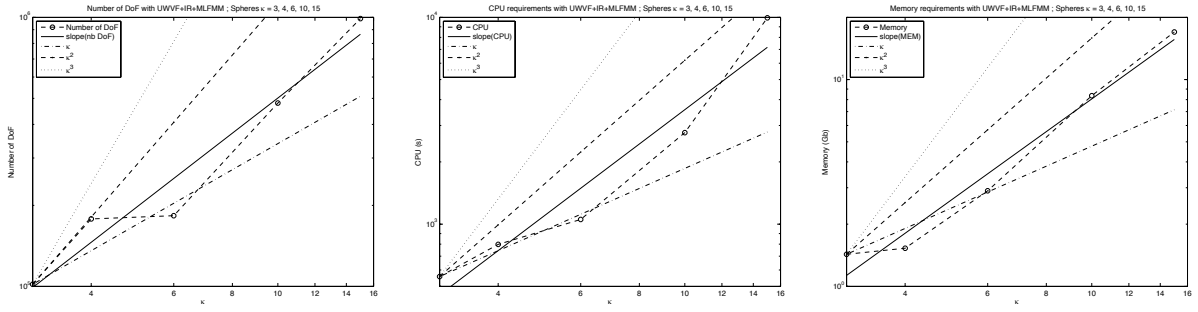

Figure 1.38. Number of degrees of freedom (left), CPU-time (middle) and memory requirements (right) with respect to the wavenumber κ, using a log-log scale. We show the data from Table 1.6 marked with a symbol in each case. The best fit line is shown as a solid line, and lines corresponding to $O(\kappa)$, $O(\kappa^2)$ and $O(\kappa^3)$ for comparison.

1.6 Perspectives

The consideration of FMM remains a mathematical challenge in some particular configurations and of great importance in the application of Mathematics. Some improvements are still under developments and combinations with current alternatives to the FMM would be pertinent.

- ⋆ With Yvon Lafranche, we are currently developing a generic library of fast methods, FastMMLib [DLnt]. The initial idea was a generic library of Fast Multipole Methods based on the general expression of the FMM expansion (1.1). The code is in C++ and the implemented skeleton is generic enough such that we can plan the integration of several different fast methods in the library like the high-order solver by O. Bruno et al [BK01b, BK01a] or the H-matrices [Hac99, BGH06, Beb08].

- ⋆ The work done with Marion Darbas and Yvon Lafranche on the combination of FMM and analytical preconditioner for Helmholtz equation can be extended to Maxwell equations using the developments done by Marion Darbas on the preconditioning aspects [Dar04, Dar06].

- ⋆ The ultra-weak variational formulation is currently derived in 2D using Bessel and Hankel functions alternatively to plane-wave functions [LHM12, HCWSC13, LHM13]. When this improvement is done for the 3D case, a combination with integral representation and FMM will certainly be worth some investigation.

Chapter 2

Volume integral operators for wave propagation

2.1 Introduction

The work presented in this chapter was realized with Martin Costabel in the context of the PhD theses of El-Hadji Koné and Hamdi Sakly [Kon10, Sak14], and it was initiated by a collaboration with Ronan Sauleau from IETR (Institut d'Électronique et de Télécommunications de Rennes). The application behind these developments was the design of lens-antennas [SB06] and it was based on volume integral formulations. If the volume integral equations are already widely used by physicists [KM00, Lu03, BS06, SF11] and numerically observed [Rah00, Bot06, SSVVA06], the mathematical analysis of these equations has been the subject of only a few studies [FP84, Pot01, Kir07, KL09]. With Martin Costabel, El-Hadji Koné, Hamdi Sakly, we contribute to the analysis of existence and uniqueness of the equations, mapping properties and spectral properties of the volume integral operators [CDK10, CDS12, CDSonb, CDSona].

The chapter is devoted to the analysis of the volume integral equation for the resolution of Maxwell equations in exterior domain. The volume formulation involves the electric and magnetic operators. The first section of the chapter is devoted to mathematical properties of the electric and magnetic operators: existence and uniqueness results and mapping properties. The second section offers the spectral properties derived from the analysis of these operators.

The physical context is defined by a bounded domain Ω^- in $\mathbb{R}^3$ representing a scatterer of electric permittivity ε and magnetic permeability μ. We use the notation $\Omega^+ = \mathbb{R}^3 \setminus \overline{\Omega^-}$ and $\Gamma = \partial\Omega^-$. We denote by $\mathbf{n}$ the unit outward normal vector to Ω^-. The electric permittivity and magnetic permeability of Ω^+ are respectively $\varepsilon_0 > 0$ and $\mu_0 > 0$. We will denote the relative permittivity and permeability by $\varepsilon_r = \dfrac{\varepsilon}{\varepsilon_0}$ and $\mu_r = \dfrac{\mu}{\mu_0}$. We will also use the notation $\eta = 1 - \varepsilon_r$ for the electric contrast and $\nu = 1 - 1/\mu_r$ for the permeability contrast. The electric conductivity σ vanishes everywhere. With the frequency ω, the wavenumber is $k = \omega\sqrt{\varepsilon_0\mu_0} > 0$.

We aim to solve the electromagnetic problem using a volume integral equation. The analysis involves several tools, we introduce here the functional spaces, the traces, the integral operators which are used in this study. For well known properties of these tools, we refer to [Cos07, CK98, Néd01, HW08, SS11].

- The functional spaces
  - ⋆ $H(\mathrm{curl}, \Omega^-) = \{\mathbf{u} \in L^2(\Omega^-)^3; \mathrm{curl}\,\mathbf{u} \in L^2(\Omega^-)^3\}$,

- $\star$ $H(\mathrm{curl}, \mathrm{div}, \Omega^-) = H(\mathrm{curl}, \Omega^-) \cap H(\mathrm{div}, \Omega^-)$,
- $\star$ $H_{\mathrm{loc}}(\mathrm{curl}, \overline{\Omega^+}) = \{\mathbf{u} \in L^2_{\mathrm{loc}}(\overline{\Omega^+})^3; \mathrm{curl}\,\mathbf{u} \in L^2_{\mathrm{loc}}(\overline{\Omega^+})^3\}$,
- $\star$ $H_{\mathrm{loc}}(\mathrm{curl}, \mathrm{div}, \overline{\Omega^+}) = H_{\mathrm{loc}}(\mathrm{curl}, \overline{\Omega^+}) \cap H_{\mathrm{loc}}(\mathrm{div}, \overline{\Omega^+})$,
- $\star$ $H(\mathrm{div}, \Omega^-)$ and $H(\mathrm{div}, \Omega^+)$ (respectively $H_{\mathrm{loc}}(\mathrm{div}, (\overline{\Omega^+}))$) are defined in the same way as $H(\mathrm{curl}, \Omega^-)$ (respectively $H_{\mathrm{loc}}(\mathrm{curl}, (\overline{\Omega^+}))$), with $\mathrm{curl}\,\mathbf{u}$ replaced by $\mathrm{div}\,\mathbf{u}$,
- $\star$ $H(\mathrm{div}\,0, \Omega) = \{\mathbf{u} \in H(\mathrm{div}, \Omega); \mathrm{div}\,\mathbf{u} = 0\}$,
- $\star$ $H_0(\mathrm{div}\,0, \Omega) = \{\mathbf{u} \in H(\mathrm{div}\,0, \Omega); \mathbf{n} \cdot \mathbf{u} = 0\}$.

- The trace operators for a scalar function u and a vector function $\mathbf{u}$
  - $\star$ trace: $\gamma_0 u = u|_\Gamma$, normal derivative: $\gamma_1 u = \mathbf{n} \cdot \nabla u|_\Gamma$,
  - $\star$ normal trace: $\gamma_n \mathbf{u} = \mathbf{n} \cdot \mathbf{u}|_\Gamma$, tangential trace: $\gamma_\times \mathbf{u} = \mathbf{n} \times \mathbf{u}|_\Gamma$,
  - $\star$ one-sided traces: $\gamma_0^\pm g = g^\pm|_\Gamma$, $\gamma_1^\pm g = (\mathbf{n} \cdot \nabla g^\pm)|_\Gamma$ and $\gamma_n^\pm \mathbf{v} = \gamma_n \mathbf{v}^\pm$, with $g^\pm = g|_{\Omega^\pm}$ and $\mathbf{v}^\pm = \mathbf{v}|_{\Omega^\pm}$ for g and $\mathbf{v}$ respectively scalar and vector fields defined on $\mathbb{R}^3$.

- The integral operators for a scalar field u defined on Γ and a vector field $\mathbf{u}$ defined on Ω^-,
  - $\star$ volume operators: using the notation G_k for the Helmholtz fundamental solution,

$$\mathcal{N}\mathbf{u}(x) = \int_{\Omega^-} \mathbf{u}(y) G_k(x,y)\, dy \quad , \quad \mathcal{M}\mathbf{u}(x) = \int_{\Omega^-} \nabla_y\, G_k(x,y) \cdot \mathbf{u}(y)\, dy\,, \tag{2.1}$$

  - $\star$ surface operators:

$$\mathcal{S}u(x) = \int_\Gamma u(y) G_k(x,y)\, ds(y)\,,$$

$$K_k' u(x) = \gamma_1 \int_\Gamma u(y) G_k(x,y)\, ds(y)\,,$$

$$M_k u(x) = \int_\Gamma \mathbf{n}(x) \times \mathrm{curl}_x(u(y) G_k(x,y))\, ds(y)\,,$$

  - $\star$ scaled operators:

$$\begin{aligned} \mathcal{M}_\eta &: \mathbf{u} \mapsto \mathcal{M}(\eta \mathbf{u})\,, \quad \mathcal{S}_\eta : u \mapsto \mathcal{S}(\eta\, u)\,, \\ \mathcal{N}_\tau &: \mathbf{u} \mapsto \mathcal{N}(\tau \cdot \mathbf{u})\,, \quad \mathcal{N}_\eta : \mathbf{u} \mapsto \mathcal{N}(\eta \mathbf{u})\,, \end{aligned} \tag{2.2}$$

    with τ this logarithmic gradient of ε_r: $\tau = -\dfrac{1}{\varepsilon_r} \nabla \varepsilon_r$,
  - $\star$ the electric volume integral operator A_k

$$A_k \mathbf{u}(x) = -\nabla\, \mathrm{div} \int_\Omega G_k(x,y)\, \mathbf{u}(y)\, dy - k^2 \int_\Omega G_k(x,y)\, \mathbf{u}(y)\, dy\,, \tag{2.3}$$

  - $\star$ the magnetic volume integral operator B_k

$$B_k \mathbf{u}(x) = \mathrm{curl} \int_\Omega G_k(x,y)\, \mathrm{curl}\,\mathbf{u}(y)\, dy\,. \tag{2.4}$$

2.2 Volume integral equations: mathematical framework

2.2.1 Mathematical properties of the electric volume integral equation

We first consider a configuration with no magnetic contrast (the magnetic permeability μ is constant in $\mathbb{R}^3$, $\mu \equiv \mu_0 > 0$) and a regular boundary Γ (at least C^2). The electric permittivity ε is considered to be a function of the space variable satisfying $\varepsilon|_{\Omega^+} = \varepsilon_0$; and ε is discontinuous across Γ, in general.

We consider a vector field $\mathbf{F} \in H(\mathrm{div}, \Omega^+)$ with compact support contained in Ω^+, representing a current density that serves as source for the incident field scattered by the dielectric body Ω^-. The physical quantity we aim to characterize is the electromagnetic field radiated by an antenna and refracted by a dielectric lens (Fig. 2.1).

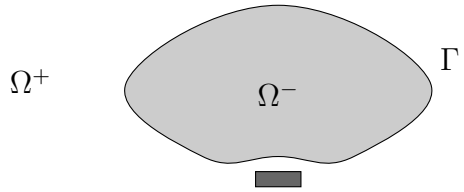

Figure 2.1. (*generated with Fig4TeX* [Laf11]) Combination of an antenna and a dielectric lens Ω^-.

The scattering problem $(\mathcal{P})$ we want to solve can be written as follows:

Find $\mathbf{E}$, $\mathbf{H}$ such that $\mathbf{E}_i \in H(\mathrm{curl}, \mathrm{div}, \Omega^-), \mathbf{E}_e \in H_{\mathrm{loc}}(\mathrm{curl}, \mathrm{div}, \overline{\Omega^+})$, $\mathbf{H}_i \in H(\mathrm{curl}, \Omega^-), \mathbf{H}_e \in H_{\mathrm{loc}}(\mathrm{curl}, \overline{\Omega^+})$, with $\mathbf{E}_i = \mathbf{E}|_{\Omega^-}$,$\mathbf{H}_i = \mathbf{H}|_{\Omega^-}$,$\mathbf{E}_e = \mathbf{E}|_{\Omega^+}$ and $\mathbf{H}_e = \mathbf{H}|_{\Omega^+}$, satisfying the equations

$$
(\mathcal{P}) \qquad \left\{ \begin{array}{llll}
\mathrm{curl}\,\mathbf{E}_i - ik\,\mathbf{H}_i = 0 & \text{and} & \mathrm{curl}\,\mathbf{H}_i + ik\varepsilon_r\,\mathbf{E}_i = 0 & \text{in } \Omega^-, \\
\mathrm{curl}\,\mathbf{E}_e - ik\,\mathbf{H}_e = 0 & \text{and} & \mathrm{curl}\,\mathbf{H}_e + ik\,\mathbf{E}_e = \mathbf{F} & \text{in } \Omega^+, \\
\mathbf{n}\times\mathbf{H}_e = \mathbf{n}\times\mathbf{H}_i & \text{and} & \mathbf{n}\cdot\mathbf{H}_e = \mathbf{n}\cdot\mathbf{H}_i & \text{on } \Gamma, \\
\mathbf{n}\times\mathbf{E}_e = \mathbf{n}\times\mathbf{E}_i & \text{and} & \mathbf{n}\cdot\mathbf{E}_e = \mathbf{n}\cdot\varepsilon_r\,\mathbf{E}_i & \text{on } \Gamma, \\
\mathbf{H}_e \times \frac{x}{r} - \mathbf{E}_e = \mathcal{O}\left(\frac{1}{r^2}\right), \ r = |x| \to +\infty. & & &
\end{array} \right.
$$

Martin Costabel and El-Hadji Koné demonstrated the equivalence of problem $(\mathcal{P})$ to a coupled surface-volume system of integral equations defined by the problem $(\mathcal{E}_1)$ and a volume integral equation defined by the problem $(\mathcal{E}_2)$ as follows:

$$
(\mathcal{E}_1) \qquad \left\{ \begin{array}{l}
\text{Find } (\mathbf{E}_*, e_*) \in (L^2(\Omega^-))^3 \times H^{-\frac{1}{2}}(\Gamma), \text{ such that} \\
\begin{pmatrix} 1 - \nabla\mathcal{N}_\tau + k^2\mathcal{N}_\eta & -\nabla\mathcal{S}_\eta \\ k^2\gamma_n^-\mathcal{N}_\eta - \gamma_1^-\mathcal{N}_\tau & 1 - \gamma_1^-\mathcal{S}_\eta \end{pmatrix} \begin{pmatrix} \mathbf{E}_* \\ e_* \end{pmatrix} = \begin{pmatrix} \mathbf{D} \\ \gamma_n^-\mathbf{D} \end{pmatrix}
\end{array} \right.
$$

and

$$
(\mathcal{E}_2) \qquad \left\{ \begin{array}{l}
\text{Find } \mathbf{E}_\circ \in (L^2(\Omega^-))^3, \text{ such that} \\
\left(1 - \nabla\mathcal{M}_\eta + k^2\mathcal{N}_\eta\right)\mathbf{E}_\circ = \mathbf{D}\ .
\end{array} \right.
$$

The equivalence results are formulated through the following theorems.

Theorem 2.1. *If* $(\mathbf{E}, \mathbf{H})$ *is a solution of the problem* $(\mathcal{P})$*, then* $(\mathbf{E}_i, \gamma_n \mathbf{E}_i)$ *is a solution of the problem* $(\mathcal{E}_1)$*.*

Theorem 2.2. *If* $(\mathbf{E}_*, e_*) \in (L^2(\Omega^-))^3 \times H^{-\frac{1}{2}}(\Gamma)$ *is a solution of the problem* $(\mathcal{E}_1)$*, then we have a solution* $(\mathbf{E}, \mathbf{H})$ *of the problem* $(\mathcal{P})$ *by defining:*

$$\mathbf{E}|_{\Omega^-} = \mathbf{E}_*,$$

$$\mathbf{E}|_{\Omega^+}(x) = \nabla \mathcal{S}(\eta\, e_*)(x) - \nabla \mathcal{N}(\operatorname{div} \mathbf{E}_*)(x) - k^2 \mathcal{N}(\eta\, \mathbf{E}_*)(x) + \mathbf{D}(x)\,,$$

$$\mathbf{H}|_{\Omega^-} = \frac{1}{ik} \operatorname{curl} \mathbf{E}_* \qquad \textit{and} \qquad \mathbf{H}|_{\Omega^+} = \frac{1}{ik} \operatorname{curl} \mathbf{E}|_{\Omega^+}.$$

In Theorems 2.1 and 2.2, we showed equivalence between the scattering problem $(\mathcal{P})$ and the first integral formulation $(\mathcal{E}_1)$. In this context, the right hand side had a particular form coming from our assumption that the sources are situated in the exterior domain. The right hand side $\mathbf{D}$ in the integral equation was the field generated by such a source, and was therefore analytic on the whole domain $\overline{\Omega^-}$. In order to study mapping properties of the integral operators, in particular the strongly singular operator appearing in $(\mathcal{E}_2)$, we need to consider more general right hand sides $\mathbf{D}$. The following equivalence theorem between the two integral formulations $(\mathcal{E}_1)$ and $(\mathcal{E}_2)$ holds in such a more general situation.

Theorem 2.3. *Let* $\mathbf{D} \in H(\operatorname{div}, \Omega^-)$, $\operatorname{div} \mathbf{D} = 0$.
(i) *If* $(\mathbf{E}_*, e_*) \in L^2(\Omega^-)^3 \times H^{-\frac{1}{2}}(\Gamma)$ *is a solution of the problem* $(\mathcal{E}_1)$*, then* $\mathbf{E}_*$ *is a solution of the problem* $(\mathcal{E}_2)$*.*
(ii) *If* $\mathbf{E}_\circ \in L^2(\Omega^-)^3$ *is a solution of the problem* $(\mathcal{E}_2)$*, then* $\mathbf{E}_\circ \in H(\operatorname{div}, \Omega^-)$ *and defining* $e_\circ = \gamma_n \mathbf{E}_\circ \in H^{-\frac{1}{2}}(\Gamma)$*, the pair* $(\mathbf{E}_\circ, e_\circ)$ *is a solution of the problem* $(\mathcal{E}_1)$ *.*

Having announced that the problems $(\mathcal{P})$, $(\mathcal{E}_1)$ and $(\mathcal{E}_2)$ are all equivalent, we now give mapping properties of the integral operators. Their well-posedness will imply the one for the transmission problem, which is of course already well known [CK98]. A more important motivation for the analysis of the integral operators in $(\mathcal{E}_1)$ and $(\mathcal{E}_2)$ is the question of their suitability for numerical computations. The easier one is $(\mathcal{E}_1)$, because it involves only weakly singular integral operators whose mapping properties are well known:

Proposition 2.4. *Let the coefficient* ε_r *be in* $C^1(\overline{\Omega^-})$ *with* $\varepsilon_r(x) \neq 0$ *in* $\overline{\Omega^-}$ *and*

$$\varepsilon_r(x) \neq -1 \quad \textit{on } \Gamma\,. \tag{2.5}$$

Then the matrix operator of the problem $(\mathcal{E}_1)$

$$\mathrm{A} = \begin{pmatrix} 1 - \nabla \mathcal{N}_\tau + k^2 \mathcal{N}_\eta & -\nabla \mathcal{S}_\eta \\ k^2 \gamma_n^- \mathcal{N}_\eta - \gamma_1^- \mathcal{N}_\tau & 1 - \gamma_1^- \mathcal{S}_\eta \end{pmatrix}$$

from $L^2(\Omega^-)^3 \times H^{-\frac{1}{2}}(\Gamma)$ *to* $L^2(\Omega^-)^3 \times H^{-\frac{1}{2}}(\Gamma)$ *is Fredholm of index zero. If there is a point on* Γ *where* (2.5) *is not satisfied, then it is not Fredholm.*

As a consequence of the equivalence theorems, Proposition 2.4 and the known uniqueness of the scattering problem, we obtain the following corollary:

Theorem 2.5. *Under the assumptions of problem $(\mathcal{P})$, the equation $(\mathcal{E}_2)$ has a unique solution depending continuously on the data.*

More general questions of mapping properties of the strongly singular integral operator of $(\mathcal{E}_2)$ in L^2 or in $H(\mathrm{div})$, in particular its spectral theory, remain largely open. We have the following partial result:

Proposition 2.6. *Let $\varepsilon_r \in C^1(\overline{\Omega^-})$ and $\eta = 1 - \varepsilon_r$.*
(i) The operator

$$\mathcal{A}_k^\eta : \mathbf{E} \mapsto \nabla \mathcal{M}(\eta \mathbf{E}) - k^2 \mathcal{N}(\eta \mathbf{E})$$

is bounded from $L^2(\Omega^-)^3$ to $L^2(\Omega^-)^3$ and from $H(\mathrm{div}, \Omega^-)$ to $H(\mathrm{div}, \Omega^-)$.
(ii) If $\mathbf{E} \in L^2(\Omega^-)^3$ is solution of

$$(1 - \mathcal{A}_k^\eta)\mathbf{E} = \mathbf{D}$$

with $\mathbf{D} \in H(\mathrm{div}, \Omega^-)$, then $\mathbf{E} \in H(\mathrm{div}, \Omega^-)$.
(iii) If $\varepsilon_r(x) \neq 0$ in $\overline{\Omega^-}$ and $\varepsilon_r(x) \neq -1$ on Γ, then the nullspace of the operator $1 - \mathcal{A}_k^\eta$ in $L^2(\Omega^-)^3$ is finite dimensional, and the codimension of the closure in $L^2(\Omega^-)^3$ of the image of $H(\mathrm{div}, \Omega^-)$ is finite.
(iv) If $\varepsilon_r(x) \geq \varepsilon_1$ for all $x \in \Omega^-$, where ε_1 is a positive constant, then the operator $1 - \mathcal{A}_k^\eta$ is a Fredholm operator of index zero in $L^2(\Omega^-)^3$, and it is strongly elliptic: There is a compact operator $\mathcal{K}_0$ and $c > 0$ such that for all $\mathbf{E} \in L^2(\Omega^-)^3$

$$\int_{\Omega^-} \overline{\mathbf{E}(x)} \cdot (1 - \mathcal{A}_k^\eta)\mathbf{E}(x)\, dx \geq c \, \|\mathbf{E}\|^2_{L^2(\Omega^-)} - \|\mathcal{K}_0 \mathbf{E}\|^2_{L^2(\Omega^-)} \,. \tag{2.6}$$

The volume integral equation $(\mathcal{E}_2)$ is well-posed in L^2 and satisfies a Gårding inequality. It is suitable for numerical approximations using L^2-conforming finite elements, because any Galerkin method will lead to a stable discretization scheme.

The proofs of these results are available in [CDK10, Kon10] and require technical tools which are all available in standard references, such as the Stratton-Chu integral representation theorem in [CK98], the basic properties of the Sobolev spaces associated with the electromagnetic energy in [GR96], trace theorems and mapping properties of singular integral operators between Sobolev spaces in [Néd01] and the unique continuation principle from [Lei86] or [Pro60].

With Daniel Martin and El-Hadji Koné, we implemented the volume integral operators in the finite element library MÉLINA++ [MDL14] and numerical results were obtained for different definitions of the relative permittivity ε_r. Figs. 2.2-2.3 show the refraction of a plane wave by the dielectric unit ball, with wavenumber $k = 5$, incident direction $(0, 0, -1)$ and polarization (0,1,0). The figures correspond to these definitions of the electric permittivity ε_r

$$\varepsilon_r^{(1)} = \begin{cases} 1.1 + 10^6 i & \text{if } x_3 \leq 0, \\ 0.95 & \text{if } x_3 > 0, \end{cases}$$

$$\varepsilon_r^{(2)} = \begin{cases} 1.1 + 10^6 i & \text{if } |x_3| \leq 3/4, \\ 0.95 & \text{if } 3/4 < |x_3| \leq 1. \end{cases}$$

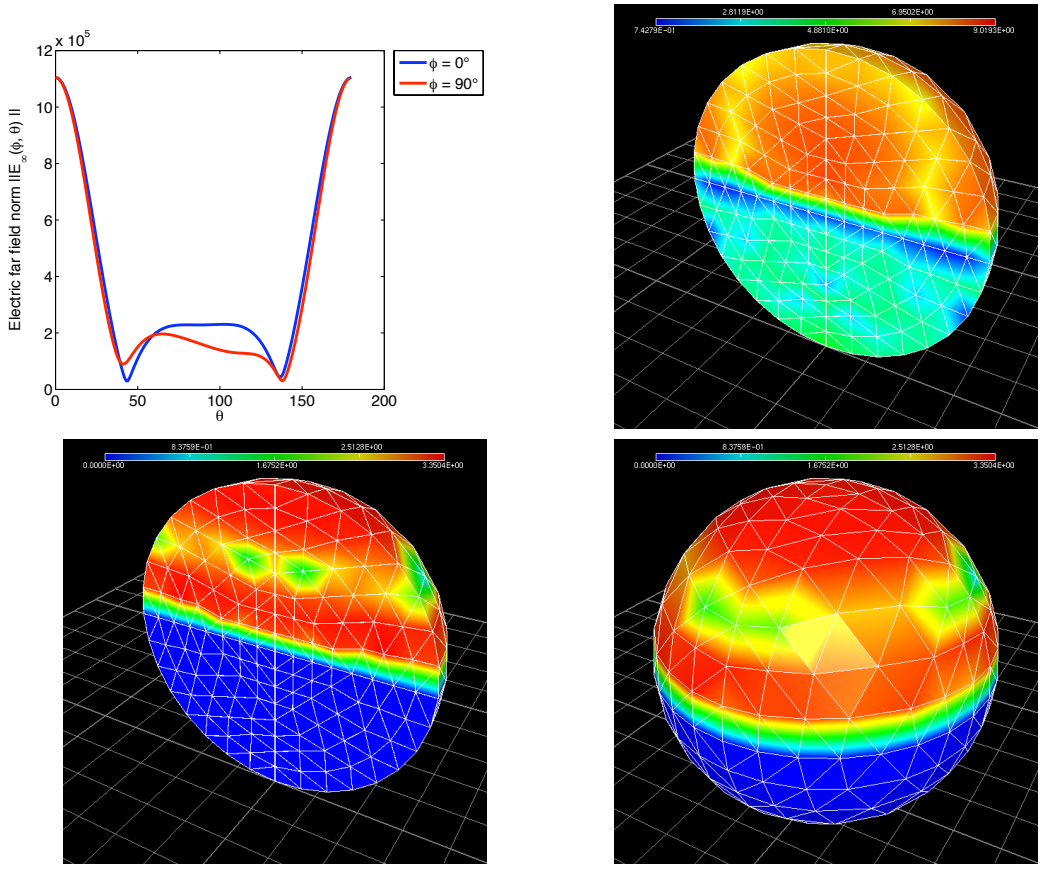

Figure 2.2. Case of $\varepsilon_r = \varepsilon_r^{(1)}$; top-left: far field; top-right: cut of the real part of the first component; bottom-left: cut of the imaginary part of the third component; bottom-right: imaginary part of the third component of the field on Γ.

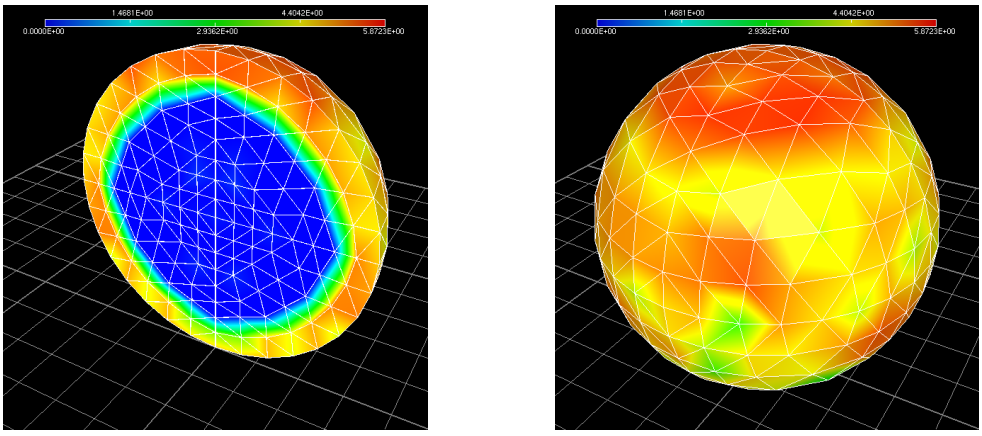

Figure 2.3. Case of $\varepsilon_r = \varepsilon_r^{(2)}$; left: cut of the imaginary part of the second component; right: imaginary part of the second component of the field on Γ.

2.2.2 Mathematical properties of the magnetic volume integral equation

For a different hypothesis on the electric permittivity and magnetic permeability, with ε_r, μ_r arbitrarily complex constant numbers, the system of Maxwell equations to be solved takes the

general form:

Find $\mathbf{E}$, $\mathbf{H}$ such that

$$(\mathcal{P}_\star) \qquad \begin{cases} \operatorname{curl}\mathbf{E} - ik\mu_r\mathbf{H} = 0 \\ \operatorname{curl}\mathbf{H} + ik\varepsilon_r\mathbf{E} = F \\ \\ [\mathbf{n}\times\mathbf{E}]_\Gamma = 0 \quad , \quad [\mathbf{n}\cdot\mu_r\mathbf{H}]_\Gamma = 0 \\ [\mathbf{n}\times\mathbf{H}]_\Gamma = 0 \quad , \quad [\mathbf{n}\cdot\varepsilon_r\mathbf{E}]_\Gamma = 0 \\ \\ \mathbf{H}\times\frac{x}{r} - \mathbf{E} = \mathcal{O}\left(\frac{1}{r^2}\right), \ r = |x| \to +\infty. \end{cases}$$

It can be shown [Kir07] that the scattering problem is equivalent to the volume integral equation considered in $H(\operatorname{curl},\Omega^-)$:

$$\mathbf{u}(x) - \eta A_k\mathbf{u}(x) - \nu B_k\mathbf{u}(x) = \mathbf{u}^{\text{inc}}(x) \ \ (x\in\Omega^-), \tag{2.7}$$

where A_k and B_k are the volume operators given in (2.3-2.4).

We now restrict ourselves to a configuration with no electric contrast (the electric permittivity ε is constant in $\mathbb{R}^3$) in order to focus on the magnetic operator. Here, we focus on a crucial mapping property which was previously ignored in the literature. With Hamdi Sakly, we studied carefully the extendability of the magnetic operator to $L^2(\Omega^-)$. In this configuration, the scattering problem is equivalent to the volume integral equation:

$$\mathbf{u} - \nu B_k\mathbf{u} = \mathbf{u}^{\text{inc}} \quad \text{ in } H(\operatorname{curl},\Omega^-)\,. \tag{2.8}$$

Andreas Kirsch and Armin Lechleiter [KL09] demonstrated that the integral operator B_k is bounded from $H(\operatorname{curl},\Omega^-)$ to itself and to $H(\operatorname{div}0,\Omega^-)$. As a next step, one could think about the extension to $L^2(\Omega^-)$ as we operated for the operator A_k. For $v\in C_0^\infty(\Omega^-)$, by elementary relations on differential operators, one can show that

$$B_k\,\mathbf{u} = A_k\,\mathbf{u} + \mathbf{u}\,.$$

However, for $\mathbf{u}\in H(\operatorname{curl},\Omega^-)$, B_k writes as follows:

$$B_k\,\mathbf{u} = \widetilde{B}_k\,\mathbf{u} - \operatorname{curl}\int_\Gamma G_k(x,y)\,\mathbf{u}(y)\times\mathbf{n}(y)\,ds(y)\,,$$

where $\widetilde{B}_k : L^2(\Omega^-)^3 \to L^2(\Omega^-)^3$ is the extended operator on $L^2(\Omega^-)$:

$$\widetilde{B}_k\mathbf{u}(x) = \operatorname{curl}\operatorname{curl}\int_{\Omega^-} G_k(x,y)\,\mathbf{u}(y)\,dy\,.$$

Since the Γ-integral term does not have a continuous extension to $L^2(\Omega^-)$, we clearly deduce that B_k cannot be extended to $L^2(\Omega^-)$.
Moreover, one can interpret the problem obtained by replacing B_k by its extension $\widetilde{B}_k$:

$$\mathbf{u} - \nu\widetilde{B}_k\mathbf{u} = \mathbf{u}^{\text{inc}}\,. \tag{2.9}$$

The following result occurs:

Theorem 2.7. *Let $\widetilde{\mathbf{u}} \in L^2(\mathbb{R}^3)^3$ be a solution of $\widetilde{\mathbf{u}} - \nu\widetilde{B}_k\widetilde{\mathbf{u}} = \mathbf{f}$ in $\mathbb{R}^3$, then $\widetilde{\mathbf{u}}$ satisfies:*

1. $\widetilde{\mathbf{u}} \in H(\mathrm{curl}, \Omega^-)$,$\widetilde{\mathbf{u}} \in H_{\mathrm{loc}}(\mathrm{curl}, \mathbb{R}^3)$ *and* $[\gamma_\times(\frac{1}{\mu_r}\widetilde{\mathbf{u}})]_\Gamma = 0$ *if* $\mathbf{f} \in H(\mathrm{curl}, \mathbb{R}^3)$
2. $[\gamma_n\widetilde{\mathbf{u}}]_\Gamma = 0$ *if* $\mathbf{f} \in H(\mathrm{div}, \mathbb{R}^3)$
3. $\frac{1}{\mu_r}\widetilde{\mathbf{u}} \in H(\mathrm{curl}, \Omega^-)$, $\frac{1}{\mu_r}\widetilde{\mathbf{u}} \in H_{\mathrm{loc}}(\mathrm{curl}, \mathbb{R}^3)$ *and* $[\gamma_\times(\frac{1}{\mu_r}\,\mathrm{curl}\,\widetilde{\mathbf{u}})]_\Gamma = 0$ *if* $\mathrm{curl}\,\mathbf{f} \in H(\mathrm{curl}, \mathbb{R}^3)$
4. $[\gamma_n(\frac{1}{\mu_r}\,\mathrm{curl}\,\widetilde{\mathbf{u}})]_\Gamma = 0$

Corollary 2.8. *Solving the volume integral equation $\mathbf{u} - \nu\widetilde{B}_k\mathbf{u} = \mathbf{u}^{\mathrm{inc}}$ in $L^2(\Omega^-)$ gives: the Maxwell equations in $\mathbb{R}^3 \setminus \Gamma$ with the transmission conditions*

$$\begin{array}{rclcrcl} [\frac{1}{\mu_r}\mathbf{E} \times n]_\Gamma &=& 0\,, & & [n \cdot \mathbf{H}]_\Gamma &=& 0\,, \\ [\mathbf{H} \times n]_\Gamma &=& 0\,, & & [n \cdot \mathbf{E}]_\Gamma &=& 0\,. \end{array}$$

The latter is not the initial transmission problem $(\mathcal{P}_\star)$ we are interested in. Solving (2.9) instead of (2.8) leads to a solution which is different in most of the usual configurations.

2.3 Analysis of the spectrum of the volume integral equations

This section is dedicated to the analysis of the spectrum of the volume integral operators when the electric permittivity and the magnetic permeability are considered constant in Ω^-. Most of the results were demonstrated by Hamdi Sakly for his PhD [Sak14]. Some more details on the proofs are given in [CDS12]. The results concerning the magnetic integral operator use the following lemma

Lemma 2.9. *Let X and Y be vector spaces and $S : Y \to X$ and $T : X \to Y$ linear operators. Then for $\lambda \neq 0$, T induces isomorphisms from $\ker(\lambda - ST)$ to $\ker(\lambda - TS)$ and from $X/(\lambda - ST)X$ to $Y/(\lambda - TS)Y$. In particular, $\lambda - ST$ is Fredholm of index 0 in X if and only if $\lambda - TS$ is Fredholm of index 0 in Y.*

2.3.1 The essential spectrum of the electric volume integral operator

The results for the electric operator are obtained from the properties annouced in Section 2.2 and the orthogonal decomposition of $L^2(\Omega^-)$:

$$L^2(\Omega) = \nabla H_0^1(\Omega^-) \oplus H(\mathrm{div}\,0, \Omega^-) \oplus \mathbf{W}$$

where $H(\mathrm{div}\,0, \Omega^-)$ is the space of divergence-free L^2 vector fields, and $\mathbf{W}$ is the space of gradients of harmonic H^1 vector fields. The essential spectrum of A_0 then results from

Theorem 2.10. *The operator A_0 is bounded and selfadjoint on $L^2(\Omega^-)$ with $\nabla H_0^1(\Omega^-)$, $H(\mathrm{div}\,0, \Omega^-)$ and $\mathbf{W}$ as invariant subspaces. On $\nabla H_0^1(\Omega^-)$: $A_0 u = u$, on $H(\mathrm{div}\,0, \Omega^-)$: $A_0 u = 0$, and on $\mathbf{W}$: $\gamma_n A_0 = (\frac{1}{2} + K_0')\gamma_n$, where K_0' is the operator of the normal derivative of the harmonic single layer potential.*

The well known properties of K_0' [Cos07] lead to the characterization of the essential spectrum of the volume integral operator A_k, denoted by $\sigma_e(A_k)$.

Corollary 2.11. *The essential spectrum of A_k is the same in $L^2(\Omega^-)$ and in $H(\mathrm{curl}, \Omega^-)$. There exist $0 < \lambda \leq \Lambda < 1$ such that $\sigma_e(A_k) \subset \{0, 1\} \cup [\lambda, \Lambda]$. If Γ is smooth, then $\lambda = \Lambda = \frac{1}{2}$, so that $\sigma_e(A_k) = \{0, \frac{1}{2}, 1\}$.*

The implementation done with El-Hadji Koné led to numerical results in the investigation of the spectrum of A_k when the dielectric is the unit ball (see Fig. 2.4).

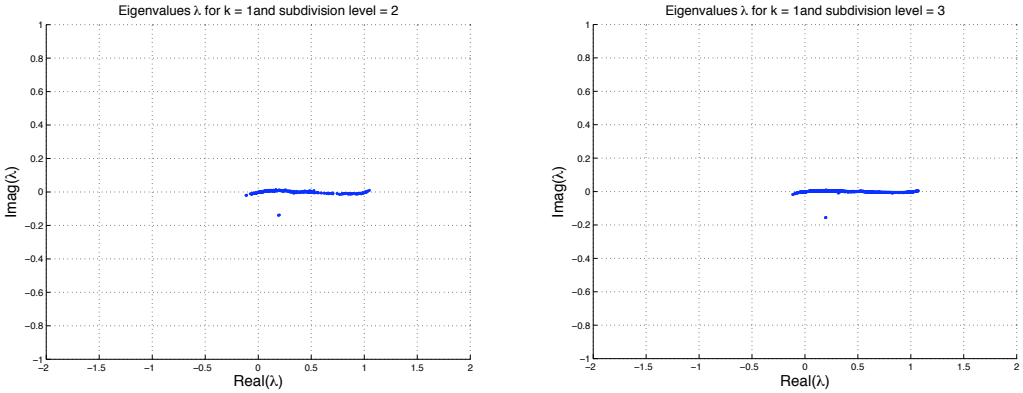

Figure 2.4. Numerical spectrum of A_k, wavenumber $k = 1$; left: mesh with 512 tetrahedra; right: mesh with 4096 tetrahedra.

2.3.2 The essential spectrum of the magnetic volume integral operator

Mapping properties show that it suffices to look at B_0 and integration by parts leads to

$$B_0 u(x) = u(x) + \nabla \int_{\Omega^-} g_0(x-y)\, \mathrm{div}\, u(y)\, dy - \nabla S_0 \gamma_n u(x) + \mathrm{curl}\, S_0 \gamma_\times u(x)\,. \tag{2.10}$$

By considering mapping properties of the involved operators and Lemma 2.9 with $T = (\gamma_n, \gamma_\times)$ and $S(v, w) = -\nabla S_0 v + \mathrm{curl}\, S_0 w$, the result is that for $\lambda \neq 1$, $\sigma_e(B_0) = \sigma_e(\widehat{B}_0)$, where $\widehat{B}_0$ is the system of boundary integral operators in the space $H^{-\frac{1}{2}}(\Gamma) \times H^{-\frac{1}{2}}(\mathrm{div}_\top, \Gamma)$

$$\widehat{B}_0 = \begin{pmatrix} \frac{1}{2} - K_0' & \gamma_n\, \mathrm{curl}\, S_0 \\ -\gamma_\times \nabla S_0 & \frac{1}{2} + M_0 \end{pmatrix}. \tag{2.11}$$

Here M_0 is defined by evaluating $n \times \mathrm{curl}\, S_0$ on the boundary. The knowledge of the surface integral operators leads to the result:

Theorem 2.12. *If Γ is smooth, then $\sigma_e(B_k) = \{0, \frac{1}{2}, 1\}$.*

Note that although we have obtained $\sigma_e(A_k) = \sigma_e(B_k^0) = \sigma_e(B_k) = \{0, \frac{1}{2}, 1\}$, the corresponding invariant subspaces are quite different for A_k and for B_k, and the commutator of A_k and B_k is not compact in $H(\mathrm{curl}, \Omega^-)$.

2.3.3 The essential spectrum of the complete volume integral operator

When both the parameters η and ν are not identically equal to zero, the operator of the volume integral equation is $\mathcal{A}_k^{\eta,\nu} = \eta A_k + \nu B_k$ on $H(\mathrm{curl}, \Omega^-)$. Repeating the arguments that led to (2.11), we find the spectrally equivalent system of boundary integral equations

$$\widehat{\mathcal{A}}_0^{\eta,\nu} = \begin{pmatrix} \frac{1}{2}(\nu+\eta) + (\eta-\nu)K_0' & \nu\gamma_n \operatorname{curl} S_0 \\ (\eta-\nu)\gamma_\times \nabla S_0 & \nu(\frac{1}{2} + M_0) \end{pmatrix} . \tag{2.12}$$

We define mappings T from $\mathbf{Y}$ to $\mathbf{Z} = H^{-\frac{1}{2}}(\Omega^-) \times H^{\frac{1}{2}}(\Omega^-) \times H^{-\frac{1}{2}}(\Omega^-)$ and S from $\mathbf{Z}$ to $\mathbf{Y}$ by $T(v,w) = (v, V_0 \operatorname{div}_\top w, V_0 \operatorname{curl}_\top w)$, $S(v,p,q) = ((\eta+\nu)v/2 + \nu q, (\nu-\eta)\,\mathbf{curl}_\top V_0 v - 2\nu\nabla_\top V_0 p + 2\nu\,\mathbf{curl}_\top V_0 q)$. Here V_0 is the boundary integral operator of the harmonic single layer potential and $\operatorname{curl}_\top$ and $\mathbf{curl}_\top$ are the scalar and vector surface curls. Then on a smooth boundary $ST - \widehat{\mathcal{A}}_0^{\eta,\nu}$ is compact in $\mathbf{Y}$, and TS acts in $\mathbf{Z}$ up to a compact perturbation as the multiplication with the constant matrix

$$A_0^{\eta,\nu} = \begin{pmatrix} \frac{\eta+\nu}{2} & 0 & \nu \\ 0 & \frac{\nu}{2} & 0 \\ \frac{\nu-\eta}{4} & 0 & \frac{\nu}{2} \end{pmatrix} .$$

Using Lemma 2.9, we see that $\sigma_e(\widehat{\mathcal{A}}_0^{\eta,\nu}) \setminus \{0\}$ in $\mathbf{Y}$ is given by the eigenvalues of the matrix $A_0^{\eta,\nu}$, which are $\{\frac{\eta}{2}, \frac{\nu}{2}, \nu\}$. It follows

Theorem 2.13. *If Γ is smooth and $\eta, \nu \in \mathbb{C}$, then for $\mathcal{A}_k^{\eta,\nu} = \eta A_k + \nu B_k$ we have $\sigma_e(\mathcal{A}_k^{\eta,\nu}) = \{0, \frac{\eta}{2}, \eta, \frac{\nu}{2}, \nu\}$.*

2.4 Perspectives

The explorations exposed in this chapter offer important information for the numerical resolution. A new PhD-project that we aim to advise with Martin Costabel consists of numerical improvements in the resolution of volume integral equations. The application of the Fast Multipole Method (Chapter 1) has to be studied. New and original numerical tools are considered in literature, the discrete dipole approximation [DF94, DF08, DF12], the reduced basis method [FHMS11, GHS12]; a thorough knowledge of their mathematical properties would be of great interest in recent applications of electromagnetic waves (photonic fibers, microresonators, ...). Collaborations with Stéphane Balac and other members of the institute FOTON (Fonctions Optiques pour les Technologies de l'informatiON) give us a favorable environment for such investigations.

Chapter 3

Integral representation: an exact artificial boundary condition

3.1 Introduction

The resolution of Maxwell equations in exterior domain can be realized using either finite elements or ultra-weak variational formulation (UWVF) [Ces96, CD03] in a bounded domain limited by an artificial boundary. The artificial boundary condition is a difficult issue which has been treated with different techniques: absorbing boundary conditions (ABC) [EM77, BGT82, ABB99], perfectly matched layers (PML) [Ber94] or integral representations [HL96]. For example, Huttunen et al [HMK02, HKM04, HMM07] considered the UWVF with PML. In this chapter, we analyse integral representations as exact boundary conditions for the resolution of Maxwell equations in exterior domain either with finite elements or ultra-weak variational formulation.

The combination of UWVF and integral representation is presented in Section 3.2 where the integral operators are numerically considered thanks to a Fast Multipole approximation [DM07, Dar08, DM12]. The impact of the FMM was shown in Section 1.5. Hereby, we focus on the application of the integral representation. This work is part of developments done with Peter Monk in the context of my postdoc position at the university of Delaware. Peter Monk's UWVF code is also a tool used to generate data for the Linear Sampling Method (LSM), an inverse problems solver. With Fioralba Cakoni and David Colton, we applied the LSM to screens [CCD03, CD05].

The second section of the chapter is devoted to a Schwarz interpretation of the combination of finite elements and integral representation. This work was done with Rania Rais and Nabil Gmati in the context of the PhD thesis of Rania Rais, with important developments in the finite element library MÉLINA++ with the contribution of Daniel Martin and Yvon Lafranche. Rania Rais first studied the case of Helmholtz equations [DGR10]. We hereby focus on the case of Maxwell equations [Rai14, DGR14, DGRon].

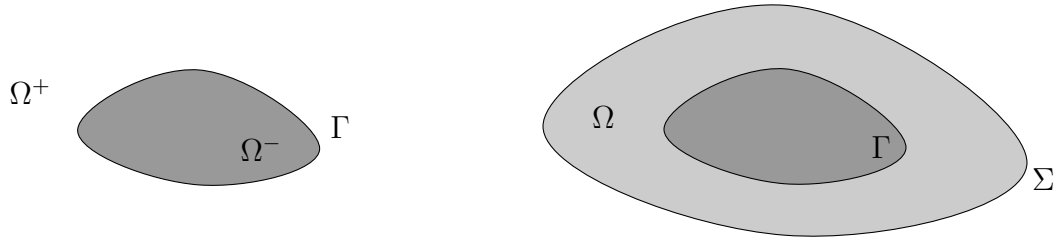

Figure 3.1. (*generated with Fig4TeX* [Laf11]) Left: the exterior unbounded domain Ω^+. Right: the computational domain Ω, the region outside the boundary of the impenetrable scatterer Ω^- and inside the artificial boundary Σ.

3.2 Ultra-Weak Variational Formulation and integral representation

3.2.1 Combination of UWVF and integral representation

To solve the time harmonic Maxwell system in the unbounded exterior of a bounded scatterer Ω^- (assumed to have connected complement and polyhedral surface Γ), we introduce a polyhedral artificial boundary Σ containing the scatterer in its interior and we denote by Ω the bounded annular domain between Γ and Σ (see Fig. 3.1). Hence, we are interested in the resolution of the time-harmonic Maxwell equations in the domain Ω: find the electric field $\mathbf{E}$ and magnetic field $\mathbf{H}$ such that the following equations hold:

$$\left.\begin{array}{l} \operatorname{curl}\mathbf{E} - \imath\omega\mu\mathbf{H} = m\,, \\ \operatorname{curl}\mathbf{H} + \imath\omega\varepsilon\mathbf{E} = j\,, \end{array}\right\} \quad \text{in } \Omega, \tag{3.1}$$

where m and j are given data vector functions specifying the volume sources, ε and μ are positive piecewise constant functions of position and $\omega > 0$ is the angular frequency of the field. Although not required by the method, we usually assume a source free region and select $m = j = 0$ (our numerical test will conform to this).

For the UWVF, it is convenient to specify the boundary condition on $\partial\Omega = \Gamma \cup \Sigma$ in the following non standard form ([CD03])

$$-\,|\,\sqrt{\varepsilon}\,|\,\mathbf{E}\times n + (|\,\sqrt{\mu}\,|\,\mathbf{H}\times n)\times n = Q(|\,\sqrt{\varepsilon}\,|\,\mathbf{E}\times n + (|\,\sqrt{\mu}\,|\,\mathbf{H}\times n)\times n) + g\,, \tag{3.2}$$

where n is the outward normal to Ω, $Q = 0$ gives the standard low order absorbing boundary condition on Σ and g is computed from the incident wave. Since we model the total field, we choose $g = 0$ on Γ and use Q to set the boundary condition. For example choosing $Q = 1$ gives the perfectly conducting boundary condition, while $|Q| < 1$ gives an impedance condition. The choice $Q = -1$ gives a magnetic wall condition that is useful for symmetric structures. On Σ, the choice of an integral representation corresponds to $Q = 0$ and g given by an integral operator.

The UWVF is based on the decomposition of the domain Ω into tetrahedra $\{\Omega_k\}_{k=1,\dots,K}$ and it computes the impedance trace of the solution on the boundaries of all these tetrahedra which can then be post processed to give the solution in the entire element. This variational formulation is defined on the Hilbert space $V = \prod_{k=1}^{K} L_t^2(\partial\Omega_k)$ where $L_t^2(\partial\Omega_k)$ is the space of

square integrable tangential fields on $\partial\Omega_k$ the boundary of Ω_k. For this space the scalar product is given by

$$(\mathcal{X},\mathcal{Y})_V = \sum_k \int_{\partial\Omega_k} \mathcal{X}|_{\partial\Omega_k}\overline{\mathcal{Y}|_{\partial\Omega_k}}.$$

Under the assumption that ε and μ are positive constants on each element Ω_k, $(\mathbf{E},\mathbf{H})$ is found through the restriction of the field $(\mathbf{E}_k,\mathbf{H}_k)$ to $\partial\Omega_k$, where $(\mathbf{E}_k,\mathbf{H}_k) = (\mathbf{E},\mathbf{H})|_{\Omega_k}$. The method then solves for an unknown function $\mathcal{X} \in V$, defined element by element by the impedance trace $\mathcal{X}|_{\partial\Omega_k} \in L_t^2(\partial\Omega_k)$ on $\partial\Omega_k$ and

$$\mathcal{X}|_{\partial\Omega_k} = \sqrt{\widetilde{\varepsilon}|_{\partial\Omega_k}}(\mathbf{E}_k \times n_k) + \sqrt{\widetilde{\mu}|_{\partial\Omega_k}}((\mathbf{H}_k \times n_k) \times n_k)\,. \tag{3.3}$$

where $\widetilde{\varepsilon}|_{\partial\Omega_k}$ and $\widetilde{\mu}|_{\partial\Omega_k}$ are quantities defined by the values of ε and μ on each side of $\partial\Omega_k$ (see [DM07] for details), and n_k is the exterior normal to $\partial\Omega_k$.

The UWVF involves two operators Π and F defined in [CD03, Ces96]. The operator $\Pi : V \to V$ switches boundary traces across faces shared by two tetrahedra and involves the boundary condition (3.2) through the function Q on faces which contribute to the boundaries Σ and Γ. More precisely if elements Ω_j and Ω_k meet at a face $f_{j,k}$ then

$$\Pi\mathcal{X}_j|_{f_{j,k}} = \mathcal{X}_k|_{f_{j,k}}$$

and on a boundary face of an element Ω_k, $\Pi\mathcal{X}_k|_{\partial\Omega} = Q\mathcal{X}_k|_{\partial\Omega}$. The operator $F : V \to V$ is a local operator that links the outgoing and incoming impedance traces of the degrees of freedom on the interfaces between tetrahedra. If (u,v) satisfy the Maxwell system on Ω_k and $\mathcal{X}_k = \sqrt{\widetilde{\varepsilon}|_{\partial\Omega_k}}(u\times n_k)+\sqrt{\widetilde{\mu}|_{\partial\Omega_k}}((v\times n_k)\times n_k)$ then $F(\mathcal{X}_k) = \sqrt{\widetilde{\varepsilon}|_{\partial\Omega_k}}(u\times n_k)-\sqrt{\widetilde{\mu}|_{\partial\Omega_k}}((v\times n_k)\times n_k)$.

The UWVF of Maxwell's equations is as follows [CD03, Ces96]: find $\mathcal{X} \in V$ such that

$$(\mathcal{X},\mathcal{Y})_V - (\Pi\mathcal{X}, F\mathcal{Y})_V = (\widetilde{b},\mathcal{Y})_V \quad \text{for all } \mathcal{Y} \in V, \tag{3.4}$$

for all $\mathcal{Y} \in V$ where $\tilde{g}$ is the extension by zero of g to a function in V.

Thus by taking a finite dimensional subspace $V_h \subset V$ and using basis functions Z_i, $i \in J$ for V_h, a Galerkin discretization of the formulation (3.4) leads to problem of finding $\mathcal{X}_h = \sum_{i\in J} X_i Z_i \in V_h$ such that $(\mathcal{X}_h,\mathcal{Y}_h)_V - (\Pi\mathcal{X}_h, F\mathcal{Y}_h)_V = (\widetilde{g},\mathcal{Y}_h)_V$ for all $\mathcal{Y}_h \in V_h$.

Equivalently, in matrix-vector form, we seek to compute $X = [X_1,\cdots,X_{\mathrm{card}(J)}]^T$ such that

$$(A-C)X = b\,, \tag{3.5}$$

where A is the matrix with (i,j)th entry $(Z_j,Z_i)_V$ and C has (i,j)th entry given by $(\Pi Z_j, FZ_i)_V$. The data vector b is derived from the right hand side above in the same way.

As usual for the UWVF, to facilitate calculating the action of F, on each element Ω_k we use a basis generated by taking the impedance trace of p_k plane waves satisfying the adjoint Maxwell system on Ω_k ($p_k/2$ directions with two polarizations for each direction). In particular to discretize the problem, we follow [CD03] and use boundary functions given by

$$\mathcal{Y}|_{\partial\Omega_k} = \sqrt{\widetilde{\varepsilon}|_{\partial\Omega_k}}(\mathbf{E}'_k \times n_k) + \sqrt{\widetilde{\mu}|_{\partial\Omega_k}}((\mathbf{H}'_k \times n_k) \times n_k)$$

where the fields $(\mathbf{E}'_k, \mathbf{H}'_k)$ are taken from the span of a set of p_k plane waves that satisfy the adjoint Maxwell problem

$$\begin{cases} \operatorname{curl} \mathbf{E}'_k - \imath\omega\overline{\mu_{\Omega_k}}\mathbf{H}'_k = 0 \text{ in } \Omega_k, \\ \operatorname{curl} \mathbf{H}'_k + \imath\omega\overline{\varepsilon_{\Omega_k}}\mathbf{E}'_k = 0 \text{ in } \Omega_k. \end{cases}$$

In (3.4), $\widetilde{b} \in V$ is derived from the right hand side of (3.1) and from g given in (3.2). At least six plane waves (and usually more) are used per element, counting polarizations.

The UWVF leads to a sparse square system of size $(\sum_{k=1}^{K} p_k)$. The number of plane waves p_k is chosen depending on the local wavelength and diameter of the element (see [HMM07]).

Compared to more classical volume methods, the UWVF enables one to reduce the number of elements in the mesh. The complexity of the method is then linked to the number of elements in the mesh and the number of basis functions per element. For concreteness, suppose the electromagnetic parameters of the domain are constant and define the wavenumber $\kappa = \omega\sqrt{\varepsilon\mu}$. A closer consideration of the complexity needs the introduction of another parameter: K_0 denotes the average number of tetrahedra taken in one dimension so that $K \sim K_0^3$. As a volume method, the UWVF method leads to a sparse system: the number of degrees of freedom is of order $K_0^3\, p$ and the complexity of the algorithm is $\mathcal{O}(K_0^3\, p^2)$ where p denotes the average number of basis functions per tetrahedron which typically satisfies $K_0\, p \sim \kappa$ [HMM07].

In this section, we focus on the coupling of integral representation and UVWF. To simplify the presentation we suppose that $\varepsilon = \mu = 1$ so that the exterior domain is entirely homogeneous and we use the perfectly conducting boundary condition on Γ (i.e. the scatterer is not penetrable and the exterior medium is homogeneous). In this case we may define the integral representation from the fields on Γ (extensions to more general domains require to introduce another intermediate boundary such that the domain is homogeneous between Σ and this intermediate boundary). In this case the artificial boundary Σ can be taken very close to the boundary of the obstacle. Following Hazard and Lenoir [HL96], the hybrid scheme consists in replacing the low order absorbing boundary condition $-\mathbf{E} \times n + (\mathbf{H} \times n) \times n = -\mathbf{E}_0 \times n + (\mathbf{H}_0 \times n) \times n$ on Σ by the boundary condition

$$-\mathbf{E} \times n + (\mathbf{H} \times n) \times n = -\mathbf{E}^s \times n + (\mathbf{H}^s \times n) \times n - \mathbf{E}_0 \times n + (\mathbf{H}_0 \times n) \times n\,,$$

where $(\mathbf{E}^s, \mathbf{H}^s)$ are given by the Stratton-Chu formula ([CK98]) in terms of $n \times \mathbf{H}$ and $n \times \mathbf{E}$ on Σ (i.e. under our assumptions on Γ) via

$$\begin{aligned} \mathbf{E}^s(x) &= \operatorname{curl}_x \int_\Gamma G(x,y)\, n_\gamma(y) \times \mathbf{E}(y)\, d\gamma(y) \\ &\quad -\frac{1}{\imath\,\omega} \operatorname{curl}_x \operatorname{curl}_x \int_\Gamma G(x,y)\, n_\gamma(y) \times \mathbf{H}(y)\, d\gamma(y)\,, \qquad (3.6) \\ \mathbf{H}^s(x) &= \operatorname{curl}_x \int_\Gamma G(x,y)\, n_\gamma(y) \times \mathbf{H}(y)\, d\gamma(y) \\ &\quad +\frac{1}{\imath\,\omega} \operatorname{curl}_x \operatorname{curl}_x \int_\Gamma G(x,y)\, n_\gamma(y) \times \mathbf{E}(y)\, d\gamma(y)\,, \qquad (3.7) \end{aligned}$$

where n_γ is the exterior normal to the surface Γ and $G(x,y) = \exp(\imath\kappa|x-y|)/(4\pi|x-y|)$ is Helmholtz fundamental solution. Thanks to the structure of the unknowns of the UWVF, as shown in [DM07], the fields in the integrands above can be computed directly from the degrees

of freedom of the UWVF (3.3) taking into account the convention for the direction of normals, and the boundary condition on Γ (3.2) where $g = 0$.

The system (3.5) becomes $(A - C - \widetilde{C})X = b$ where $\widetilde{C}$ couples the degrees of freedom on Γ and Σ. The matrix $\widetilde{C}$ can be split into different discrete integral operators $\widetilde{C}_i\,,\ i = 1, ..., 4$ of the form

$$(\widetilde{C}_i\,\mathcal{X}_h)_{kl} = \int_{\Sigma_{kk}^{\text{ext}}} c_k\, S_i(\mathcal{X}_h)\ \cdot\ \overline{F\mathcal{Y}_{kl}}\, d\sigma\ ,$$

where

- Σ_{kk}^{ext} is the face on Σ of a tetrahedron intersects the exterior boundary,
- c_k depends only on ε and μ on Σ_{kk}^{ext},
- F is the local operator introduced in (3.4),
- S_i is a global operator which comes from the right hand side of (3.6)-(3.7), for instance

$$(S_1(\mathcal{X}))(x) = \left(- \int_\Gamma f_Q(y)\, \nabla_y G(x,y) \times \mathcal{X}(y)\, d\gamma(y) \right) \times n(x)\ ,$$

  where f_Q is a function involving Q and ε. The action of these integral operators can be evaluated by the FMM.

In this work, the solution of the new system $(A - C - \widetilde{C})X = b$ is obtained by the same method (BiCGStab) as used for the classical UWVF system $(A - C)X = b$, considering $C + \widetilde{C}$ as a small perturbation of C. It is important to note that we never compute $\widetilde{C}$ explicitly, but evaluate its action as needed by the FMM.

The integral representation aims to reduce the distance of the absorbing boundary from the scatterer to a number of elements independent of κ. We then have a number of elements in the mesh of order K_0^2. This reduces the complexity related to the volume calculation. The FMM is used to control the cost of the calculation related to the integral operators which give rise to large dense blocks in the discrete system.

In the sequel, numerical results illustrate the impact of the use of an integral representation as an exact boundary artificial condition for the UWVF. These results are for the problem of approximating scattering by a perfectly conducting unit sphere. This very simple example has the advantage that a Mie series solution is available for comparison (other geometrical configurations were considered in [DM12]). Results from four codes are presented: the classical UWVF with a Silver-Müller type low order auxilliary boundary condition of order 0 (i.e the standard UWVF with the boundary condition described earlier setting $Q = 0$), the code UWVF+IR with integral representation but without FMM, the code UWVF+IR+SLFMM using a single-level FMM and the code UWVF+IR+MLFMM using a multilevel FMM. All the resuts concerned by computational costs comparisons were obtained on an Apple Mac Pro with 2×3GHz quad-core Xeon processors using 16 Gb RAM.

For approximating scattering by the unit sphere, the exterior boundary Σ is taken to be a concentric sphere. We have experimented with several exterior boundaries giving rise to different meshes as defined in [DM07]. Table 3.1 describes those considered in this section. The names "Sxxx" denote the different meshes, where "xxx" denotes the distance between Γ and Σ in centimeters. For $\kappa = 4$ the distance from the perfect conductor to the artificial boundary ranges from 0.16λ (S025) to 2.6λ (S400) where $\lambda = 2\pi/\kappa$ is the wavelength.

Table 3.1. A summary of the meshes used in this study.

Name	S400	S200	S100	S075	S050	S025
Radius in m	5	3	2	1.75	1.5	1.25
Distance between Γ and Σ	$\approx 2.6\lambda$	$\approx 1.3\lambda$	$\approx 2\lambda/3$	$\approx \lambda/2$	$\approx \lambda/3$	$\approx \lambda/6$
Number of tetrahedra	16179	14526	40609	30133	21083	11008
Number of basis functions per tetrahedron	8 to 128	8 to 72	10 to 32	10 to 30	8 to 28	10 to 24
Number of DoF	880200	508450	753616	536874	356666	178146

All the meshes have been generated using FEMLab. The meshes S400 and S200 are appropriate for a classical use of the UWVF. The other meshes have been generated optimizing the ratio between the average edge-length h and the wavelength λ to $h \approx \lambda/5$. These meshes are quite uniform (the $S400$ and $S200$ meshes are graded to give larger elements away from the scatterer). The large number of tetrahedra in S025 might appear to be a disadvantage for the UWVF+IR+[S/M]LFMM codes (the number of tetrahedra is comparable to S400). However the number of degrees of freedom (DoF) is much less than for S400 because fewer plane waves are used per element due to the smaller size of elements as shown in the bottom row of Table 3.1.

In Figs. 3.2 and 3.3, we clearly see the impact of the integral representation on the accuracy of the result: when considering a closer and closer exterior boundary, the classical UWVF code, as is well known, gives worse and worse results. On the other hand, with the different meshes, the code UWVF+IR+SLFMM gives more or less identical results which fit with the Mie series solution, even with the thin mesh S025. Similar results are obtained for the TM polarization (see Fig. 3.4). The results obtained with the code UWVF+IR+MLFMM, in Fig. 3.5, are comparable to those of the code UWVF+IR+SLFMM, indicating that use of the multilevel scheme does not degrade the FMM accuracy.

The algorithm complexity is derived in details in Section 1.5. CPU-time, memory requirements and error measures are given in the case of the TE polarization in Table 3.2. The results are given for the meshes S400 and S200 using the classical UWVF code and for the mesh S025 using the codes UWVF+IR+SLFMM (S025 - S) and UWVF+IR+MLFMM (S025 - M). In the table we use the notation introduced in Section 1.5 (units are seconds and Giga-bytes).

The RCS curve obtained with S200 using the UWVF code could be acceptable, however its accuracy is quite poor in comparison with the one obtained with S025 using the codes UWVF+IR+SLFMM and UWVF+IR+MLFMM hence we should compare results for S400 and S025 in Table 3.2. That case shows that the UWVF+IR+MLFMM code reduces computer time by approximately 50% and the memory needed by almost 75% for roughly the same RMS error.

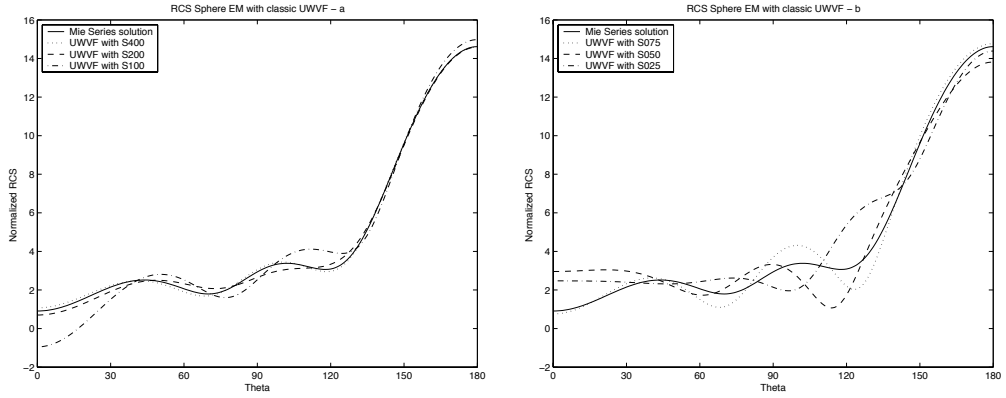

Figure 3.2. The TE-polarized RCS as a function of polar coordinate θ computed using the classical UWVF code with the meshes in Table 3.1 compared to the Mie series solution. Left: the larger diameter meshes (S400, S200, S100). Right: the smaller diameter meshes (S025, S050, S075). Only the meshes S400 and S200 gives results close to the Mie series.

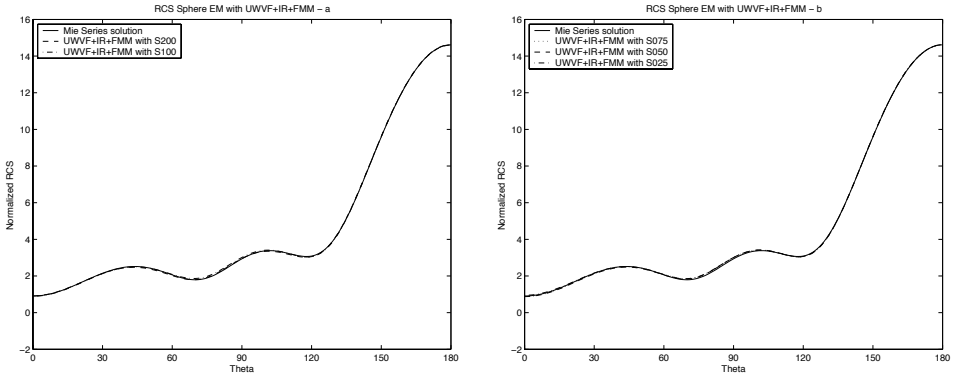

Figure 3.3. The TE-polarized RCS as a function of polar coordinate θ computed using the new UWVF+IR+SLFMM code with meshes in Table 3.1 compared to the Mie series solution. Left: results for the larger diameter meshes (S200, S100). Right: the smaller diameter meshes (S075, S050, S025). All the meshes give results in good agreement with the Mie series.

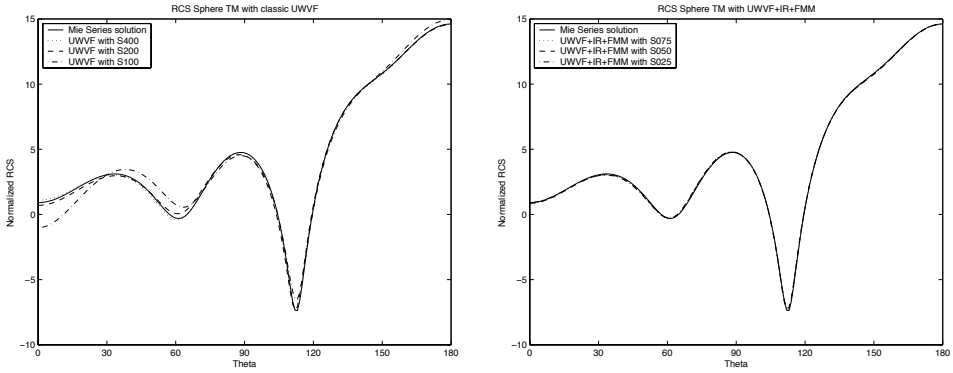

Figure 3.4. The TM-polarized RCS as a function of polar coordinate θ computed using the two codes in the study. Left: results for the classical UWVF code with meshes S400, S200 and S100. Right: results for the new code with the meshes S025, S050 and S075. For the UWVF+IR+SLFMM the results are almost independent of the distance of the auxiliary boundary from the scatterer, whereas the classical UWVF requires to mesh a large region of space.

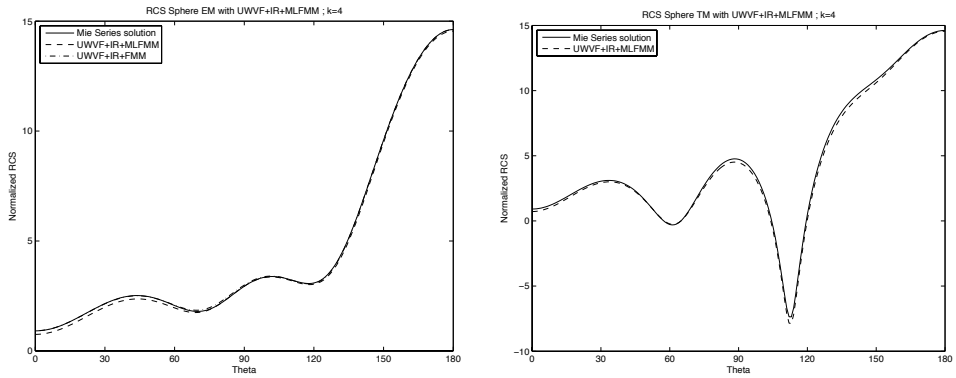

Figure 3.5. The RCS as a function of polar coordinate θ computed using the three codes in the study, with $\kappa = 4$. Left: TE-polarized RCS with the codes UWVF+IR+SLFMM and UWVF+IR+MLFMM with the mesh S025. Right: TM-polarized RCS with the code UWVF+IR+MLFMM (dashed line) with the mesh S025 and the exact solution (solid line).

Table 3.2. Computational costs comparisons between the UWVF (S400; S200), UWVF+IR+SLFMM (S025 - S) and UWVF+IR+MLFMM (S025 - M) for scattering by a unit sphere at constant κ. For more details of the meshes see Table 3.1. The RCS error is computed via the Mie series.

Case	κ	CPU	MEM.	Rel Err 2	Rel Err ∞	RMS error
S400	4	1725	6.2	$1.5\ 10^{-2}$	$1.1\ 10^{-2}$	$9.5\ 10^{-2}$
S200	4	462	1.8	$3.2\ 10^{-2}$	$2.5\ 10^{-2}$	$2\ 10^{-1}$
S025 - S	4	838	2.8	$4.6\ 10^{-3}$	$5.1\ 10^{-3}$	$2.8\ 10^{-2}$
S025 - M	4	798	1.6	$1.7\ 10^{-2}$	$1.1\ 10^{-2}$	$1.1\ 10^{-1}$

3.2.2 Linear sampling method

Peter Monk's UWVF code is a tool used to generate data for the Linear Sampling Method (LSM), an inverse problems solver. The LSM solves the inverse problem of determining the shape of a body from the knowledge of the incident electromagnetic plane wave and the electric far field pattern of the scattered wave. The method was introduced by D. Colton and A. Kirsch ([CK96]) for the Helmholtz equation with Dirichlet boundary conditions and was further developed for more complicated boundary conditions and Maxwell equations (see e.g. [CCM04, CC03a, CHP03]). In [CC03b], the LSM was adapted to obstacles with empty interior by D. Colton and F. Cakoni for the case of mixed cracks in $\mathbb{R}^2$. In papers [CCD03, CD05], with D. Colton and F. Cakoni, we applied the LSM to screens and mixed screens, open surfaces in $\mathbb{R}^3$. The theoretical results show that the LSM is very suitable to arrive at the solution of the inverse problem for perfectly conducting screens or for screens with mixed type boundary conditions (perfectly conducting boundary condition on one side and impedance boundary condition one the other side).

Some numerical results are illustrated in this section. Figs. 3.6, 3.7, 3.8 give the reconstruction of perfectly conducting screens and mixed screens. For more details on the method and its use, we refer to the given references.

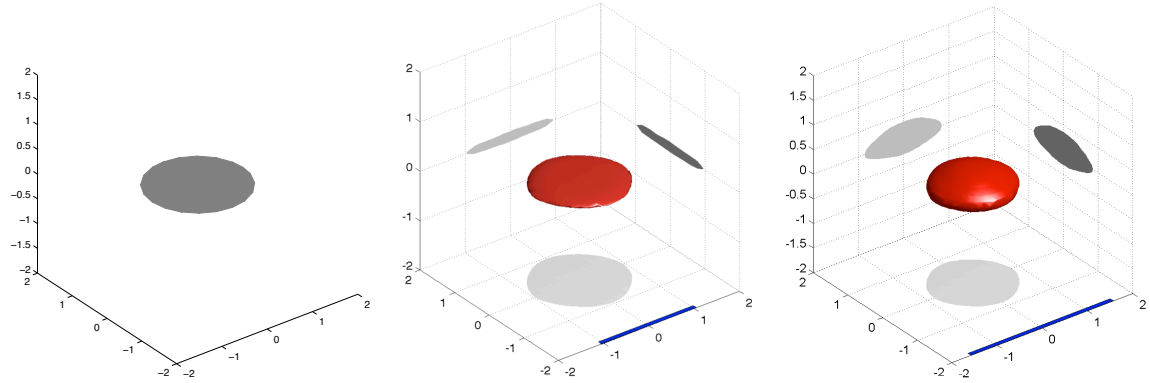

Figure 3.6. The unit disc: exact and reconstructed objects. Center: the screen is a perfect conductor. Right: the upper side of the screen satisfies an impedance boundary condition.

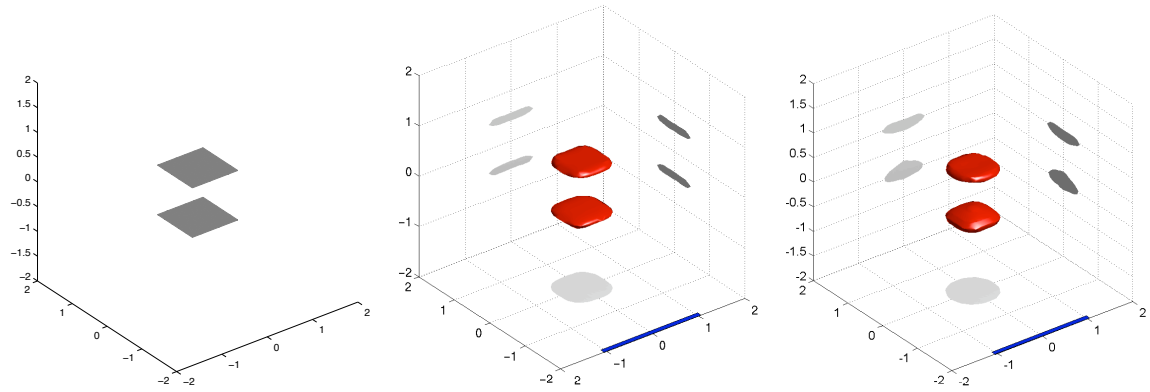

Figure 3.7. Two parallel squares: exact and reconstructed objects. Center: the screen is a perfect conductor. Right: the upper square is a perfect conductor on both sides, and the upper side of the lower square satisfies an impedance boundary condition while the other side is perfectly conducting.

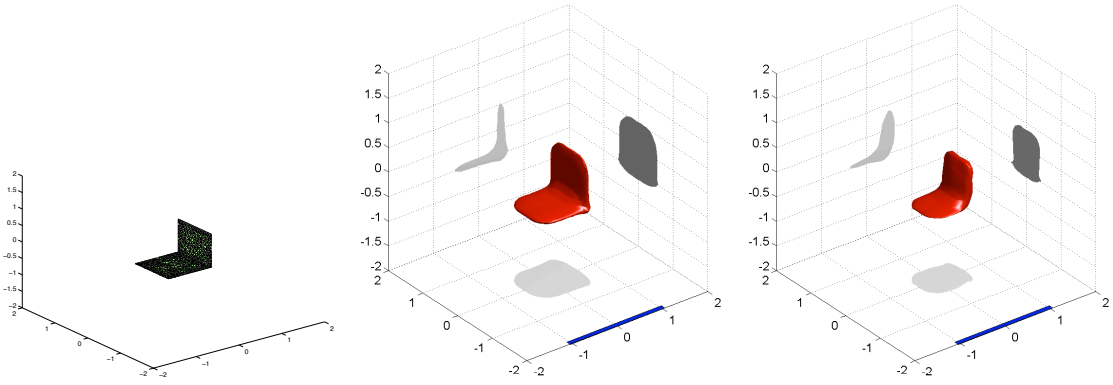

Figure 3.8. A L-shape object: exact and reconstructed objects. Center: the screen is a perfect conductor. Right: the screen satisfies a perfectly conducting boundary condition on all sides except for the inner side of the vertical square which satisfies an impedance boundary condition.

3.3 Coupling of finite elements and integral representation

In this section, the resolution of the 3D exterior time-harmonic Maxwell equations is done by a combination of finite elements and integral representation ([HL96]). Like in previous section, this strategy leads to an equivalent problem on a reduced bounded domain delimited by the surface of the scatterer and an artificial boundary with exact artificial boundary condition. No *a priori* condition is required on the distance between the scatterer and the artificial boundary but a difficult issue consists in the elaboration of a resolution strategy. A relevant idea was suggested in [LJ01]. We propose the interpretation of this idea as an application of the Schwarz method, following the work done in [BBFGJ05] for Helmholtz equation. Hence, the theory on the Schwarz method justifies the use of Krylov solvers and the choice of a preconditioner.

Let us consider Ω^- a bounded scatterer in $\mathbb{R}^3$ with a regular boundary Γ and Ω^+ its unbounded complementary. We are concerned with the scattering of a time-harmonic electromagnetic wave by the perfect conductor Ω^-. Our purpose is to determine the total field $\mathbf{E} = \mathbf{E}^s + \mathbf{E}^{\text{inc}}$ where $\mathbf{E}^{\text{inc}}$ is the incident wave and $\mathbf{E}^s$ is the scattered field, solution to the regularized Maxwell equations with essential boundary condition on Γ and radiation condition at infinity. Considering an integral representation on an artificial boundary Σ (see Fig. 3.1), the exterior problem reduces to a problem on the bounded domain Ω delimited by Γ and Σ (see [HL96]): Find $\mathbf{E}$ such that

$$\left\{\begin{array}{l} \operatorname{curl}\operatorname{curl}\mathbf{E} - t^{-1}\nabla(\operatorname{div}\mathbf{E}) - k_s^2\mathbf{E} = 0 \text{ in } \Omega, \\ \mathbf{E}\times n_\gamma = 0, \operatorname{div}\mathbf{E} = 0 \text{ on } \Gamma, \\ T_{\nu_1}(\mathbf{E}) = T_{\nu_1}(\mathbf{E}^{\text{inc}} - \mathcal{I}_\Gamma(\mathbf{E})) \text{ and } N_{\nu_2}(\mathbf{E}) = N_{\nu_2}(\mathbf{E}^{\text{inc}} - \mathcal{I}_\Gamma(\mathbf{E})) \text{ on } \Sigma, \end{array}\right. \tag{3.8}$$

where n_γ is the exterior normal to Γ (outgoing from Ω^-); the regularization term $t^{-1}\nabla(\operatorname{div}\mathbf{E})$ allows the use of a Galerkin finite element method (see [HL96]) and the regularization parameter t^{-1} depends on the permittivity and the permeability of the air; k_s is the wavenumber; ν_1 and ν_2 are complex numbers which have a negative imaginary part. The two operators T_{ν_1} and N_{ν_2} are defined by $T_{\nu_1}\mathbf{E} = \operatorname{curl}\mathbf{E}\times n_\sigma + \nu_1\, n_\sigma \times (\mathbf{E}\times n_\sigma)$ and $N_{\nu_2}\mathbf{E} = \operatorname{div}\mathbf{E} + \nu_2\mathbf{E}\cdot n_\sigma$ with n_σ the exterior normal to Σ (outgoing from Ω). The boundary conditions on Σ are derived from the integral representations satisfied by the scattered field and identified by the following expression ([HL96]): for $x \in \Omega^+$,

$$\begin{aligned} \mathcal{I}_\Gamma(\mathbf{E})(x) \;=\; & -k_s^2\int_\Omega \mathcal{R}\mathcal{G}_t(x,.)\mathbf{E} + \int_\Omega \operatorname{curl}\mathcal{R}\mathcal{G}_t(x,.)\operatorname{curl}\mathbf{E} \\ & + t^{-1}\int_\Omega \operatorname{div}\mathcal{R}\mathcal{G}_t(x,.)^T\operatorname{div}\mathbf{E} - t^{-1}\int_\Gamma \operatorname{div}\mathcal{G}_t(x,.)^T(\mathbf{E}\cdot n_\gamma)d\gamma, \end{aligned}$$

where $\mathcal{G}_t = G_{k_s}I + \dfrac{1}{k_s^2}\operatorname{Hess}(G_{k_s} - G_{k_p})$ is the outgoing Green tensor associated with the differential operator $\operatorname{curl}\operatorname{curl} - t^{-1}\nabla(\operatorname{div}) - k_s^2 I$ of the regularized Maxwell equation; I is the identity matrix in $\mathbb{R}^3$; Hess stands for Hessian operator; $k_p = \sqrt{t}k_s$ and G_k is the fundamental solution of Helmholtz equation; $\mathcal{R}$ is a linear operator that maps every regular function φ defined on Γ into a regular function $\mathcal{R}\varphi$ defined on Ω which satisfies $\mathcal{R}\varphi = \varphi$ on Γ and $\mathcal{R}\varphi = 0$ on Σ. The consideration of the Hilbert space

$$\mathcal{H}_t = \left\{\mathbf{E} \in H(\operatorname{curl},\Omega)/\operatorname{div}\mathbf{E} \in L^2(\Omega), \mathbf{E}\times n_\gamma = 0 \text{ on } \Gamma, \mathbf{E}\times n_\sigma \in L^2(\Sigma)^3, \mathbf{E}\cdot n_\sigma \in L^2(\Sigma)\right\},$$

enables one to write a variational formulation of the problem (3.8): Find $\mathbf{E} \in \mathcal{H}_t$ such that

$$(\mathcal{A}_t + \mathcal{C}_t)\mathbf{E} = F_t, \tag{3.9}$$

where the operators $\mathcal{A}_t$ and $\mathcal{C}_t : \mathcal{H}_t \to \mathcal{H}_t$ are defined as follows

$$\begin{aligned}(\mathcal{A}_t\mathbf{E}, \mathbf{E}')_t &= \int_\Omega (\operatorname{curl}\mathbf{E} \cdot \operatorname{curl}\mathbf{E}' + t^{-1}\operatorname{div}\mathbf{E}\operatorname{div}\mathbf{E}' - k_s^2\mathbf{E}\cdot\mathbf{E}') \\ &\quad + \int_\Sigma (\nu_1(n_\sigma\times\mathbf{E})\cdot(n_\sigma\times\mathbf{E}') + t^{-1}\nu_2(n_\sigma\cdot\mathbf{E})(n_\sigma\cdot\mathbf{E}'))d\sigma,\end{aligned}$$

$$(\mathcal{C}_t\mathbf{E}, \mathbf{E}')_t = \int_\Sigma T_{\nu_1}(\mathcal{I}_\Gamma(\mathbf{E}))\cdot\mathbf{E}'d\sigma + t^{-1}\int_\Sigma N_{\nu_2}(\mathcal{I}_\Gamma(\mathbf{E}))(n_\sigma\cdot\mathbf{E}')d\sigma,$$

and F_t is given by $(F_t, \mathbf{E}')_t = \int_\Sigma (T_{\nu_1}(\mathbf{E}^{\text{inc}})\cdot\mathbf{E}' + t^{-1}N_{\nu_2}(\mathbf{E}^{\text{inc}})(n_\sigma\cdot\mathbf{E}'))d\sigma$, where $(\cdot,\cdot)_t$ is the scalar product on $\mathcal{H}_t$.

The problem (3.9) is well posed as explained in [HL96] and the operator $\mathcal{A}_t$ is invertible.

The question of the resolution has been tackled by J. Jin and J.-M. Liu [LJ01] who suggested to solve (3.9) by considering $\mathcal{C}_t$ in the right hand side. An application of the fixed point algorithm leads to finding $\mathbf{E}_{n+1}$ such that

$$\begin{cases} \operatorname{curl}\operatorname{curl}\mathbf{E}_{n+1} - t^{-1}\nabla(\operatorname{div}\mathbf{E}_{n+1}) - k_s^2\mathbf{E}_{n+1} = 0 \text{ in } \Omega, \\ \mathbf{E}_{n+1}\times n_\gamma = 0, \operatorname{div}\mathbf{E}_{n+1} = 0 \text{ on } \Gamma, \\ T_{\nu_1}(\mathbf{E}_{n+1}) = T_{\nu_1}(\mathbf{E}^{\text{inc}} - \mathcal{I}_\Gamma(\mathbf{E}_n)) \text{ and } N_{\nu_2}(\mathbf{E}_{n+1}) = N_{\nu_2}(\mathbf{E}^{\text{inc}} - \mathcal{I}_\Gamma(\mathbf{E}_n)) \text{ on } \Sigma. \end{cases} \tag{3.10}$$

In papers [DGR14, DGRon], we interprete the algorithm defined by (3.10) as a Schwarz method. This interpretation has been initially proposed for the case of Helmholtz equation in [BBFGJ05]. The strategy is designed by the Total Overlapping Schwarz Method. Indeed the overlapping area is the total domain Ω. We hereby extend their work to the case of Maxwell equations: it consists in replacing equivalently the problem (3.10) by the two following subproblems. The first one is a transmission problem:

$$\begin{cases} \operatorname{curl}\operatorname{curl}\mathbf{E}_{2n+1} - t^{-1}\nabla(\operatorname{div}\mathbf{E}_{2n+1}) - k_s^2\mathbf{E}_{2n+1} = 0 \text{ in } \Omega^-\cup\Omega^+, \\ n_\gamma\times[\mathbf{E}_{2n+1}] = 0,\ n_\gamma\times[\operatorname{curl}\mathbf{E}_{2n+1}] = -n_\gamma\times\operatorname{curl}\mathbf{E}_{2n} \text{ on } \Gamma, \\ [\operatorname{div}\mathbf{E}_{2n+1}] = 0,\ n_\gamma\cdot[\mathbf{E}_{2n+1}] = -n_\gamma\cdot\mathbf{E}_{2n} \text{ on } \Gamma, \\ \lim\limits_{\rho\to\infty}\int_{||x||=\rho} ||\operatorname{curl}\mathbf{E}^s_{2n+1}\times n_\sigma - ik_s n_\sigma\times(\mathbf{E}^s_{2n+1}\times n_\sigma)||^2 d\sigma = 0, \\ \lim\limits_{\rho\to\infty}\int_{||x||=\rho} |\sqrt{t^{-1}}\operatorname{div}\mathbf{E}^s_{2n+1} - ik_s\mathbf{E}^s_{2n+1}\cdot n_\sigma|^2 d\sigma = 0. \end{cases} \tag{3.11}$$

The second one consists in finding $\mathbf{E}_{2n+2}$ such that

$$\begin{cases} \operatorname{curl}\operatorname{curl}\mathbf{E}_{2n+2} - t^{-1}\nabla(\operatorname{div}\mathbf{E}_{2n+2}) - k_s^2\mathbf{E}_{2n+2} = 0 \text{ in } \Omega, \\ \mathbf{E}_{2n+2}\times n_\gamma = 0,\ \operatorname{div}\mathbf{E}_{2n+2} = 0 \text{ on } \Gamma, \\ T_{\nu_1}(\mathbf{E}_{2n+2}) = T_{\nu_1}(\mathbf{E}_{2n+1}) \text{ and } N_{\nu_2}(\mathbf{E}_{2n+2}) = N_{\nu_2}(\mathbf{E}_{2n+1}) \text{ on } \Sigma. \end{cases} \tag{3.12}$$

The solution $\mathbf{E}_{2n+1}$ of (3.11) has an explicit expression given by an integral representation. By inserting this representation in the second condition of (3.12) we effectively obtain the solution

of (3.10). At the iteration n, the Schwarz algorithm is defined by $\mathcal{A}_t\mathbf{E}_{n+1} = -\mathcal{C}_t\mathbf{E}_n + F_t$. Numerically, we use the scheme suggested by J. Jin and J.-M. Liu and do not use the subproblems (3.11) and (3.12). The intermediate problems (3.11) and (3.12) are used for theoretical justifications. This enables one to derive convergence estimations that cannot be obtained directly from the system (3.10).

In [Rai14], Rania Rais investigated an analytical calculation of the rate of convergence of the Total Overlapping Schwarz method in a spherical configuration, case where Ω^- is a perfectly conducting ball. Let us consider the scatterer to be a ball of radius R_*. We suppose that the artificial boundary Σ is a sphere concentric to Γ with radius $R > R_*$. We first introduce some notations: We denote by j_l the spherical Bessel function of degree l, by h_l the spherical Hankel function of the first kind of degree l and $H_l(r) = h_l(r) + rh_l'(r)$, $J_l(r) = j_l(r) + rj_l'(r)$. We introduce the tangential vector spherical harmonics on the unit sphere S^2, $U_{lm} = (1/\sqrt{l(l+1)})\nabla Y_l^m$ and $V_{lm} = n_\gamma \times U_{lm}$, where Y_l^m, $l > 0$, $m = -l, ..., l$ are the orthonormal scalar spherical harmonics (complete basis of $L^2(S^2)$). The sets of U_{lm} and V_{lm} form a complete orthonormal basis for $T^2(S^2) := \{a : S^2 \to \mathbb{C}^3 \ / \ a \in (L^2(S^2))^3, a \cdot n_\gamma = 0\}$.

We define the error $(\mathbf{w}_n)_n$ on the field $\mathbf{E}$ at each iteration by:

$$\mathbf{w}_{2n+1} = \mathbf{E}_{2n+1} - \mathbf{E} \text{ in } \Omega^+, \quad \mathbf{w}_{2n+1} = \mathbf{E}_{2n+1} \text{ in } \Omega^-, \quad \mathbf{w}_{2n+2} = \mathbf{E}_{2n+2} - \mathbf{E} \text{ in } \Omega.$$

For all n, we define $\Lambda_n = T_{\nu_1}(\mathbf{w}_{2n})$ and $\delta_n = N_{\nu_2}(\mathbf{w}_{2n})$. In order to prove that the error $(\mathbf{w}_n)_n$ converges to zero, we first show that $\Lambda_{n+1} = K\Lambda_n$ and $\delta_{n+1} = L\delta_n$ with $K : T^2(S^2) \to T^2(S^2)$ and $L : L^2(S^2) \to L^2(S^2)$ two linear maps. K (resp. L) has a diagonal representation in the basis $(U_{lm}, V_{lm})_{lm}$ of $T^2(S^2)$ (resp. Y_l^m of $L^2(S^2)$). Let us denote by $\tau_{1,lm}, \tau_{2,lm}$ (resp. $\tau_{3,lm}$) the eigenvalues of K (resp. L). These eigenvalues define the rate of convergence of the Total Overlapping Schwarz method. Taking into account the boundary and transmission conditions, we obtain:

$$\tau_{1,lm} = \left(1 - \frac{H_l(k_sR_*)}{J_l(k_sR_*)}\frac{J_l(k_sR) - ik_sRj_l(k_sR)}{H_l(k_sR) - ik_sRh_l(k_sR)}\right)^{-1},$$

$$\tau_{2,lm} = \left(1 - \frac{h_l(k_sR_*)}{j_l(k_sR_*)}\frac{J_l(k_sR) - ik_sRj_l(k_sR)}{H_l(k_sR) - ik_sRh_l(k_sR)}\right)^{-1}, \ \tau_{3,lm} = \left(1 - \frac{H_l(k_sR_*)}{J_l(k_sR_*)}\frac{j_l(k_sR)}{h_l(k_sR)}\right)^{-1}.$$

The convergence of the Total Overlapping Schwarz method is ensured if $|\tau_{i,lm}| < 1$, $\forall i = 1, ..., 3$, $\forall l$. The reader can see that these eigenvalues are independent of the parameter m. For $R_* = 1$, the asymptotic behavior of the spherical Bessel functions for large l leads to the asymptotic estimation $\tau_{i,lm} \sim (1 - R^{2l})^{-1}$, $i = 1, ..., 3$. As a consequence, for small values of R, there exists a finite number of coefficients $\tau_{i,lm}$ outside of the unit disk, and for sufficiently large values of R, all the coefficients $\tau_{i,lm}$ are in the interior to the unit disk. We conclude that the linear convergence of the Schwarz method would be reachable for R large enough. The numerical tests illustrate this theoretical result. In Fig. 3.9, we consider $R_* = 1$ and $R = R_* + e$ with different values of e: $\lambda/100$, $\lambda/10$ or $\lambda/5$. The cases $e = \lambda/100$ and $e = \lambda/10$ exhibit some coefficients larger than 1 while the maximum value of $|\tau_{2,lm}|$ is strictly lower than 1 at the considered wavenumbers for the thickness $e = \lambda/5$ but the results are strongly dependent on the wavenumber. Similar asymptotic observations can be done on $|\tau_{1,lm}|$ and $|\tau_{3,lm}|$. As a consequence, a Krylov method is a relevant alternative to the algorithm defined by (3.10): due to the properties of Krylov solvers demonstrated in [GP08], the convergence of a Krylov method is ensured for the resolution of the problem (3.9) using $\mathcal{A}_t$ as a preconditioner. In

[Rai14, DGRon], the superlinear convergence of GMRES solver is analytically demonstrated for the spherical configuration.

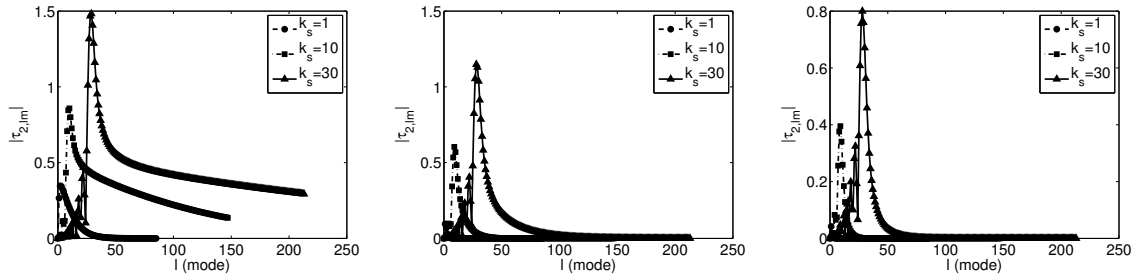

Figure 3.9. Modulus of $\tau_{2,lm}$ for thickness $e = \lambda/100$ (left), $\lambda/10$ (center) and $\lambda/5$ (right). Cases $k_s = 1$, 10 or 30.

The use of $\mathcal{A}_t$ as a preconditioner to solve the problem (3.9) using a Krylov solver has been numerically tested. We hereby consider the resolution of problem (3.9) using the GMRES. After a finite element discretization, the linear system is written under the form $(A + C)[\mathbf{E}] = F$ and the preconditioned system becomes $(I + A^{-1}C)[\mathbf{E}] = A^{-1}F$ where the matrix C involves the integral operators and the matrix A related to the differential operators involves a term resulting from the essential condition considered by a penalization technique:

$$\varepsilon_p \, (n_\gamma \times \operatorname{curl} \mathbf{E}) + \mathbf{E} \times n_\gamma = 0 \text{ on } \Gamma, \quad \text{with } \varepsilon_p > 0.$$

The numerical implementation were done using and developing new integrands in the library MÉLINA++ [MDL14]. The validation of the code was done by considering an intermediate problem the solution of which is known

$$\begin{cases} \operatorname{curl}\operatorname{curl} \mathbf{E} - \nabla(\operatorname{div} \mathbf{E}) - k_s^2 \mathbf{E} = 0 \text{ in } \Omega^+, \\ \mathbf{E} \times n_\gamma = \mathcal{G}_1^1 \times n_\gamma, \operatorname{div} \mathbf{E} = \operatorname{div} \mathcal{G}_1^1 \text{ on } \Gamma, \\ \lim\limits_{\rho\to\infty} \int_{||x||=\rho} || \operatorname{curl} \mathbf{E}^s \times n_\sigma - ik_s n_\sigma \times (\mathbf{E}^s \times n_\sigma)||^2 d\sigma = 0, \\ \lim\limits_{\rho\to\infty} \int_{||x||=\rho} |\operatorname{div} \mathbf{E}^s - ik_s \mathbf{E}^s \cdot n_\sigma|^2 d\sigma = 0, \end{cases} \tag{3.13}$$

where $\mathcal{G}_1^1$ is the first vector component of $\mathcal{G}_1$. The scatterer is the unit sphere and the artificial boundary Σ is the sphere concentric to Γ with radius $R = 1.5$. Fig. 3.10-left shows the convergence of the relative error with respect to the mesh density: the relative error is plotted with respect to the average size of the mesh elements, for different values of the penalization parameter ε_p, for the wavenumber $k_s = 3$.

To illustrate the superlinear convergence of the GMRES applied to the preconditioned system, we exhibit the GMRES residuals in Fig. 3.10-right for different values of the wavenumber, with $\varepsilon_p = 10^{-4}$. The considered meshes were adapted to the wavenumber such that the average edge length is about the wavelength over ten and there are about two layers of mesh elements between Γ and Σ.

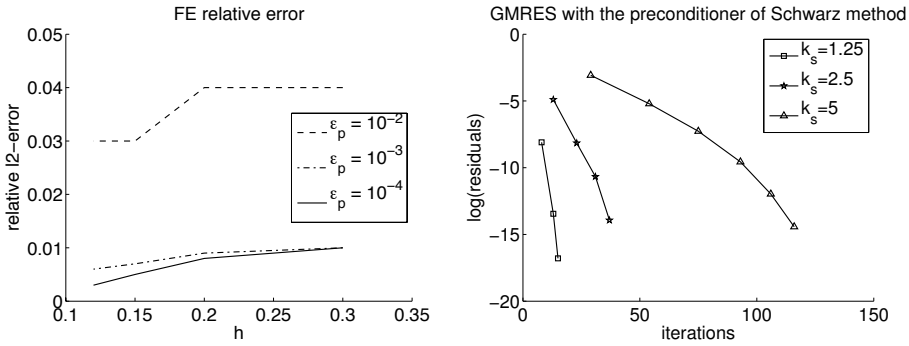

Figure 3.10. Relative l^2-error with respect to the mesh density (left); behavior of the GMRES residuals, case $k_s h = 2\pi/10$ (right)

3.4 Perspectives

The work done with Rania Rais and Nabil Gmati on the justification and the implementation of an integral representation for 3D Maxwell equations is a significant progress which offers several perspectives. These first developments were done in a rather simple context in term of geometry or numerical tools used for the resolution. Next steps would consist of the consideration of Nédélec finite elements for a more systematic formulation valuable for any geometry, an efficient implementation of the essential condition, the application of a Multilevel Fast Multipole Method. Related to the last item, Rania Rais contributes to the implementation of the library FastMMLib [DLnt].

Chapter 4

Singularities of the integral operators

4.1 Introduction

In this chapter, we focus on the integration of singular integrands. Within the works presented in the document, we considered a numerical strategy based on Duffy transformation which was robust enough for the considered applications but suffers from a lack of efficiency in the most singular cases. Alternatives are detailed in literature and should be considered for comparisons and combinations. In next section, we express the numerical strategy as used in the works presented in the previous chapters. The last section is devoted to perspectives of combinations with other approaches, either numerical or analytical.

4.2 Treatment of the singularities in MÉLINA++

In this section, we explain the strategy used to deal with the singularities of the Helmholtz fundamental solution and derivatives involved in surface or volume integral equations. With Daniel Martin, we implemented surface integral operators in the finite element library MÉLINA++ [MDL14]. To deal with the singularities of the Green kernel, we integrated a strategy based on singular changes of variables involving Duffy transformation [Duf82]. Indeed, we extended a technique developed by Jean Gay, retired engineer from CEA-CESTA, and essentially described in PhD theses of the university of Bordeaux I ([Lec97, Lan95, Dar02a]). With El-Hadji Koné, in the context of his PhD thesis [Kon10], we derived the evaluation of singular integrands on tetrahedra related to volume integral operators. We, hereby, explain the strategy in the case of surface configurations as it is implemented in the library MÉLINA++ for $\mathbb{P}_1$ finite elements. The case of volume integrands is similar and can be found in [Kon10].

The strategy is applied to kernels of the following forms

$$G(x,y) = \sum_{i=1}^{I} \frac{F_i(x,y)}{|x-y|^{\alpha_i}} \ , \qquad \nabla_x G(x,y) = \sum_{i=1}^{I} \frac{F_i(x,y)}{|x-y|^{\alpha_i}} (x-y) \ ,$$

$$\nabla_x \nabla_y G(x,y) = \sum_{i=1}^{I} \frac{F_i(x,y)}{|x-y|^{\alpha_i}} (x-y)(x-y)^\top + \sum_{i=1}^{I} \frac{\widetilde{F}_i(x,y)}{|x-y|^{\beta_i}} I_3 \ .$$

In the following, we detail the formulae for the evaluation of the expression

$$I_{KL} = \int_K \int_L \frac{F(x,y)}{|x-y|^\alpha}\, \varphi_c(y)\varphi_r(x) dx\, dy\,,$$

where K and L are mesh triangles sharing vertices. The evaluation of expressions involving $\nabla_x G(x,y)$ or $\nabla_x \nabla_y G(x,y)$ is similar, taking advantage of the factor $(x-y)$.

Let us denote X_i and Y_i, $i = 1, ..., 3$ the vertices of K and L respectively. according to the number of shared vertices, three different configurations occur. In the library MÉLINA++, the triangles are considered as the image of a reference triangle $\hat{K}$ by a linear function. Hence, $K = F_K(\hat{K})$ and $L = F_L(\hat{K})$, with F_K and F_L linear functions. The reference triangle is defined by the vertices $(1,0), (0,1), (0,0)$. We also denote by $\hat{X}_i$, $\hat{Y}_i$ the points of $\hat{K}$ satisfying $X_i = F_K(\hat{X}_i)$ and $Y_i = F_K(\hat{Y}_i)$.

4.2.1 1st case : K and L share exactly one vertex

Let us number the vertices such that $X_1 = Y_1$ (see Fig. 4.1).

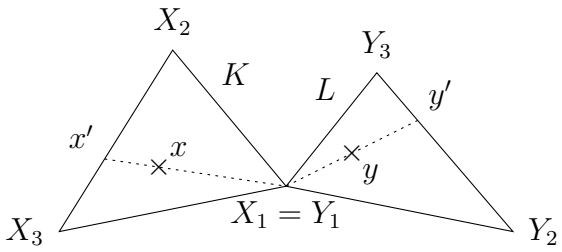

Figure 4.1. (*generated with Fig4TeX* [Laf11]) Two triangles sharing one vertex

The integral to be evaluated is

$$I_{KL} = \int_{\hat{K}} \int_{\hat{K}} \frac{F(F_K(\hat{x}), F_L(\hat{y}))}{|F_K(\hat{x}) - F_L(\hat{y})|^\alpha}\, \hat{\varphi}_c(\hat{y})\hat{\varphi}_r(\hat{x})\ |\mathrm{det} F_K(\hat{x})|\ |\mathrm{det} F_L(\hat{y})|\, d\hat{x}\, d\hat{y}\,.$$

A first change of variables is (see Fig. 4.1)

$$\begin{array}{l} \hat{x}' = (1-\lambda_x)\hat{X}_2 + \lambda_x \hat{X}_3, \quad \lambda_x \in [0,1] \\ \hat{y}' = (1-\lambda_y)\hat{Y}_2 + \lambda_y \hat{Y}_3, \quad \lambda_y \in [0,1] \end{array} \quad \text{and} \quad \begin{array}{ll} \hat{x}_1 = (1-\xi)\hat{X}_1 + \xi\, \hat{x}', & \xi \in [0,1], \\ \hat{y}_1 = (1-\xi\eta)\hat{Y}_1 + \xi\eta\, \hat{y}', & \eta \in [0,1], \\ \hat{y}_2 = (1-\xi)\hat{Y}_1 + \xi\, \hat{y}', & \xi \in [0,1], \\ \hat{x}_2 = (1-\xi\eta)\hat{X}_1 + \xi\eta\, \hat{x}', & \eta \in [0,1]. \end{array}$$

Let us introduce the notation (which leads to $x_i - y_i = \xi x\_y(i)$)

$$x\_y(1) = (\eta-1)X_1 - \eta F_L(\hat{y}') + F_K(\hat{x}') \quad \text{et} \quad x\_y(2) = (1-\eta)X_1 + \eta F_K(\hat{x}') - F_L(\hat{y}').$$

This change of variables involve Duffy transformation and cancel the singularity. The integral then reads

$$\sum_{i=1}^{2} \iiiint_{[0,1]^4} \frac{F(F_K(\hat{x}_i), F_L(\hat{y}_i))}{|x\_y(i)|^\alpha}\, \hat{\varphi}_c(\hat{y}_i)\hat{\varphi}_r(\hat{x}_i)\, |\mathrm{det} F_K(\hat{x}_i)|\ |\mathrm{det} F_L(\hat{y}_i)|\, \xi^{3-\alpha}\eta\, d\eta\, d\xi\, d\lambda_y\, d\lambda_x\,,$$

and more precisely

$$\iiiint_{[0,1]^4} \frac{F(F_K(\hat{x}_{\lambda_x,\xi}), F_L(\hat{y}_{\lambda_y,\xi\eta}))}{|(\eta-1)X_1 - \eta F_L(\hat{y}'_{\lambda_y}) + F_K(\hat{x}'_{\lambda_x})|^\alpha} \hat{\varphi}_c(\hat{y}_{\lambda_y,\xi\eta})\hat{\varphi}_r(\hat{x}_{\lambda_x,\xi})$$
$$|\mathrm{det} F_K(\hat{x}_{\lambda_x,\xi})| \left|\mathrm{det} F_L(\hat{y}_{\lambda_y,\xi\eta})\right| \xi^{3-\alpha}\eta \, d\eta \, d\xi \, d\lambda_y \, d\lambda_x$$

$$+ \iiiint_{[0,1]^4} \frac{F(F_K(\hat{x}_{\lambda_x,\xi\eta}), F_L(\hat{y}_{\lambda_y,\xi}))}{|(1-\eta)X_1 + \eta F_K(\hat{x}'_{\lambda_x}) - F_L(\hat{y}'_{\lambda_y})|^\alpha} \hat{\varphi}_c(\hat{y}_{\lambda_y,\xi})\hat{\varphi}_r(\hat{x}_{\lambda_x,\xi\eta})$$
$$|\mathrm{det} F_K(\hat{x}_{\lambda_x,\xi\eta})| \left|\mathrm{det} F_L(\hat{y}_{\lambda_y,\xi})\right| \xi^{3-\alpha}\eta \, d\eta \, d\xi \, d\lambda_y \, d\lambda_x \ .$$

For $(\lambda_x, \lambda_y, \xi, \eta)$, the default quadrature rule is Gauss-Legendre of degree 3 on $[0, 1]$.

4.2.2 2nd case: K and L share exactly one edge

Let us number the vertices such that $X_2 = Y_3$ and $X_3 = Y_2$ (see Fig. 4.2).

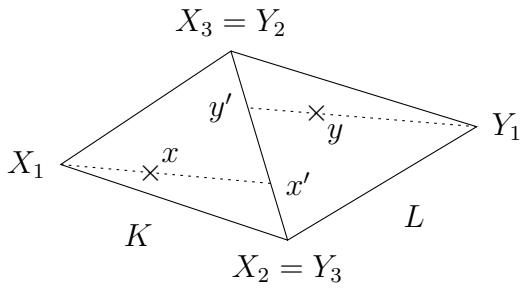

Figure 4.2. (*generated with Fig4TeX* [Laf11]) Two triangles sharing one edge

The integral to be evaluated is

$$I_{KL} = \int_{\hat{K}} \int_{\hat{K}} \frac{F(F_K(\hat{x}), F_L(\hat{y}))}{|F_K(\hat{x}) - F_L(\hat{y})|^\alpha} \hat{\varphi}_c(\hat{y})\hat{\varphi}_r(\hat{x}) \ |\mathrm{det} F_K(\hat{x})| \ |\mathrm{det} F_L(\hat{y})| \, d\hat{x} \, d\hat{y} \ .$$

Successive changes of variables ($\hat{x} \to (\lambda_x, \mu_x)$, $\hat{y} \to (\lambda_y, \mu_y)$; split of the unit square into two triangles, Fig. 4.3-left, and Duffy transformation for $(\lambda_x, \lambda_y) \to (u, w)$; split of the unit cube into three pyramids, Fig. 4.3-right, and Duffy transformation for $(\mu_x, \mu_y, w) \to (\eta, \zeta, \xi)$) lead to the following expression

$$I_{KL} = \sum_{i=1}^{6} \iiiint_{[0,1]^4} \frac{F(F_K(\hat{x}_i), F_L(\hat{y}_i))}{|x\_y(i)|^\alpha} \hat{\varphi}_c(\hat{y}_i)\hat{\varphi}_r(\hat{x}_i) \, |\mathrm{det} F_K(\hat{x}_i)| \, |\mathrm{det} F_L(\hat{y}_i)| \, \mathrm{Jac}(i) \, d\eta \, du \, d\zeta \, d\xi \ ,$$

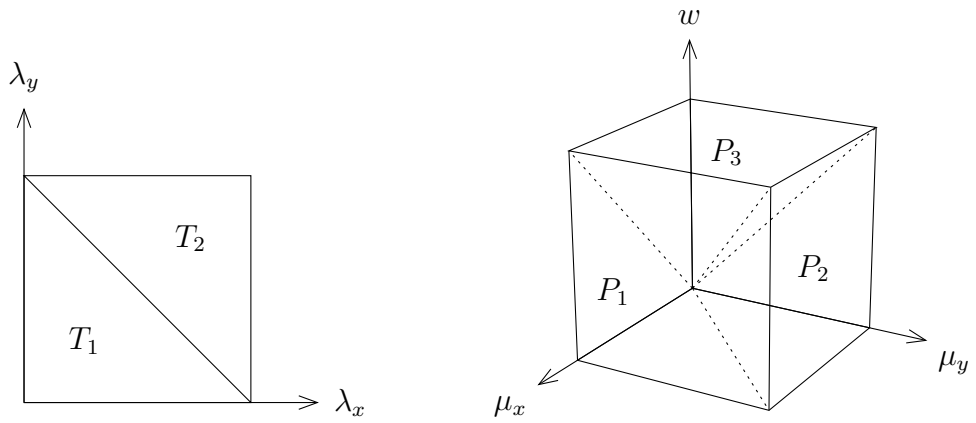

Figure 4.3. (*generated with Fig4TeX* [Laf11]) integration domain splits for application of Duffy transformation

with the following definition of the different quantities (each column corresponds to one of the triangles in Fig. 4.3, each line corresponds to one of the pyramids in Fig. 4.3)

$\hat{x}'_1 = (1-(1-\xi\zeta)u)\hat{X}_2 + (1-\xi\zeta)u\hat{X}_3$ $\hat{y}'_1 = (1-(1-\xi\zeta)(1-u))\hat{Y}_2 + (1-\xi\zeta)(1-u)\hat{Y}_3$ $\hat{x}_1 = \xi\hat{X}_1 + (1-\xi)\hat{x}'_1$ $\hat{y}_1 = \xi\eta\hat{Y}_1 + (1-\xi\eta)\hat{y}'_1$ $\mathrm{Jac}(1) = \xi^2(1-\xi)(1-\xi\eta)(1-\xi\zeta)$ $x\_y(1) = \xi[S_x + \eta S_y$ $+((1-\eta)(1-\xi\zeta)u + (1-\xi\eta)\zeta)S_{23}]$	$\hat{x}'_2 = (1-(1-\xi\zeta)u-\xi\zeta)\hat{X}_2 + ((1-\xi\zeta)u+\xi\zeta)\hat{X}_3$ $\hat{y}'_2 = (1-(1-\xi\zeta)(1-u)-\xi\zeta)\hat{Y}_2 + ((1-\xi\zeta)(1-u)+\xi\zeta)\hat{Y}_3$ $\hat{x}_2 = \xi\hat{X}_1 + (1-\xi)\hat{x}'_2$ $\hat{y}_2 = \xi\eta\hat{Y}_1 + (1-\xi\eta)\hat{y}'_2$ $\mathrm{Jac}(2) = \mathrm{Jac}(1) = \xi^2(1-\xi)(1-\xi\eta)(1-\xi\zeta)$ $x\_y(2) = \xi[S_x + \eta S_y$ $+((1-\eta)(1-\xi\zeta)u - (1-\xi)\zeta)S_{23}]$
$\hat{x}'_3 = (1-(1-\eta\zeta)u)\hat{X}_2 + (1-\eta\zeta)u\hat{X}_3$ $\hat{y}'_3 = (1-(1-\eta\zeta)(1-u))\hat{Y}_2 + (1-\eta\zeta)(1-u)\hat{Y}_3$ $\hat{x}_3 = \xi\eta\hat{X}_1 + (1-\xi\eta)\hat{x}'_3$ $\hat{y}_3 = \eta\hat{Y}_1 + (1-\eta)\hat{y}'_3$ $\mathrm{Jac}(3) = \eta^2(1-\xi\eta)(1-\eta)(1-\eta\zeta)$ $x\_y(3) = \eta[\xi S_x + S_y$ $+(-(1-\xi)(1-\eta\zeta)u + (1-\eta)\zeta)S_{23}]$	$\hat{x}'_4 = (1-(1-\eta\zeta)u-\eta\zeta)\hat{X}_2 + ((1-\eta\zeta)u+\eta\zeta)\hat{X}_3$ $\hat{y}'_4 = (1-(1-\eta\zeta)(1-u)-\eta\zeta)\hat{Y}_2 + ((1-\eta\zeta)(1-u)+\eta\zeta)\hat{Y}_3$ $\hat{x}_4 = \xi\eta\hat{X}_1 + (1-\xi\eta)\hat{x}'_4$ $\hat{y}_4 = \eta\hat{Y}_1 + (1-\eta)\hat{y}'_4$ $\mathrm{Jac}(4) = \mathrm{Jac}(3) = \eta^2(1-\xi\eta)(1-\eta)(1-\eta\zeta)$ $x\_y(4) = \eta[\xi S_x + S_y$ $+(-(1-\xi)(1-\eta\zeta)u - (1-\xi\eta)\zeta)S_{23}]$
$\hat{x}'_5 = (1-(1-\zeta)u)\hat{X}_2 + (1-\zeta)u\hat{X}_3$ $\hat{y}'_5 = (1-(1-\zeta)(1-u))\hat{Y}_2 + (1-\zeta)(1-u)\hat{Y}_3$ $\hat{x}_5 = \xi\zeta\hat{X}_1 + (1-\xi\zeta)\hat{x}'_5$ $\hat{y}_5 = \eta\zeta\hat{Y}_1 + (1-\eta\zeta)\hat{y}'_5$ $\mathrm{Jac}(5) = \zeta^2(1-\xi\zeta)(1-\eta\zeta)(1-\zeta)$ $x\_y(5) = \zeta[\xi S_x + \eta S_y$ $+((\xi-\eta)(1-\zeta)u + (1-\eta\zeta))S_{23}]$	$\hat{x}'_6 = (1-(1-\zeta)u-\zeta)\hat{X}_2 + ((1-\zeta)u+\zeta)\hat{X}_3$ $\hat{y}'_6 = (1-(1-\zeta)(1-u)-\zeta)\hat{Y}_2 + ((1-\zeta)(1-u)+\zeta)\hat{Y}_3$ $\hat{x}_6 = \xi\zeta\hat{X}_1 + (1-\xi\zeta)\hat{x}'_6$ $\hat{y}_6 = \eta\zeta\hat{Y}_1 + (1-\eta\zeta)\hat{y}'_6$ $\mathrm{Jac}(6) = \mathrm{Jac}(1) = \zeta^2(1-\xi\zeta)(1-\eta\zeta)(1-\zeta)$ $x\_y(6) = \zeta[\xi S_x + \eta S_y$ $+((\xi-\eta)(1-\zeta)u - (1-\xi\zeta))S_{23}]$

and, $S_x = F_K(\hat{X}_1 - \hat{X}_2)$, $S_y = F_K(\hat{X}_2 - \hat{Y}_1)$ et $S_{23} = F_K(\hat{X}_2 - \hat{X}_3)$. The default quadrature rule for (ξ, η, ζ, u) is Gauss-Legendre of degree 3 on $[0, 1]$.

4.2.3 3rd case: K and L are identical

There is no requirement on the numbering of the vertices.

The integral to be evaluated is

$$I_{KK} = \int_{\hat{K}}\int_{\hat{K}} \frac{F(F_K(\hat{x}), F_K(\hat{y}))}{|F_K(\hat{x}) - F_K(\hat{y})|^\alpha}\, \hat{\varphi}_c(\hat{y})\hat{\varphi}_r(\hat{x})\ |\mathrm{det}F_K(\hat{x})|\ |\mathrm{det}F_K(\hat{y})|\, d\hat{x}\, d\hat{y}\,.$$

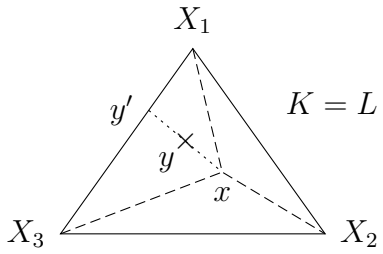

Figure 4.4. (*generated with Fig4TeX* [Laf11]) Auto-influence case, $K = L$

For this case, the principle is rather basic and non optimal: we consider a usual quadrature rule on triangle, for the variable $\hat{x}$ and we cancel the singularity by changes of variables on $\hat{y}$ considered one by one in the triangles $\hat{x}\hat{X}_2\hat{X}_3$, $\hat{X}_1\hat{x}\hat{X}_3$ and $\hat{X}_1\hat{X}_2\hat{x}$ (see Fig. 4.4). $\hat{y}$ is expressed like a combination of $\hat{x}$ and a point on the opposite edge of the considered triangle. This leads to the expression

$$I_{KK} = \int_{\hat{K}} \sum_{i=1}^{3} \iint_{[0,1]^2} \frac{F(F_K(\hat{x}), F_K(\hat{y}_i))}{\mu_y^{\alpha} \, |x\_y(i)|^{\alpha}} \hat{\varphi}_c(\hat{y}_i)\hat{\varphi}_r(\hat{x}) \, |\det F_K(\hat{x})| \, |\det F_K(\hat{y}_i)| \, \mathrm{Jac}(i) \, d\mu_y \, d\lambda_y \, d\hat{x} \, ,$$

with the following definition of the different quantities

$\hat{y}'_1 = (1-\lambda_y)\hat{X}_2 + \lambda_y\hat{X}_3$ $\mathrm{Jac}(1) = 2\,\mu_y\,\mathrm{meas}(\hat{x}\hat{X}_2\hat{X}_3)$	$\hat{y}_1 = (1-\mu_y)\hat{x} + \mu_y\hat{y}'_1$ $x\_y(1) = F_K(\hat{x} - \hat{y}'_1)$
$\hat{y}'_2 = (1-\lambda_y)\hat{X}_3 + \lambda_y\hat{X}_1$ $\mathrm{Jac}(2) = 2\,\mu_y\,\mathrm{meas}(\hat{X}_1\hat{x}\hat{X}_3)$	$\hat{y}_2 = (1-\mu_y)\hat{x} + \mu_y\hat{y}'_2$ $x\_y(2) = F_K(\hat{x} - \hat{y}'_2)$
$\hat{y}'_3 = (1-\lambda_y)\hat{X}_1 + \lambda_y\hat{X}_2$ $\mathrm{Jac}(3) = 2\,\mu_y\,\mathrm{meas}(\hat{X}_1\hat{X}_2\hat{x})$	$\hat{y}_3 = (1-\mu_y)\hat{x} + \mu_y\hat{y}'_3$ $x\_y(3) = F_K(\hat{x} - \hat{y}'_3)$

For the variable x, the default quadrature rule is a misc rule of degree 5 for triangles. For the variables (λ_y, μ_y), the default quadrature rule is Gauss-Legendre of degree 3 on $[0, 1]$.

4.3 Alternatives for a library on the treatment of the singularities – Perspectives

Section 4.2 was dedicated to a numerical strategy developed by Jean Gay, retired engineer from CEA-CESTA, and implemented in the library MÉLINA++ [MDL14]. In literature, one can find two alternatives

- ⋆ Stefan Sauter and Christoph Schwab describe in [SS11] another numerical approach which is also based on Duffy transformation and rather similar. Their method is derived for triangles and quadrangles.

- ⋆ Nicolas Salles and Marc Lenoir developed an analytic strategy to evaluate the singular integrals in the case of triangles [LS12]. The method is based on the properties of homogeneous functions. The drawback of this approach is the fact that the developments should be derived independently for each integrand depending on the kernel, the operator applied to the kernel, the degree of the finite element interpolation.

- ⋆ In the case of two-dimensional problems, the singular integrands are evaluated very efficiently with a numerical scheme by Javier Sayas et al [DLS14b, DLS14a, DLSon]. The strategy is based on a careful mathematical analysis which justifies a choice of quadrature rules with a surprisingly low number of quadrature points. The three-dimensional equivalent would be a wonderful result.

These works motivate the idea of a library devoted to strategies of integration of singular integrands. The numerical methods have to be compared. They share a disadvantage: they are efficient for the cases of non identical elements but are very costly for the auto-influence case. The analytical approach leads to expressions which are easier to derive in the case of auto-influence. Both approaches should be combined. One could also think about a lower-dimension numerical integration, for example for some 1D integrals involved in the derivation of the analytical expression: in some configurations, it may be better to use 1D numerical integration schemes instead of deriving the analytical approach till the last step involving special functions such as hyperbolic cosine. With Nicolas Salles, in the context of his PhD thesis [Sal13], we implemented his developments for triangles in the library MÉLINA++. First tests shew the relevance of a combination of numerical and analytical approaches. Marc Lenoir already wrote the analytical expression of the auto-influence case for tetrahedra in the framework of volume integral equations.

Bibliography

[•••••] Personal bibliography

[BDMN03] Alain Bachelot, Eric Darrigrand, and Katherine Mer-Nkonga. Coupling of a multilevel fast multipole method and a microlocal discretization for the 3-D integral equations of electromagnetism. *C. R. Math. Acad. Sci. Paris*, 336(6):505–510, 2003.

[CCD03] Fioralba Cakoni, David Colton, and Eric Darrigrand. The inverse electromagnetic scattering problem for screens. *Inverse Problems*, 19(3):627–642, 2003.

[CD05] Fioralba Cakoni and Eric Darrigrand. The inverse electromagnetic scattering problem for a mixed boundary value problem for screens. *J. Comput. Appl. Math.*, 174(2):251–269, 2005.

[CDF10] Philippe Chartier, Eric Darrigrand, and Erwan Faou. A regular fast multipole method for geometric numerical integrations of Hamiltonian systems. *BIT*, 50(1):23–40, 2010.

[CDK10] Martin Costabel, Eric Darrigrand, and El-Hadji Koné. Volume and surface integral equations for electromagnetic scattering by a dielectric body. *J. Comput. Appl. Math.*, 234(6):1817–1825, 2010.

[CDS12] Martin Costabel, Eric Darrigrand, and Hamdi Sakly. The essential spectrum of the volume integral operator in electromagnetic scattering by a homogeneous body. *C. R. Math. Acad. Sci. Paris*, 350(3–4):193–197, 2012.

[CDSona] Martin Costabel, Eric Darrigrand, and Hamdi Sakly. The essential spectrum of the integral operator for the magnetic scattering problem with smooth and non-smooth domains. in preparation.

[CDSonb] Martin Costabel, Eric Darrigrand, and Hamdi Sakly. The essential spectrum of the volume integral operator for the magnetic scattering problem – 2D case. in preparation.

[Dar02a] Eric Darrigrand. *Couplage Méthodes multipôles - Discrétisation Microlocale pour les Equations Intégrales de l'Electromagnétisme*. Thèse de doctorat, Université Bordeaux I, Septembre 2002.

[Dar02b] Eric Darrigrand. Coupling of fast multipole method and microlocal discretization for the 3-D Helmholtz equation. *J. Comput. Phys.*, 181(1):126–154, 2002.

[Dar08] Eric Darrigrand. Ultra-weak variational formulation and efficient integral representation in electromagnetism: a thorough study of the algorithm complexity. *ESAIM, Proc.*, 22:190–197, 2008.

[DDL13] Marion Darbas, Eric Darrigrand, and Yvon Lafranche. Combining analytic preconditioner and fast multipole method for the 3-D Helmholtz equation. *J. Comput. Phys.*, 236:289–316, 2013.

[DGR10] Eric Darrigrand, Nabil Gmati, and Rania Rais. Méthode multipôles rapide pour le couplage entre éléments finis et représentation intégrale. In *CARI'10: 10th African Conference on Research in Computer Science*, 8 pages. Yamoussoukro – Côte d'Ivoire, October 2010.

[DGR14] Eric Darrigrand, Nabil Gmati, and Rania Rais. Schwarz method justification of a coupling between finite elements and integral representation for Maxwell exterior problem. *C. R. Math. Acad. Sci. Paris*, 352:311–315, 2014.

[DGRon] Eric Darrigrand, Nabil Gmati, and Rania Rais. Convergence of Krylov subspace solvers with Schwarz' preconditioner for Maxwell exterior problem. in preparation.

[DLnt] Eric Darrigrand and Yvon Lafranche. https://sourcesup.cru.fr/projects/fastmmlib/. FastMMLib documentation, Université Rennes 1, under development.

[DM07] Eric Darrigrand and Peter Monk. Coupling of the ultra-weak variational formulation and an integral representation using a fast multipole method in electromagnetism. *J. Comput. Appl. Math.*, 204(2):400–407, 2007.

[DM09] Eric Darrigrand and Daniel Martin. Résolution des équations intégrales de B. Després avec la librairie éléments finis MÉLINA++. Support de l'atelier MÉLINA++ 2009, http://perso.univ-rennes1.fr/eric.darrigrand-lacarrieu/Publi/eid.pdf, Université Rennes 1, 2009.

[DM12] Eric Darrigrand and Peter Monk. Combining the ultra-weak variational formulation and the multilevel fast multipole method. *Appl. Numer. Math.*, 62(6):709–719, 2012.

[MDL14] Daniel Martin, Eric Darrigrand, and Yvon Lafranche. http://anum-maths.univ-rennes1.fr/melina/melina++_distrib/. MÉLINA++ documentation, Université Rennes 1, last update: jan 2014.

[•••••] Complete bibliography

[ABB99] Xavier Antoine, Hélène Barucq, and Abderrahmane Bendali. Bayliss-Turkel-like radiation conditions on surfaces of arbitrary shape. *J. Math. Anal. Appl.*, 229(1):184–211, 1999.

[ABL07] François Alouges, Sophie Borel, and David P. Levadoux. A stable well-conditioned integral equation for electromagnetism scattering. *J. Comput. Appl. Math.*, 204(2):440–451, 2007.

[AD05] Xavier Antoine and Marion Darbas. Alternative integral equations for the iterative solution of acoustic scattering problems. *Quart. J. Mech. Appl. Math.*, 58(1):107–128, 2005.

[AD07] Xavier Antoine and Marion Darbas. Generalized combined field integral equations for the iterative solution of the three-dimensional Helmholtz equation. *M2AN Math. Model. Numer. Anal.*, 41(1):147–167, 2007.

[ADL06] Xavier Antoine, Marion Darbas, and Ya Yan Lu. An improved surface radiation condition for high-frequency acoustic scattering problems. *Comput. Methods Appl. Mech. Engrg.*, 195(33-36):4060–4074, 2006.

[Ant08] Xavier Antoine. Advances in the On-Surface Radiation Condition Method: Theory, Numerics and Applications. In *Computational Methods for Acoustics Problems*, volume 406, pages 169–194. F. Magoulès, 2008.

[ANZ94] Toufic Abboud, J.-C. Nédélec, and Bin Zhou. Méthodes des équations intégrales pour les hautes fréquences. *C. R. Acad. Sci. Paris*, 318, serie I:165–170, 1994.

[ANZ95] Toufic Abboud, J.-C. Nédélec, and Bin Zhou. Improvement of the Integral Equation Method for High Frequency Problems. *Third international conference on mathematical aspects of wave propagation phenomena, SIAM*, pages 178–187, 1995.

[AS72] Milton Abramowitz and Irene A. Stegun. *Handbook of Mathematical Functions with Formulas, Graphs, and Mathematical Tables*. John Wiley, New York, 1972.

[BBFGJ05] Faker Ben Belgacem, Michel Fournié, Nabil Gmati, and Faten Jelassi. On the Schwarz algorithms for the elliptic exterior boundary value problems. *M2AN Math. Model. Numer. Anal.*, 39(4):693–714, 2005.

[BC00] Nathalie Bartoli and Francis Collino. Integral Equations via Saddle Point Problem for Acoustic Problems. *M2AN*, 34(5):1023–1049, 2000.

[BDMN03] Alain Bachelot, Eric Darrigrand, and Katherine Mer-Nkonga. Coupling of a multilevel fast multipole method and a microlocal discretization for the 3-D integral equations of electromagnetism. *C. R. Math. Acad. Sci. Paris*, 336(6):505–510, 2003.

[Beb08] Mario Bebendorf. *Hierarchical matrices*, volume 63 of *Lecture Notes in Computational Science and Engineering*. Springer-Verlag, Berlin, 2008. A means to efficiently solve elliptic boundary value problems.

[Ber94] Jean-Pierre Berenger. A perfectly matched layer for the absorption of electromagnetic waves. *J. Comput. Phys.*, 114:185–200, October 1994.

[BET12] Oscar Bruno, Tim Elling, and Catalin Turc. Regularized integral equations and fast high-order solvers for sound-hard acoustic scattering problems. *Internat. J. Numer. Methods Engrg.*, 91(10):1045–1072, 2012.

[BGH06] Steffen Börm, Lars Grasedyck, and Wolfgang Hackbusch. *Hierarchical Matrices*. Lecture note 21. Max-Planck-Institut, Leipzig, second edition, 2006.

[BGT82] Alvin Bayliss, Max Gunzburger, and Eli Turkel. Boundary conditions for the numerical solution of elliptic equations in exterior regions. *SIAM J. Appl. Math.*, 42(2):430–451, 1982.

[BH05] Annalisa Buffa and Ralf Hiptmair. Regularized combined field integral equations. *Numer. Math.*, 100(1):1–19, 2005.

[BK01a] Oscar P. Bruno and Leonid A. Kunyansky. A Fast High Order Algorithm for the Solution of Surface Scattering Problems: Basic Implementation, tests, and Applications. *J. Comput. Phys.*, 169(1):80–110, May 2001.

[BK01b] Oscar P. Bruno and Leonid A. Kunyansky. Surface Scattering in 3-D: An Accelerated High Order Solver. *R. Soc. Lond. Proc. Ser. A Math. Phys. Eng. Sci.*, 457(2016):2921–2934, 2001.

[Bot06] Matthys M. Botha. Solving the volume integral equations of electromagnetic scattering. *Journal of Computational Physics*, 218(1):141 – 158, 2006.

[BS06] Neil V. Budko and Alexander B. Samokhin. Spectrum of the volume integral operator of electromagnetic scattering. *SIAM J. Sci. Comput.*, 28(2):682–700, 2006.

[BSSF96a] John C. Burant, Matthew C. Strain, Gustavo E. Scuseria, and Michael J. Frisch. Analytic energy gradients for the Gaussian very fast multipole method (GvFMM). *Chem. Phys. Lett.*, 248(1–2):43–49, 1996.

[BSSF96b] John C. Burant, Matthew C. Strain, Gustavo E. Scuseria, and Michael J. Frisch. Kohn-Sham analytic energy second derivatives with the Gaussian very fast multipole method (GvFMM). *Chem. Phys. Lett.*, 258(1–2):45–52, 1996.

[CC03a] Fioralba Cakoni and David Colton. Combined far-field operators in electromagnetic inverse scattering theory. *Math. Meth. Appl. Sci.*, 26:413–429, 2003.

[CC03b] Fioralba Cakoni and David Colton. The linear sampling method for cracks. *Inverse Problems*, 19(2):279–295, 2003.

[CCCS04] Tie Jun Cui, Weng Cho Chew, Guang Chen, and J. Song. Efficient MLFMA, RPFMA, and FAFFA algorithms for EM scattering by very large structures. *IEEE Trans. on Antennas and Propagation*, 52(3):759–770, 2004.

[CCD03] Fioralba Cakoni, David Colton, and Eric Darrigrand. The inverse electromagnetic scattering problem for screens. *Inverse Problems*, 19(3):627–642, 2003.

[CCM04] Fioralba Cakoni, David Colton, and Peter Monk. The electromagnetic inverse scattering problem for partially coated Lipschitz domains. *Proc. Royal Society of Edinburgh*, 134:661–682, 2004.

[CD03] Olivier Cessenat and Bruno Després. Using plane waves as base functions for solving time harmonic equations with the ultra weak variational formulation. *J. Comput. Acoust.*, 11(2):227–238, 2003. Medium-frequency acoustics.

[CD05] Fioralba Cakoni and Eric Darrigrand. The inverse electromagnetic scattering problem for a mixed boundary value problem for screens. *J. Comput. Appl. Math.*, 174(2):251–269, 2005.

[CDF10] Philippe Chartier, Eric Darrigrand, and Erwan Faou. A regular fast multipole method for geometric numerical integrations of Hamiltonian systems. *BIT*, 50(1):23–40, 2010.

[CDK10] Martin Costabel, Eric Darrigrand, and El-Hadji Koné. Volume and surface integral equations for electromagnetic scattering by a dielectric body. *J. Comput. Appl. Math.*, 234(6):1817–1825, 2010.

[CDS12] Martin Costabel, Eric Darrigrand, and Hamdi Sakly. The essential spectrum of the volume integral operator in electromagnetic scattering by a homogeneous body. *C. R. Math. Acad. Sci. Paris*, 350(3–4):193–197, 2012.

[CDSona] Martin Costabel, Eric Darrigrand, and Hamdi Sakly. The essential spectrum of the integral operator for the magnetic scattering problem with smooth and non-smooth domains. in preparation.

[CDSonb] Martin Costabel, Eric Darrigrand, and Hamdi Sakly. The essential spectrum of the volume integral operator for the magnetic scattering problem – 2D case. in preparation.

[Ces96] Olivier Cessenat. *Application d'une nouvelle formulation variationnelle aux équations d'ondes harmoniques - problèmes de Helmholtz 2D et de Maxwell 3D*. Thèse de doctorat, Université Paris IX, December 1996.

[CHP03] David Colton, Houssem Haddar, and Michele Piana. The linear sampling method in inverse electromagnetic scattering theory. *Inverse Problems*, 19(6):105–137, 2003.

[CJL+97] Weng Cho Chew, Jian-Ming Jin, Cai-Cheng Lu, Eric Michielssen, and Jiming M. Song. Fast Solution Methods in Electromagnetics. *IEEE Trans. on Antennas and Propagation*, 45(3):533–543, March 1997.

[CK96] David Colton and Andreas Kirsch. A simple method for solving inverse scattering problems in the resonance region. *Inverse Problems*, 12(4):383–393, 1996.

[CK98] David Colton and Rainer Kress. *Inverse acoustic and electromagnetic scattering theory*, volume 93 of *Applied Mathematical Sciences*. Springer-Verlag, Berlin, second edition, 1998.

[CN02] Snorre Christiansen and Jean-Claude Nédélec. A preconditioner for the electric field integral equation based on Calderon formulas. *SIAM J. Numer. Anal.*, 40(3):1100–1135, 2002.

[Cos07] Martin Costabel. Some historical remarks on the positivity of boundary integral operators. In *Boundary element analysis*, volume 29 of *Lect. Notes Appl. Comput. Mech.*, pages 1–27. Springer, Berlin, 2007.

[CRW93] Ronald Coifman, Vladimir Rokhlin, and Stephen Wandzura. The Fast Multipole Method for the Wave Equation: A Pedestrian Prescription. *IEEE Antennas and Propagation Magazine*, 35(3):7–12, June 1993.

[Dar00a] Eric Darve. The Fast Multipole Method (I): Error Analysis and Asymptotic Complexity. *SIAM J. Numer. Anal.*, 38(1):98–128, 2000.

[Dar00b] Eric Darve. The Fast Multipole Method: Numerical Implementation. *J. Comput. Phys.*, 160(1):195–240, 2000.

[Dar02a] Eric Darrigrand. *Couplage Méthodes multipôles - Discrétisation Microlocale pour les Equations Intégrales de l'Electromagnétisme*. Thèse de doctorat, Université Bordeaux I, Septembre 2002.

[Dar02b] Eric Darrigrand. Coupling of fast multipole method and microlocal discretization for the 3-D Helmholtz equation. *J. Comput. Phys.*, 181(1):126–154, 2002.

[Dar04] Marion Darbas. *Préconditionneurs analytiques de type Calderon pour les formulations intégrales des problèmes de diffraction d'ondes*. Thèse de doctorat, INSA de Toulouse, 2004.

[Dar06] Marion Darbas. Generalized CFIE for the iterative solution of 3-D Maxwell equations. *Appl. Math. Lett.*, 19:834–839, 2006.

[Dar08] Eric Darrigrand. Ultra-weak variational formulation and efficient integral representation in electromagnetism: a thorough study of the algorithm complexity. *ESAIM, Proc.*, 22:190–197, 2008.

[DDL13] Marion Darbas, Eric Darrigrand, and Yvon Lafranche. Combining analytic preconditioner and fast multipole method for the 3-D Helmholtz equation. *J. Comput. Phys.*, 236:289–316, 2013.

[Des97] Bruno Després. Fonctionnelle quadratique et équations intégrales pour les problèmes d'onde harmonique en domaine extérieur. *M2AN*, 31(6):679–732, 1997.

[DF94] Bruce T. Draine and Piotr J. Flatau. Discrete dipole approximation for scattering calculations. *J. Opt. Soc. Am. A*, 11(4):1491–1499, 1994.

[DF08] Bruce T. Draine and Piotr J. Flatau. Discrete-dipole approximation for periodic targets: theory and tests. *J. Opt. Soc. Am. A*, 25(11):2693–2703, 2008.

[DF12] Bruce T. Draine and Piotr J. Flatau. Fast near field calculations in the discrete dipole approximation for regular rectilinear grids. *Optics Express*, 20(2):1247–1252, 2012.

[DGR10] Eric Darrigrand, Nabil Gmati, and Rania Rais. Méthode multipôles rapide pour le couplage entre éléments finis et représentation intégrale. In *CARI'10: 10th African Conference on Research in Computer Science*, 8 pages. Yamoussoukro – Côte d'Ivoire, October 2010.

[DGR14] Eric Darrigrand, Nabil Gmati, and Rania Rais. Schwarz method justification of a coupling between finite elements and integral representation for Maxwell exterior problem. *C. R. Math. Acad. Sci. Paris*, 352:311–315, 2014.

[DGRon] Eric Darrigrand, Nabil Gmati, and Rania Rais. Convergence of Krylov subspace solvers with Schwarz' preconditioner for Maxwell exterior problem. in preparation.

[DH04] Eric Darve and Pascal Havé. Efficient fast multipole method for low-frequency scattering. *J. Comput. Phys.*, 197(1):341–363, 2004.

[DLS14a] Víctor Domínguez, Sijiang L. Lu, and Francisco-Javier Sayas. Fully discrete Calderón calculus for the two dimensional time harmonic waves. *Int. J. Numer. Anal. Model.*, 11(2):332–345, 2014.

[DLS14b] Víctor Domínguez, Sijiang L. Lu, and Francisco-Javier Sayas. A Nyström flavored Calderón calculus of order three for two dimensional waves, time-harmonic and transient. *Comput. Math. Appl.*, 67(1):217–236, 2014.

[DLSon] Víctor Domínguez, Sijiang L. Lu, and Francisco-Javier Sayas. A Nyström method for the two dimensional hypersingular operator for the Helmholtz equation. *Adv. Comput. Math.*, In revision.

[DLnt] Eric Darrigrand and Yvon Lafranche. https://sourcesup.cru.fr/projects/fastmmlib/. FastMMLib documentation, Université Rennes 1, under development.

[DM07] Eric Darrigrand and Peter Monk. Coupling of the ultra-weak variational formulation and an integral representation using a fast multipole method in electromagnetism. *J. Comput. Appl. Math.*, 204(2):400–407, 2007.

[DM09] Eric Darrigrand and Daniel Martin. Résolution des équations intégrales de B. Després avec la librairie éléments finis MÉLINA++. Support de l'atelier MÉLINA++ 2009, http://perso.univ-rennes1.fr/eric.darrigrand-lacarrieu/Publi/eid.pdf, Université Rennes 1, 2009.

[DM12] Eric Darrigrand and Peter Monk. Combining the ultra-weak variational formulation and the multilevel fast multipole method. *Appl. Numer. Math.*, 62(6):709–719, 2012.

[Duf82] Michael G. Duffy. Quadrature over a pyramid or cube of integrands with a singularity at a vertex. *SIAM J. Numer. Anal.*, 19(6):1260–1262, 1982.

[EB96] William D. Elliott and John A. Board. Fast Fourier transform accelerated fast multipole algorithm. *SIAM J. Sci. Comput.*, 17(2):398–415, 1996.

[EM77] Björn Engquist and Andrew Majda. Absorbing boundary conditions for the numerical simulation of waves. *Math. Comp.*, 31(139):629–651, 1977.

[FHMS11] M'Barek Fares, Jan Hesthaven, Yvon Maday, and Benjamin Stamm. Reduced basis method for the parametrized electric field integral equation. *J. Comput. Phys.*, 230(14):5532–5555, 2011.

[FP84] Mark J. Friedman and Joseph E. Pasciak. Spectral properties for the magnetization integral operator. *Math. Comp.*, 43(168):447–453, 1984.

[GHRW98] Leslie Greengard, Jingfang Huang, Vladimir Rokhlin, and Stephen Wandzura. Accelerating Fast Multipole Methods for the Helmholtz Equation at Low Frequency. *IEEE Comp. Sci. Engineering Magazine*, pages 32–38, July 1998.

[GHS12] Mahadevan Ganesh, Jan Hesthaven, and Benjamin Stamm. A reduced basis method for multiple electromagnetic scattering in three dimensions. *J. Comput. Phys.*, 231(23):7756–7779, 2012.

[GP08] Nabil Gmati and Bernard Philippe. Comments on the GMRES convergence for preconditioned systems. In *Large-scale scientific computing*, volume 4818 of *Lecture Notes in Comput. Sci.*, pages 40–51. Springer, Berlin, 2008.

[GR88] Leslie Greengard and Vladimir Rokhlin. The Rapid Evaluation of Potential Fields in Three Dimensions. In *Vortex Methods in Lecture Notes in Mathematics, 1360, Springer Verlag*, pages 121–141, 1988.

[GR96] Vivette Giraud and Pierre-Arnaud Raviart. *Finite Element Methods for the Navier-Stokes Equations, Theory and Algorithms*. Springer Series in Computat. Math. Springer-Verlag, Berlin, 1996.

[GR97] Leslie Greengard and Vladimir Rokhlin. A New Version of the Fast Multipole Method for the Laplace Equation in Three Dimensions. *Acta Numerica*, 6:229–269, 1997.

[GR09] Christophe Geuzaine and Jean-François Remacle. Gmsh: A 3-D finite element mesh generator with built-in pre- and post-processing facilities. *Internat. J. Numer. Methods Engrg.*, 79(11):1309–1331, 2009.

[Hac99] Wolfgang Hackbusch. A Sparse Matrix Arithmetic Based on H-Matrices. Part I: Introduction to H-Matrices. *Computing*, 62:89–108, 1999.

[HCWSC13] Charlotta J. Howarth, Simon N. Chandler-Wilde, Langdon Steven, and Paul N. Childs. Enriching a Hankel basis by ray tracing in the ultra weak variational formulation. In *11th International Conference on Mathematical and Numerical Aspects of Waves (Waves 2013)*. INRIA – ENIT, Tunis, june 2013.

[HKM04] Tomi Huttunen, Jari P. Kaipio, and Peter Monk. The perfectly matched layer for the ultra weak variational formulation of the 3D Helmholtz equation. *Internat. J. Numer. Methods Engrg.*, 61(7):1072–1092, 2004.

[HL96] Christophe Hazard and Marc Lenoir. On the solution of time-harmonic scattering problems for Maxwell's equations. *SIAM J. Math. Anal.*, 27(6):1597–1630, 1996.

[HLL00] Yao Houndonougbo, Brian Laird, and Ben Leimkuhler. Molecular dynamics algorithms for mixed hard-core/continuous potentials. *Mol. Phys.*, 98(5):309–316, 2000.

[HLW06] Ernst Hairer, Christian Lubich, and Gerhard Wanner. *Geometric numerical integration*, volume 31 of *Springer Series in Computational Mathematics*. Springer-Verlag, Berlin, second edition, 2006. Structure-preserving algorithms for ordinary differential equations.

[HMK02] Tomi Huttunen, Peter Monk, and Jari P. Kaipio. Computational aspects of the ultra-weak variational formulation. *J. Comput. Phys.*, 182(1):27–46, 2002.

[HMM07] Tomi Huttunen, Matti Malinen, and Peter Monk. Solving Maxwell's equations using the ultra weak variational formulation. *J. Comput. Phys.*, 223(2):731–758, 2007.

[HN89] Wolfgang Hackbusch and Z.P. Nowak. On the Fast Matrix Multiplication in the Boundary Element Method by Panel Clustering. *Numer. Math.*, 54:463–491, 1989.

[Hör83] Lars Hörmander. *The Analysis of Linear Partial Differential Operators I*. Springer-Verlag, 1983.

[HW08] George C. Hsiao and Wolfgang L. Wendland. *Boundary integral equations*, volume 164 of *Applied Mathematical Sciences*. Springer-Verlag, Berlin, 2008.

[IS07] Artur F. Izmaylov and Gustavo E. Scuseria. Efficient evaluation of analytic vibrational frequencies in Hartree-Fock and density functional theory for periodic nonconducting systems. *J. Chem. Phys.*, 127:144106–144106–9, 2007.

[JL77] Adrien Jami and Marc Lenoir. Formulation variationnelle pour le couplage entre une méthode d'éléments finis et une représentation intégrale. *C. R. Acad. Sci. Paris Sér. A-B*, 285(4):A269–A272, 1977.

[Jon88] D.S. Jones. An approximate boundary condition in acoustics. *Journal of Sound and Vibration*, 121(1):37 – 45, 1988.

[Kir07] Andreas Kirsch. An integral equation approach and the interior transmission problem for Maxwell's equations. *Inverse Probl. Imaging*, 1(1):159–179, 2007.

[KL00] Anne Kværnø and Ben Leimkuhler. A time-reversible, regularized, switching integrator for the N-body problem. *SIAM J. Sci. Comput.*, 22(3):1016–1035, 2000.

[KL09] Andreas Kirsch and Armin Lechleiter. The operator equations of Lippmann-Schwinger type for acoustic and electromagnetic scattering problems in L^2. *Appl. Anal.*, 88(6):807–830, 2009.

[KLss] Nicolas Kielbasiewicz and Eric Lunéville. http://uma.ensta-paristech.fr/soft/XLiFE++/. XLiFE++ documentation, ENSTA, in progress.

[KM00] Jörg Kottmann and Olivier Martin. Accurate solution of the volume integral equation for high-permittivity scatterers. *IEEE Trans. on Antennas and Propag.*, 48(11):1719–1726, 2000.

[Kon10] El-Hadji Koné. *Equations intégrales de volume et de surface pour l'analyse d'antennes-lentilles millimétriques*. Thèse de doctorat, Université Rennes 1, june 2010.

[KS99] Konstantin N. Kudin and Gustavo E. Scuseria. Range definitions for Gaussian-type charge distributions in fast multipole methods. *J. Chem. Phys.*, 111(6):2351–2356, 1999.

[KSC99] Sencer Koc, Jiming Song, and Weng Cho Chew. Error analysis for the numerical evaluation of the diagonal forms of the scalar spherical addition theorem. *SIAM J. Numer. Anal.*, 36(3):906–921, 1999.

[KTU87] Gregory A. Kriegsmann, Allen Taflove, and Korada R. Umashankar. A new formulation of electromagnetic wave scattering using an on-surface radiation boundary condition approach. *IEEE Trans. Antennas and Propagation*, 35(2):153–161, 1987.

[Laf11] Yvon Lafranche. http://perso.univ-rennes1.fr/yvon.lafranche/fig4tex/index.html. Fig4TeX documentation, Université Rennes 1, last update: november 2011.

[Lan95] Virginie Lange. *Equations intégrales espace-temps pour les équations de Maxwell. Calcul du champ diffracté par un obstacle dissipatif*. Thèse de doctorat, Université Bordeaux I, Octobre 1995.

[LC10] Yang G. Liu and Weng Cho Chew. A low frequency vector fast multipole algorithm with vector addition theorem. *Commun. Comput. Phys.*, 8(5):1183–1207, 2010.

[Lec97] Agnès Lecompte. *Compatibilité électromagnétique d'un téléphone portable avec son environnement*. Thèse de doctorat, Université Bordeaux I, Juillet 1997.

[Lei86] Rolf Leis. *Initial boundary value problems in mathematical physics*. John Wiley, New York, 1986.

[LHM12] Teemu Luostari, Tomi Huttunen, and Peter Monk. The ultra weak variational formulation using Bessel basis functions. *Commun. Comput. Phys.*, 11(2):400–414, 2012.

[LHM13] Teemu Luostari, Tomi Huttunen, and Peter Monk. Improvements for the ultra weak variational formulation. *Internat. J. Numer. Methods Engrg.*, 94(6):598–624, 2013.

[LJ01] Jian Liu and Jian-Ming Jin. A novel hybridization of higher order finite element and boundary integral methods for electromagnetic scattering and radiation problems. *IEEE Trans. Antennas and Propagation*, 49(12):1794–1806, 2001.

[LS12] Marc Lenoir and Nicolas Salles. Evaluation of 3-D singular and nearly singular integrals in Galerkin BEM for thin layers. *SIAM J. Sci. Comput.*, 34(6):A3057–A3078, 2012.

[Lu03] Cai-Cheng Lu. A fast algorithm based on volume integral equation for analysis of arbitrarily shaped dielectric radomes. *IEEE Trans. on Antennas and Propag.*, 51(3):606–612, 2003.

[MDL14] Daniel Martin, Eric Darrigrand, and Yvon Lafranche. http://anum-maths.univ-rennes1.fr/melina/melina++_distrib/. MÉLINA++ documentation, Université Rennes 1, last update: jan 2014.

[MH78] J. R. Mautz and R. F. Harrington. H-field, E-field, and combined-field solutions for conducting bodies of revolution. *Arch. Elektron. Übertragungstech.*, 32:157–164, 1978.

[Néd01] Jean-Claude Nédélec. *Acoustic and electromagnetic equations*, volume 144 of *Applied Mathematical Sciences*. Springer-Verlag, New York, 2001.

[Pot01] Roland Potthast. *Point sources and Multipoles in Inverse Scattering theory*. Chapman & Hall, London, 2001.

[Pro60] M. H. Protter. Unique continuation for elliptic equations. *Trans. Amer. Math. Soc.*, 95(1):81–91, 1960.

[PSPS94] Henrik G. Petersen, Dorthe Sølvason, John W. Perram, and Edgar R. Smith. The very fast multipole method. *J. Chem. Phys.*, 101(10):8870–8876, 1994.

[Rah96] Jussi Rahola. Diagonal Forms of the Translation Operators in the Fast Multipole Algorithm for Scattering Problems. *BIT*, 36(2):333–358, 1996.

[Rah00] Jussi Rahola. On the eigenvalues of the volume integral operator of electromagnetic scattering. *SIAM J. Sci. Comput.*, 21(5):1740–1754, 2000.

[Rai14] Rania Rais. *Couplage entre éléments finis et représentation intégrale pour les problèmes de diffraction acoustique et électromagnétique : analyse de convergence des méthodes de Krylov et méthodes multipôles rapides*. Thèse de doctorat, Université Rennes 1, feb. 2014.

[Sak14] Hamdi Sakly. *Opérateur intégral volumique en théorie de diffraction électromagnétique*. Thèse de doctorat, Université Rennes 1, may 2014.

[Sal13] Nicolas Salles. *Stabilization of the calculation of singularities in variational integral equations methods*. Thèse de doctorat, Université de Paris Sud, september 2013.

[Sau00] Stefan A. Sauter. Variable Order Panel Clustering. *Computing*, 64:223–261, 2000.

[SB06] Ronan Sauleau and Barbara Barès. A complete procedure for the design and optimization of arbitrarily-shaped integrated lens antennas. *IEEE Trans. on Antennas and Propag.*, 54(4):1122–1133, 2006.

[SC95] Jiming M. Song and Weng Cho Chew. Multilevel Fast Multipole Algorithm for Solving Combined Field Integral Equations of Electromagnetic Scattering. *Microwave Opt. Tech. Letter*, 10(1):14–19, September 1995.

[SD99] Bruno Stupfel and Bruno Després. A domain decomposition method for the solution of large electromagnetic scattering problems. *J. Electromag. Waves and Appl.*, 1999.

[SF11] Alexander B Samokhin and Yasuhide Fukumoto. Singular electromagnetic modes in an anisotropic medium. Technical report, Education-and-Research Hub for Mathematics-for-Industry, 2011.

[SS11] Stefan A. Sauter and Christoph Schwab. *Boundary element methods*, volume 39 of *Springer Series in Computational Mathematics*. Springer-Verlag, Berlin, 2011. Translated and expanded from the 2004 German original.

[SSF96] Matthew C. Strain, Gustavo E. Scuseria, and Michael J. Frisch. Achieving linear scaling for the electronic quantum Coulomb problem. *Science*, 271(5245):51–53, 1996.

[SSVVA06] Maurice I. Sancer, Kubilay Sertel, John L. Volakis, and Peter Van Alstine. On volume integral equations. *IEEE Trans. Antennas and Propagation*, 54(5):1488–1495, 2006.

[Stu01] Bruno Stupfel. A Hybrid Finite Element and Integral Equation Domain Decomposition Method for the Solution of the 3-D Scattering Problem. *J. Comput. Phys.*, 172:451–471, 2001.

[SWHG01] Yihan Shao, Christopher White, and Martin Head-Gordon. Efficient evaluation of the Coulomb force in density-functional theory calculations. *J. Chem. Phys.*, 114(15):6572–6577, 2001.

[WHG96] Christopher A. White and Martin Head-Gordon. Rotating around the quartic angular momentum barrier in fast multipole method calculation. *J. Chem. Phys.*, 105(12):5061–5067, 1996.

[WJGHG94] Christopher A. White, Benny G. Johnson, Peter M.W. Gill, and Martin Head-Gordon. The continuous fast multipole method. *Chem. Phys. Lett.*, 230(1–2):8–16, 1994.

[WJGHG96] Christopher A. White, Benny G. Johnson, Peter M.W. Gill, and Martin Head-Gordon. Linear scaling density functional calculations via the continuous fast multipole method. *Chem. Phys. Lett.*, 253(3–4):268–278, 1996.

[Zho95] Bin Zhou. *Méthode des équations intégrales pour la résolution des problèmes de diffraction à hautes fréquences*. Thèse de doctorat, Université Paris XI, Novembre 1995.